

NEW EXPERIMENTAL OBSERVATIONS IN THE COLLISION-INDUCED
INFRARED SPECTRA OF MOLECULAR HYDROGEN

CENTRE FOR NEWFOUNDLAND STUDIES

**TOTAL OF 10 PAGES ONLY
MAY BE XEROXED**

(Without Author's Permission)

K. S. CHANG

385612



CONTENTS

NEW EXPERIMENTAL OBSERVATIONS IN THE COLLISION-INDUCED INFRARED SPECTRA OF MOLECULAR HYDROGEN	Page
ABSTRACT	
CHAPTER 1 INTRODUCTION	
CHAPTER 2 APPARATUS AND EXPERIMENTAL METHOD	11
2.1 The $\Delta \nu$ Absorption	11
K. S. Chang	
2.2 Optical Arrangement, Electronics and Calibration	
of the Spectral Region	15
2.3 Gas Handling	21
2.4 Isothermal Data	22
2.5 Measurement of Experimental Data	22
CHAPTER 3 COLLISION-INDUCED VIBRATION-ROTATION U TRANSITIONS ($\Delta J = \pm 1$) IN HI2	25
3.1 Normal Hydrogen at 77 K	27
(a) Absorption Profiles	27
(b) Profile Analysis: Separation of the Quadrupolar Transitions from the Observed Absorption Profiles	31
(c) Derived Absorption Profiles of the U(1) Group	42
3.2 $D_2 - Xe$ Mixtures at 293 K	47
3.3 Heredityless Invert Matrix Elements of H ₂	51
Submitted in partial fulfilment of the requirements for the degree of Doctor of Philosophy Memorial University of Newfoundland	54
4.1 Department of Physics	55
September 1974	
4.2 Analysis of the Results of Enhancement of Absorption	59



CONTENTS

	<u>Page</u>
ABSTRACT	iv
CHAPTER 1 INTRODUCTION	1
CHAPTER 2 APPARATUS AND EXPERIMENTAL METHOD	11
2.1 The 2 m Absorption Cell	11
2.2 Optical Arrangement, Electronics and Calibration of the Spectral Region	16
2.3 Gas Handling	21
2.4 Isothermal Data	22
2.5 Measurement of Experimental Data	22
CHAPTER 3 COLLISION-INDUCED VIBRATION-ROTATION U TRANSITIONS ($\Delta J = 4$) IN HYDROGEN	25
3.1 Normal Hydrogen at 77 K	27
(a) Absorption Profiles	27
(b) Profile Analysis: Separation of the Quadrupolar Transitions from the Observed Absorption Profiles ..	31
(c) Derived Absorption Profiles of the U(1) Group ..	42
3.2 H ₂ - Xe Mixtures at 298 K	47
3.3 Hexadecapole Moment Matrix Elements of H ₂	51
CHAPTER 4 COLLISION-INDUCED FIRST OVERTONE SPECTRA OF H ₂ IN H ₂ - Kr AND H ₂ - Xe MIXTURES AT ROOM TEMPERATURE	54
4.1 Experimental Results	55
4.2 Analysis of the Profiles of Enhancement of Absorption ..	59

	<u>Page</u>
4.3 Results of Profile Analysis	69
(i) Frequency Shifts	69
(ii) Half-widths	78
CHAPTER 5 APPARENT COLLISION-INDUCED EMISSION IN HYDROGEN	82
5.1 Experimental Observation	82
5.2 Speculation on the Cause of the Phenomenon	91
APPENDIX A Normalized Boltzmann Factors for Normal Hydrogen at Different Temperatures	97
APPENDIX B Binary Absorption Coefficient Due to Electrostatic Induction between Two Homonuclear Diatomic Molecules ...	99
APPENDIX C Quadrupolar Matrix Elements of H ₂ in Supplement to the Matrix Elements Given by Birnbaum and Poll (1969)	104
ACKNOWLEDGMENTS	106
REFERENCES	107
PUBLICATIONS	110

New Experimental Observations in the Collision-Induced
Infrared Spectra of Molecular Hydrogen

ABSTRACT

This work describes several new experimental observations made by the author in the collision-induced infrared absorption spectra of molecular hydrogen at liquid nitrogen and room temperatures for densities up to 660 amagat. The experiments were carried out with a 2 m low-temperature high-pressure absorption cell of the transmission type. The spectral region investigated extends from 3500 to $10,000 \text{ cm}^{-1}$.

Collision-induced vibration-rotation U transitions ($\Delta J = +4$) of the hydrogen molecule in its fundamental band have been observed for the pure gas at 77 K for densities in the range 430 - 660 amagat and for the binary mixtures, hydrogen-xenon, and hydrogen-krypton at 298 K for total gas densities ~ 450 amagat. The high frequency tail of the quadrupolar S transitions which overlaps the U transitions has been separated from the experimental profiles by the method of profile analysis. The spectrum of the U transitions is interpreted in terms of the hexadecapolar induction mechanism. From the experimental integrated binary absorption coefficients of the U transitions, appropriate values of the hexadecapole moment matrix elements of the hydrogen molecule are derived.

Spectra of the collision-induced first overtone band of hydrogen in binary mixtures with krypton and xenon at 298 K for densities up to ~ 450 amagat have been recorded for the first time. From an analysis of the profiles of the enhancement of absorption, the frequency shifts $\Delta\nu_0$ and

the half-widths δ have been determined. Unusual occurrence of some H_2 double transitions was observed. The observed frequency shifts of the quadrupolar lines are negative and level off at high densities, qualitatively in the same way, but with larger shifts, as those observed in the fundamental. The observed half-widths of the quadrupolar lines were found to increase with the density of the inert gas, and to be quite sensitive to the base density of the hydrogen. Both observed line-shifts and half-widths are expected to have larger values than the true ones because of overlapping double transitions obscuring the single transition lines.

During the above mentioned experiments with hydrogen, it was observed that especially in the spectral region $6800 - 7400 \text{ cm}^{-1}$ more light reached the detector with compressed hydrogen in the cell than when the cell was evacuated. The spectral profiles of this phenomenon in the region $6800 - 7400 \text{ cm}^{-1}$ and their density dependence have been determined and it is speculated that upper states are populated by collision-induced absorption in the region of the first overtone and the subsequent radiative emission transitions follow the same selection rules that are known for collision-induced absorption.

CHAPTER 1

Introduction

Isolated homonuclear diatomic molecules, like hydrogen, in their electronic ground states have no permanent electric dipole moment on account of the symmetry of their charge configurations. Consequently, unlike polar molecules, they have no electric dipole absorption at their rotational or vibrational frequencies. However, an electric dipole moment is induced in two or more colliding molecules by intermolecular forces because of an asymmetric distortion of the electron charge configuration during collisions. This induced dipole moment is modulated by the rotation, vibration, and relative translational motion of the colliding molecules and causes the phenomenon of collision-induced absorption in which normally forbidden transitions occur. Collision-induced absorption was first observed in compressed oxygen and nitrogen by Crawford, Welsh, and Locke (1949) in the regions of their fundamental vibrational frequencies. In general, collision-induced spectra are broad and diffuse because the duration of the induced dipole is very short.

The present thesis reports on studies carried out in the following areas of the collision-induced infrared spectra of molecular hydrogen:

- (i) new rotational transitions $\Delta J = 4$ in the fundamental region of H_2 in the pure gas at 77 k and in $H_2 - Kr$ and $H_2 - Xe$ binary mixtures at 298 K,
- (ii) the infrared first overtone band of H_2 in $H_2 - Kr$ and $H_2 - Xe$ binary mixtures at 298 K,
- and (iii) apparent collision-

induced emission in hydrogen, especially in the region 6800 to 7300 cm^{-1} . A brief account of the collision-induced absorption of hydrogen will be presented in the following paragraphs with emphasis on the aspects having considerable bearing on the work presented in this thesis.

Since the discovery of collision-induced infrared absorption, the induced fundamental band of gaseous hydrogen has been the subject of numerous studies under a variety of experimental conditions. The reasons for the greatest interest in the study of the spectra of hydrogen are many: the H_2 molecule is the simplest of all diatomic molecules; it can be treated more rigorously by theoretical calculations; various rotational component bands are somewhat separated in spite of their broad and diffuse nature because of its small moment of inertia. Thus the collision-induced spectra of hydrogen have been instrumental in understanding the process involved and in verifying the results of the theoretical studies. The collision-induced fundamental band of gaseous hydrogen, first observed by Welsh, Crawford, and Locke (1949) has been extensively studied in the last 25 years in pure H_2 and in binary mixtures of H_2 with He, Ne, Ar, Kr, Xe, N_2 and O_2 under wide ranges of pressures and temperatures. An exhaustive list of references on this work is readily obtained from a recent excellent review paper by Welsh (1972) on collision-induced absorption of hydrogen. The attention of the reader is also drawn to the following more recent references from our laboratory on the fundamental band of hydrogen: Varghese, Ghosh and Reddy (1972) and Reddy and Chang (1973).

The collision-induced first overtone band of gaseous hydrogen in the

pure gas was first observed by Welsh, Crawford, McDonald and Chisholm (1951), and later studied by Hare and Welsh (1958) at room temperature at very high pressures, and Watanabe, Hunt, and Welsh (1971) and Watanabe (1971) at various temperatures down to 24 K. McKellar and Welsh (1971) obtained improved data on this band in pure H_2 and in binary mixtures of H_2 - Ar and H_2 - N_2 at temperatures in the range 85 to 116 K at a path length of 137 m.

One important difference in the experimental findings between the fundamental and the first overtone bands of H_2 is the absence of an overlap contribution to the first overtone band. It is also important to mention the first overtone band experimental work of Mactaggart (1971) in dense H_2 - Ar mixtures, in which he observed absorption peaks evidently corresponding to simultaneous transitions of two hydrogen molecules, which would not be expected to occur frequently in dilute mixtures of hydrogen with argon. This was explained as due to collisions of the type H_2 - Ar - H_2 .

The theory of binary collision-induced fundamental band of homonuclear diatomic gases has been interpreted theoretically by Van Kranendonk (1957, 1958), who used the so called "exponential-4" model for the induced dipole moment to show that the absorption is caused by two different mechanisms: One is the dipole moment induced by the isotropic short range overlap force, which decreases exponentially with increasing intermolecular distance R. The other is a dipole moment induced by the electrostatic quadrupole interaction force, which is anisotropic and arises from the polarization of one molecule in the colliding pair by the quadrupole moment (Q)

field of the second molecule, $\mu \propto \frac{Q_1' \alpha_2}{R^4}$ and vice versa, $\mu \propto \frac{\alpha_1' Q_2}{R^4}$.

Here Q_1' and α_1' are respectively the derivatives of the quadrupole moment and polarizability of molecule 1 with respect to its internuclear separation, and Q_2 and α_2 are the quadrupolar moment and polarizability of molecule 2. The short-range moment contributes to the intensity of the broader Q_1 lines (i.e., Q_{overlap}) ($\Delta J = 0$) and the long-range moment produces the S_1 ($\Delta J = +2$), Q_1 (i.e., Q_{quad} ; $\Delta J = 0$) and O_1 ($\Delta J = -2$) lines.* In addition to these single transitions, in which only one molecule of the colliding pair makes the vibrational or vibrational-rotational transition while the internal energy of the other molecule does not change, double transitions of the type $S_0(J) + Q_1(J)$ contribute appreciably to the intensity of the band. In a double transition, each of the molecules in a binary collision can perform a molecular transition with the absorption of a single photon. If one takes into account the anisotropy, γ , of the polarizability of the H_2 molecule (which is rather small), double rotational transitions of the type $S_1(J) + S_0(J)$ are expected to occur. However, these transitions are very weak.

* The subscript indicates the change Δv in the vibrational quantum number, i.e., 0 for the pure rotational band, 1 for the fundamental band, etc. The observed dip in the Q branch of the collision-induced fundamental band of H_2 is characteristic of the short-range overlap interaction. The observation of small dips in the $S_1(1)$ and $S_1(0)$ lines of H_2 in H_2 - He and H_2 - Ne (see for example Reddy and Chang, 1973) indicates that there is some contribution of the anisotropy of overlap moment to the intensity of the so-called "quadrupolar" S lines in these mixtures.

Recent theoretical calculations of Karl and Poll (1967), Birnbaum and Poll (1969), Dalgarno et al. (1969) and Poll (1970) indicate that the matrix elements of the quadrupole moment and polarizability between different vibrational states of H_2 , $\langle vJ | Q | v'J' \rangle$ and $\langle vJ | \alpha | v'J' \rangle$ are sensitive to the initial and final rotational quantum numbers J and J' . It is therefore necessary to use these matrix elements rather than Q , Q' , α and α' in the calculations of the quadrupole-induced part of the absorption of hydrogen. In particular, Poll (1970) has given explicit expressions which are quite exhaustive for the quadrupolar part of the binary absorption coefficient for an arbitrary transition $(v_1'J_1', v_2'J_2') \leftarrow (v_1J_1, v_2J_2)$ in terms of these matrix elements, thus extending the theory of Van Kranendonk (1957, 1958) to the collision-induced overtone bands as well. The anisotropy of the polarizability can also be taken into account by an extension of the expressions given by Poll (1970) (see McKellar and Welsh, 1971). The above mentioned 'exp-4' model satisfactorily explains most collision-induced spectra, and up to the present has been used almost exclusively.

The first non-vanishing electric multipole moment for symmetric diatomic molecules such as hydrogen is the quadrupole moment. As noted earlier in this chapter the quadrupole-induced dipole moment in the colliding pairs of molecules produces transitions with the selection rule $\Delta J = -2, 0$ and $+2$. The next higher electric multipole moment for symmetric diatomic molecules is the hexadecapole moment. In a binary collision, the induced dipole moment in one molecule by the hexadecapolar field of the other molecule, and vice versa, gives rise to transitions with the selection rule $\Delta J = -4, -2, 0, +2$ and $+4$, which would be

designated as M, O, Q, S and U branches, respectively. Also possible are double transitions corresponding to one molecule making any of the above mentioned transitions and the second molecule making an O, Q or S transition.

Because of the small magnitude of the hexadecapole moment of H₂ (Karl, Obryk, and Poll, 1973) the intensity of the hexadecapole-induced transitions in the fundamental band of hydrogen is expected to be very weak. As a matter of fact, the hexadecapole-induced transitions with the selection rule $\Delta J = -2, 0$ and $+2$ cannot be experimentally separated from the corresponding quadrupole-induced transitions.

In the fundamental band of H₂, all possible double transitions of the type S₁(J) + S₀(J), Q₁(J) + U₀(J) and single transitions U₁(J) between the lower and upper rotational states at 77 K are illustrated in Fig. 1. Also included in Figure 1 are the wave numbers of these transitions. In the calculation of the wave numbers the molecular constants of H₂ given by Foltz, Rank, and Wiggins (1966) were used. Sample absorption profiles for the fundamental and the first overtone bands of normal hydrogen at ~ 80 K at moderate pressures of the gas are shown in Fig. 2. Transitions Q₁(J), S₁(J) for the fundamental band and transitions Q₂(J), ... S₂(J) for the overtone band are marked in the figure. Also marked in the figure is the expected region of the U(1) group transitions in the fundamental band.

The observation of the U transitions in normal H₂ at 195 K on the basis of the initial preliminary experiments has been reported by us very recently in a short communication in Physical Review Letters

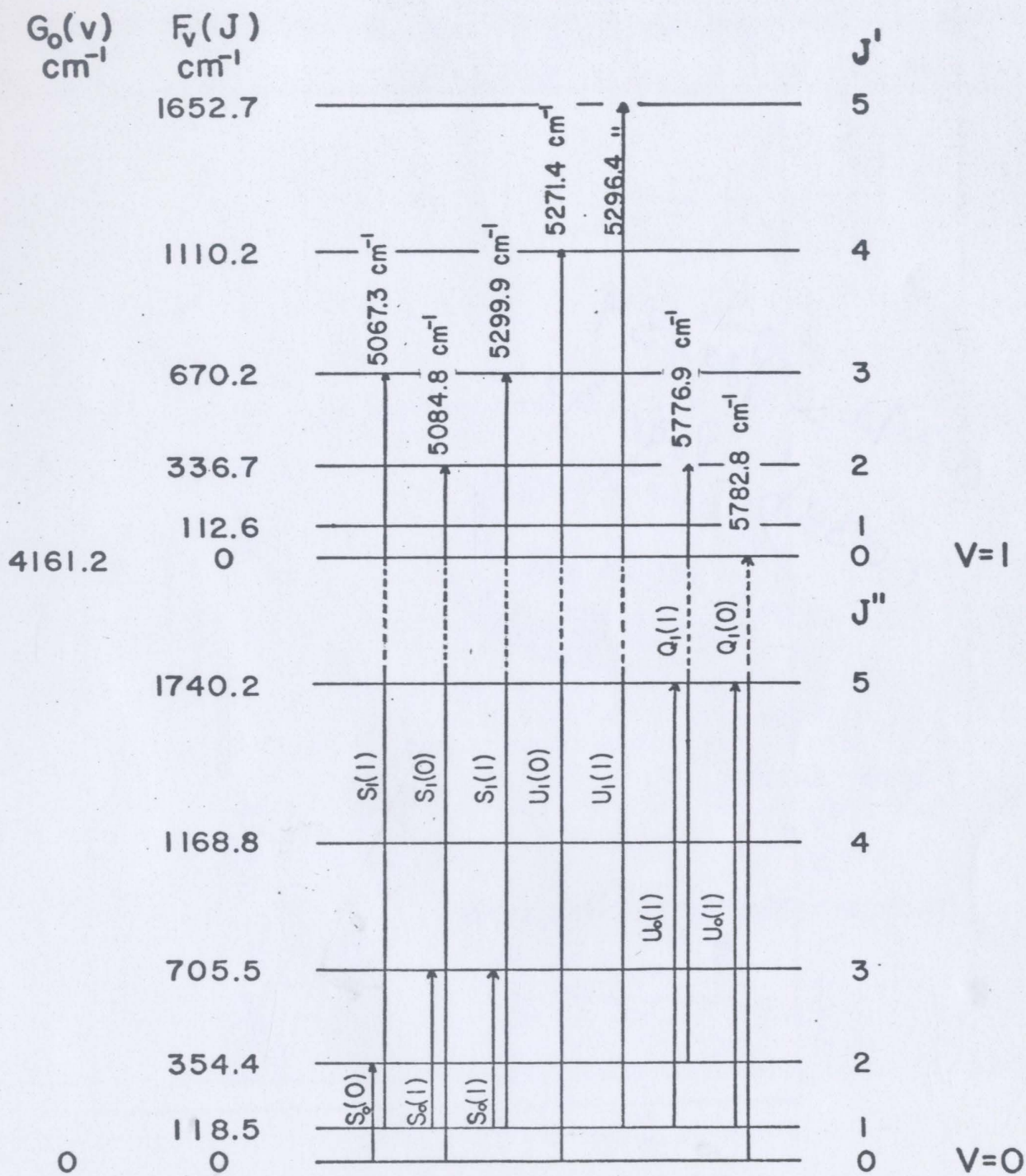


Fig. 1. Single and double transitions in the high wave number wing of the fundamental band of hydrogen at 77 K.

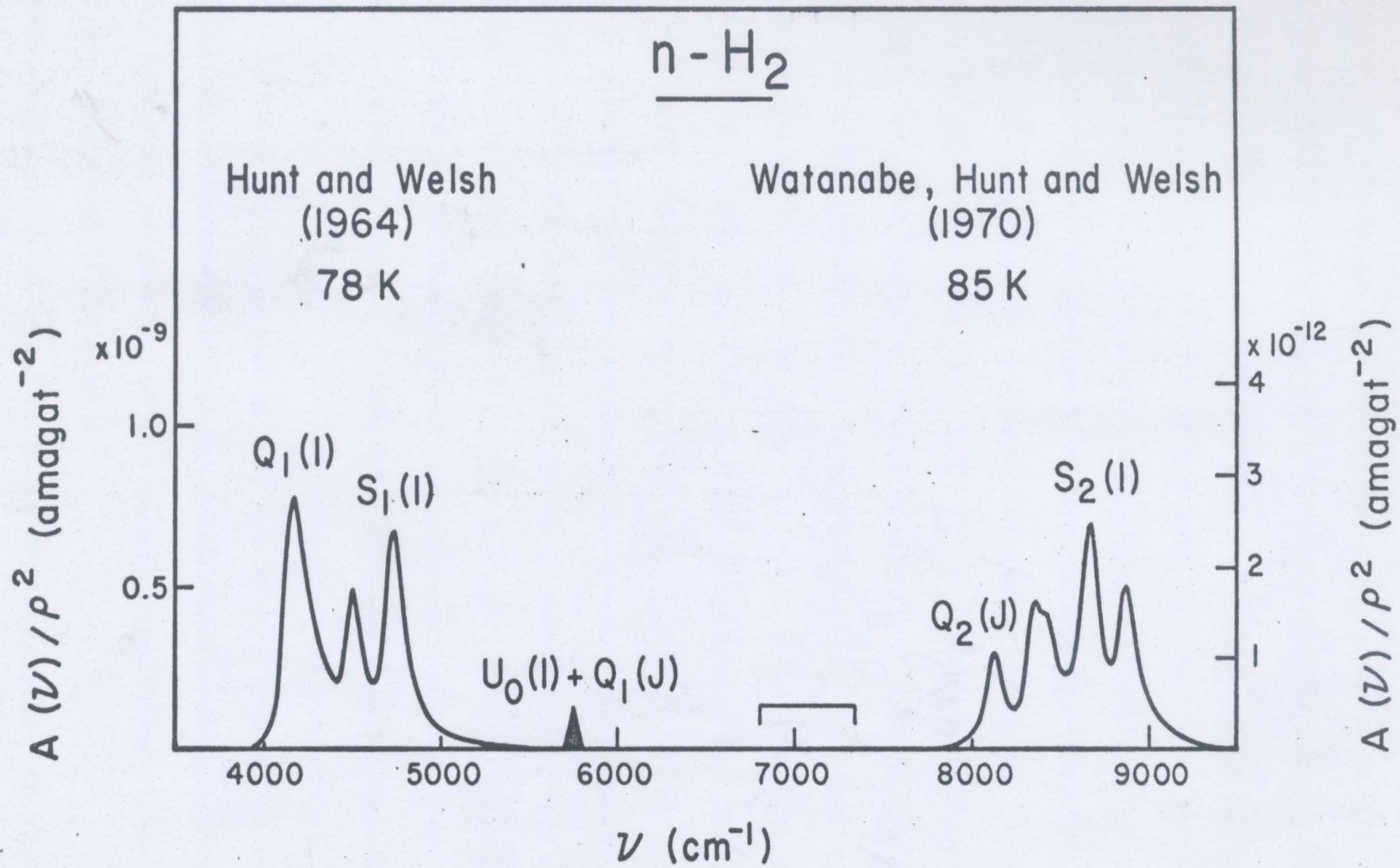


Fig. 2. Locations of the spectral regions where the U transitions and the apparent emission occur, between the fundamental and the first overtone bands.

(Gibbs et al, 1973). One of the objects of the present work is to investigate the hexadecapolar induced transitions in H_2 . A two meter high pressure cell which was previously used in our laboratory for work at room temperature was converted for work at low temperatures. The same cell was used for the entire work reported in this thesis. The hexadecapolar induced transitions in the fundamental band of H_2 have been investigated in normal hydrogen for densities up to ~ 660 amagat and in binary mixtures with Xe and Kr at room temperature for total densities up to 300 amagat. These studies are described in Chapter 3.

The collision-induced first overtone band of H_2 has been studied in binary mixtures of H_2 - Kr and H_2 - Xe at room temperature at densities up to ~ 450 and 350 amagat, respectively. The evidence of double transitions observed by Mactaggart (1971) can be seen. The absorption coefficients were measured and found very sensitive to the base density of the hydrogen. No binary absorption coefficient is quoted, as the density range of hydrogen in the present study is limited. The line shifts at different densities were obtained by means of contour analysis. Negative shifts as much as 23 cm^{-1} and 34 cm^{-1} were measured for H_2 - Kr and H_2 - Xe experiments, respectively. Again these are only qualitative measurements, as the double transition peaks could not be resolved from those of single transitions. This effect could also cause the apparent broadening of the single transition lines. These studies are described in Chapter 4.

During the course of all the above investigations in the regions

where there were no strong molecular absorptions, one very peculiar phenomenon always happened - that actually more signal was detected with the gas in the absorption cell than without, especially in the regions between ~ 6800 to 7400 cm^{-1} , where a few broad peaks could be seen. The small signal increases due to the decrease in reflection loss at windows when gases were introduced to the cell cannot account for the signal increases.

It is tentatively suggested that collision-induced emission is seen, where the upper states have been populated by collision-induced absorption, their thermal populations being totally negligible. Chapter 5 of this thesis describes the observations and discusses speculations on explaining them.

CHAPTER 2

Apparatus and Experimental Method

The present research project on the collision-induced infrared spectra of molecular hydrogen, whose objectives were outlined in Chapter 1, was carried out with a 2 meter low-temperature high-pressure absorption cell of the transmission type. A description of the absorption cell, the optical arrangement, the electronics, and the high pressure gas handling system, used in the present experimental investigation, is given in this chapter. Also included in this chapter are details of the experimental procedure and the isothermal data of gases.

2.1 The 2 m Absorption Cell

This is a transmission type 2 m absorption cell which was originally constructed in our laboratory for the study of the collision-induced absorption of gases under high pressures at room temperature (Reddy and Kuo, 1971). In order to adapt this cell for work at 77 K in the present work a few modifications and many additions to it were made. The constructional details of this low temperature cell are shown in Fig. 3.

The absorption tube B was constructed from a 2 m stainless steel (type 303) bar, 3 in. in diameter. The central bore of 1 in.^w with an accuracy of ± 0.010 in. in the body of the cell was drilled by Industrial Machining Limited, Montreal. A highly polished stainless steel light guide G made in five linear sections has a rectangular

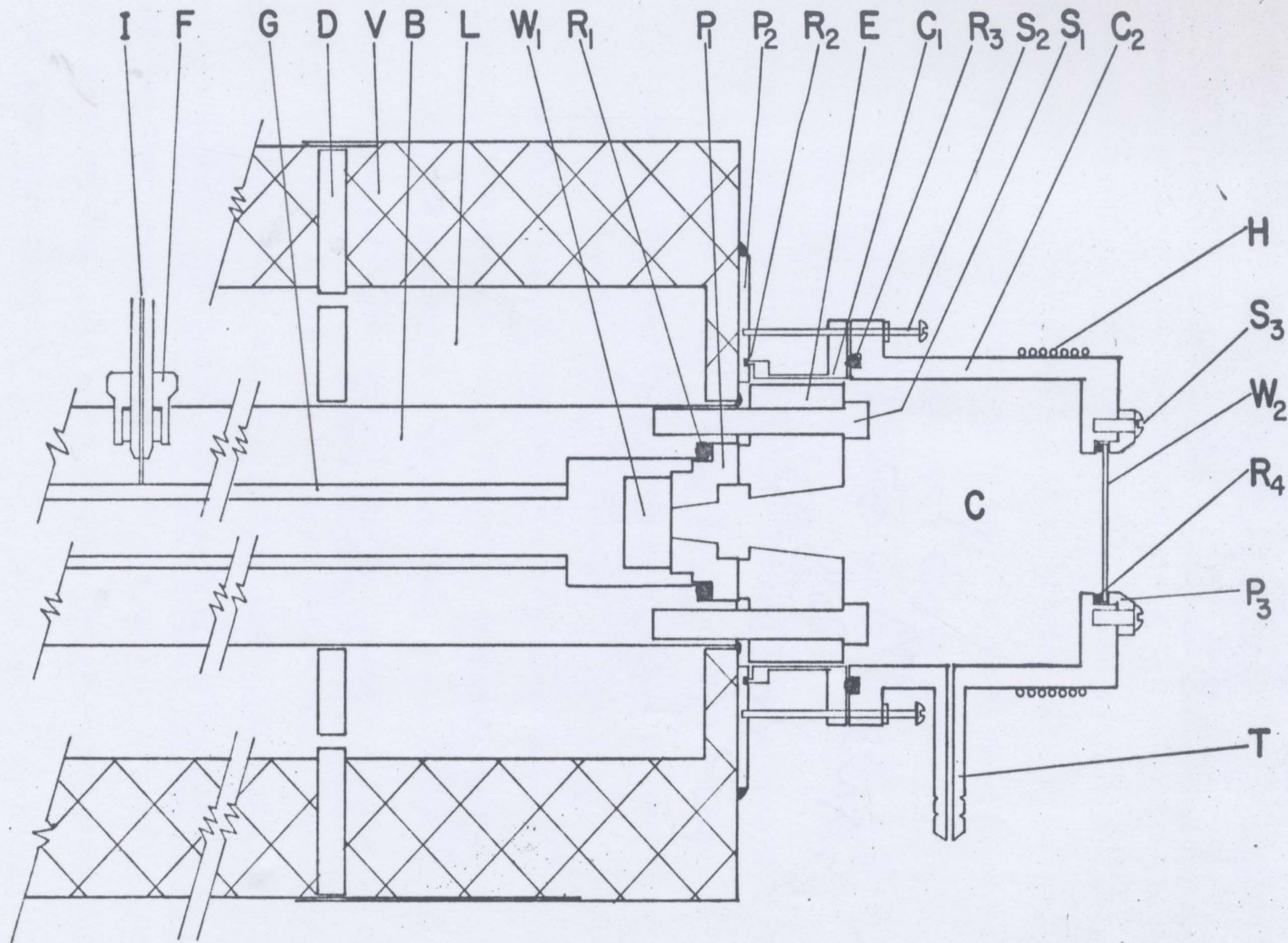


Fig. 3. A cross-section of one end of the 2 m high-pressure, low-temperature transmission type absorption cell.

aperture 1 cm x 0.5 cm. Optically flat synthetic sapphire windows W_1 , 1 in. in diameter and 1 cm thick, were attached with General-Electric RTV-108 silicone rubber cement to polished stainless steel window seats P_1 which have rectangular apertures 0.4 in. x 0.2 in. A high-pressure seal between the window seat and the absorption tube was achieved by the use of invar rings R_1 between them and by tightening each of the end pieces E against the body of the cell by means of eight Allenoy steel Allen head screws S_1 . As the coefficient of thermal expansion of invar is much less than that of the steel screws, a pressure-tight seal was obtained at low temperatures.

The absorption cell was surrounded by two concentric cylinders made of stainless steel sheet 1/32 in. thick. The inner cylinder holding the coolant L is 5-7/8 in. in diameter and welded on to two 1/4 in. thick stainless steel discs D which support the weight of the absorption cell. The holes (not shown in Fig. 3) drilled through these discs allow the coolant to flow freely through them. The outer cylinder 11 in. in diameter and consisting of three pieces of stainless steel sheet wrapped around D is capable of accommodating the thermal contraction of the inner cylinder when the absorption cell is cooled. The inner and outer cylinders were welded to two stainless steel end sheets which were in turn welded to a stainless steel cylinder tube which fits around the absorption cell. The outer jacket was then sealed to the body of the cell at its ends by means of stainless steel welding. The space between the outer and inner jackets was insulated with vermiculite V .

To prevent the window W_1 of the absorption cell from frosting during the low-temperature experiments, there was constructed at each end of the cell a vacuum chamber C , which essentially consists of two cylindrical adapters C_2 (made of plexiglass) and C_1 (made of steel) which was made thin in the central portion so that the flanges connecting C_1 and C_2 would not be too cold. Aluminum foils were wrapped over the end piece E and screws S_1 and also inside C_1 in order that heat from the outside would be reflected back. The window W_2 is a flat synthetic sapphire plate 2 in. in diameter and 3 mm thick and was sealed with a neoprene O-ring R_4 against the plexiglass adapter by the plexiglass end plate P_3 by means of three screws S_3 . Adapter C_1 was sealed to C_2 with a neoprene O-ring R_3 by tightening six screws S_2 into a 1/4 in. thick stainless steel plate P_2 welded on to the outer jacket. These screws also serve to obtain a seal between P_2 and C_1 with indium ring R_2 . Heating coils H wound around the plexiglass chamber, and carrying variable current, prevent the window W_2 from frosting. The chamber C was evacuated through the side tube T .

Gases were admitted into the absorption cell through a steel capillary tube I which was connected to the cell by means of a 1/2 in. Aminco fitting F . The coolant used for the low-temperature work was liquid nitrogen (77 K). An opening in the central section of the jackets was provided in order to admit the coolant. A vertical cross-section of the entire low-temperature cell is schematically shown in Fig. 4. The temperature of the cell was measured with a copper-constantan thermocouple mounted inside the cell through the capillary tube I . The sample path lengths of the absorption tube were 195.3 cm. at room

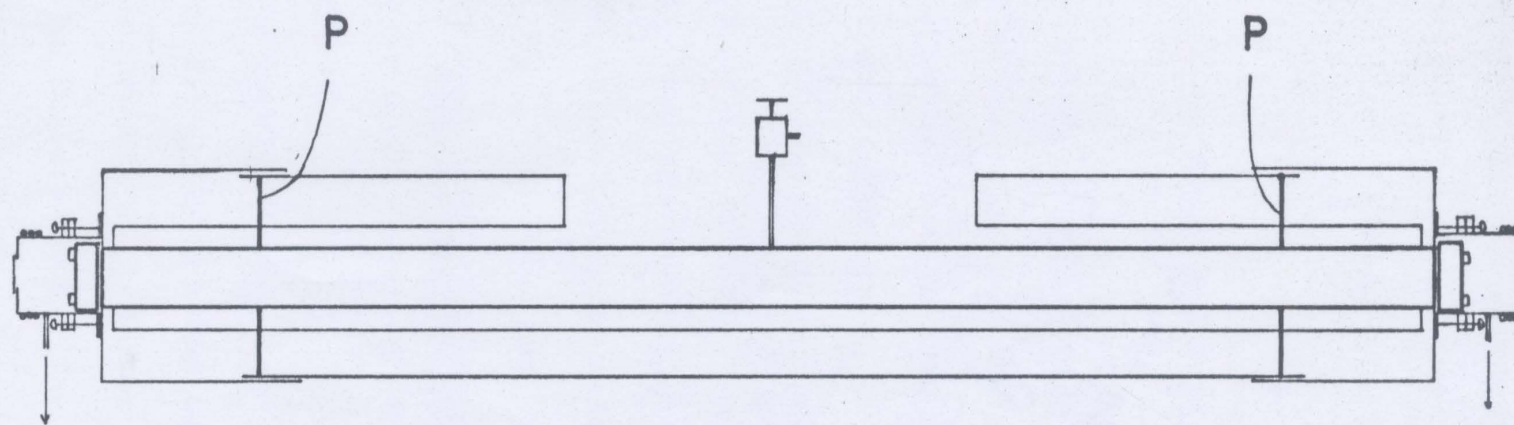


Fig. 4. A cross-section of the 2 m high-pressure, low-temperature transmission type absorption cell with cooling jacket.

temperature (298 K) and 194.9 cm at liquid nitrogen temperature.

Calculations showed that the average path length of the radiation within the absorption cell when multiple reflections in the light guide were taken into account was less than 4% longer than the actual sample path length and was not taken into account.

2.2 Optical Arrangement, Electronics and Calibration of the Spectral Region

A schematic representation of the optical arrangement is shown in Fig. 5. The infrared radiation source S is a 600 watt General Electric FFJ quartzline projection lamp mounted in a specially prepared water-cooled brass housing [Fig. 6]. It was operated at a power of \sim 400 watts obtained from a Sorenson ACR-2000 a.c. regulator. Radiation from S was focused on the entrance window of the absorption cell by the concave mirror M_1 and the radiation from the exit window of the cell was focused on the entrance slit of the spectrometer A by another concave mirror M_2 . Both M_1 and M_2 are aluminum-front-coated spherical mirrors each with a radius of curvature of 60 cm and a diameter of 15 cm. These light cones of f/4 were maintained throughout the optical arrangement.

The spectrometer A is a Perkin-Elmer model 112 G single-beam double-pass instrument, fitted with a Bausch and Lomb plane grating (either a 300 lines/mm grating blazed at 1.2μ , or a 300 lines/mm grating blazed at 3.0μ , in the first order). The filter F is either Perkin-Elmer 203-1104 or Corning CS 7-57, for the spectral region between fundamental and first overtone bands of tH_2 , or for the region

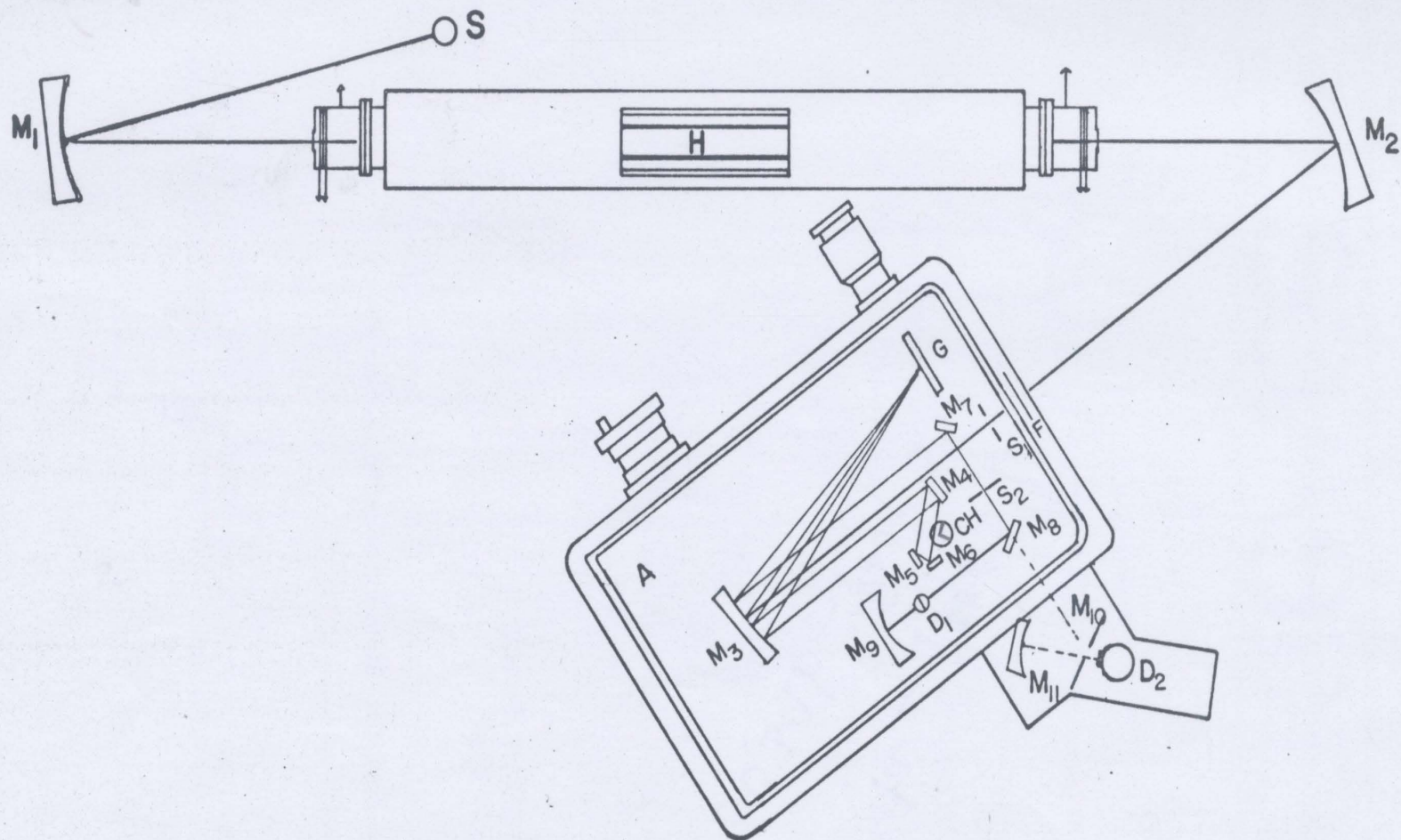


Fig. 5. Top view of the 2 m cell with the Perkin-Elmer 112 G monochromator.

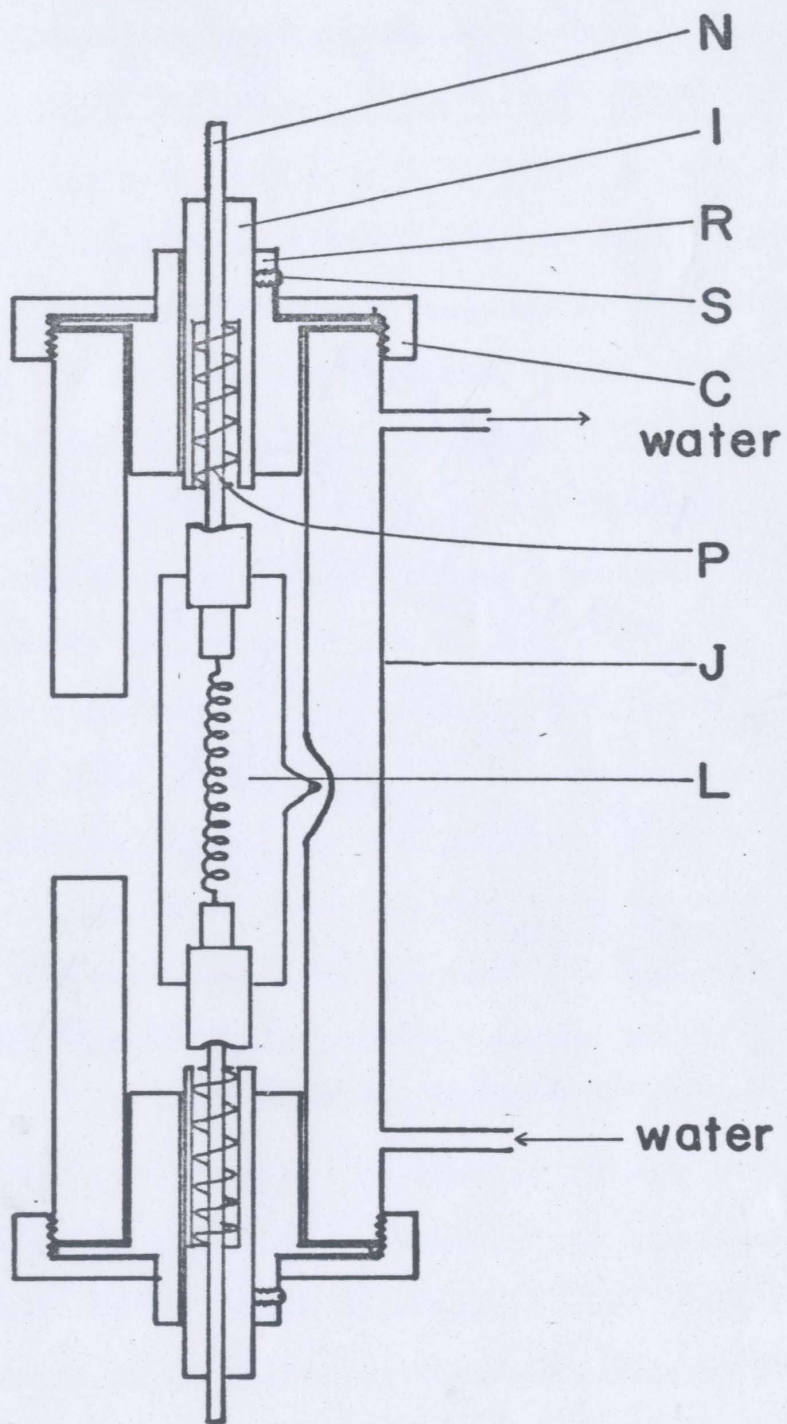


Fig. 6. Infrared continuum source with cooling jacket: L = CGE FFJ
Quartz-line projector lamp; N = connector; I = ceramic insulator;
R = retaining ring with retainer screw, S; C = brass cap; P =
retaining spring; J = brass jacket.

of the first overtone band of H_2 , respectively. The detector D is a PbS cell mounted on a ceramic or brass support which served as a heat sink and was operated at room temperature. The 13 Hz mechanical chopper CH is located such that only light which has doubly passed the grating is modulated. The resulting signal from D was first amplified by a preamplifier and then amplified and demodulated by a Perkin-Elmer 13 Hz lock-in amplifier model 107 and recorded on a Leeds and Northrup strip-chart recorder. In the present set up, the reference signal for the rectifier in the amplifier was produced by two sets of cam-operated breaker points mounted under the monochromator and actuated by rotation of the chopper shaft. In order to get optimum signal to noise ratio it was necessary to adjust the phasing of the two cams so that a bipolar square wave reference signal was obtained and the modulated signal from the detector and the reference signal from chopper were in phase in the amplifier. One of the other main causes of noise in the electronics is the dirt picked up by the breaker points. Care was taken to maintain the breaker points free from dust.

A lead sulphide detector is expected to give an optimum signal to noise ratio when the radiation signal is modulated with a chopper having much higher frequency than 13 Hz. Some experiments were therefore carried out in the present work by replacing the Perkin-Elmer 13 Hz chopper in the 112 G spectrometer (Fig. 5) with an American Time Product model L-40 400Hz tuning fork chopper which is small enough to fit in the monochromator to chop only the second pass signal. The

Perkin-Elmer model 107 amplifier was replaced by a Brower Laboratories model 131 lock-in voltmeter coupled with their model 500 frequency programmer. The reference signal was supplied by the power supply unit for the tuning fork and the phasing adjustment is a part of the lock-in voltmeter. The detector was a PbS cell operated at either room temperature or 77 K. With these modifications in the experimental set up, it was possible to obtain an optimum signal-to-noise-ratio of the PbS cell, which is close to the manufacturers' specification. Unfortunately electronics trouble developed in the model 500 frequency programmer subsequently, and it was sent back to Brower Laboratories, Ltd. for repair and most of the final experiments were therefore carried out by the original Perkin-Elmer 13 Hz chopper and model 107 amplifier.

The slit of the monochromator maintained at a width of 150μ gave an experimental spectral resolution of $\sim 7 \text{ cm}^{-1}$ at 5800 cm^{-1} and $\sim 12 \text{ cm}^{-1}$ at 8075 cm^{-1} . In specifying the spectral resolution, factors such as the rise-time of the amplifiers, the scanning speed of the grating, etc. were taken into account. It must, however, be noted that for experiments at high-pressure and low temperature the above-specified spectral resolutions could not be obtained because of the density fluctuations of the gas in the cell.

The spectral region 4700 to 9000 cm^{-1} was calibrated using mercury emission lines (Zaidel' et al., 1970), neon emission lines (Humphreys, 1953; Plyler, Blaine and Tidwell, 1955) and absorption peaks of atmospheric water vapour (Sleator and Phelps, 1925; Plyler et al., 1952). The slit width, rise-time of the amplifier, and the scanning speed of the grating were the same for both calibration and actual experiments.

2.3 Gas Handling

For the pure gas experiments, 'ultra-high pure' hydrogen from a cylinder supplied by Matheson of Canada Limited was first passed through a trap of coiled copper tubing, maintained at 77 K, and then admitted at required pressure into the absorption cell which was initially evacuated.

For each of the mixture experiments, the hydrogen gas was first admitted into the evacuated cell to obtain a particular base pressure. The perturbing gas, krypton or xenon (each of which is of research grade), from a stainless steel cylinder, also supplied by Matheson of Canada Limited, was first condensed into two stainless steel thermal compressors maintained at 77 K. These thermal compressors were used to obtain required pressures of the perturbing gases. The perturbing gas was then admitted into the cell in a few quick pulses to obtain the desired total pressure of a hydrogen - foreign-gas mixture. Thus, in a given mixture experiment, the partial density of hydrogen was kept constant and a series of pressures of the binary mixtures of hydrogen was obtained with krypton or xenon. After the required experimental traces were taken, both krypton and xenon were recovered from the mixtures with hydrogen in the absorption cell, as these gases were very expensive. This was done by first condensing them into the original storage cylinders immersed in liquid nitrogen and then pumping out the residual hydrogen gas slowly through a two-stage stainless steel trap. This trap was necessary to arrest the flow of powdery solid krypton or xenon with hydrogen. Gas pressures were measured using Bourdon-type pressure gauges

calibrated against an Ashcroft dead weight tester.

2.4 Isothermal Data

Densities of hydrogen at room temperature and liquid nitrogen temperature for pressures up to 350 atm were obtained directly from the isothermal data given by Dean (1961) and Goodwin et al. (1963). The densities of hydrogen for pressures above 350 atm were obtained by the method of extrapolation.

The isothermal data of krypton and xenon at 298 K were obtained directly from Trappeniers, Wassenaar, and Wolkers (1966), and Michels, Wassenaar, and Louwerse (1954), respectively. The partial density, ρ_b , of the foreign gas in a binary gas mixture was determined using an interpolation formula (see, for example, Chang, 1971).

2.5 Measurement of Experimental Data

For pure hydrogen absorption experiments, the absorption coefficient $\alpha(v)$ at a given wave-number v (in cm^{-1}) with the absorption cell of sample path length ℓ containing hydrogen at a density ρ_a is defined as

$$I(v) = I_0(v) \exp[-\alpha(v)\ell] ,$$

or

$$\alpha(v) = (1/\ell) \ln [I_0(v)/I(v)] ,$$

where $I_0(v)$ is the intensity transmitted by the evacuated cell and $I(v)$ is the intensity transmitted by the cell with the gas. For the

mixture experiments, the enhancement in the absorption coefficient per unit path length $\alpha_{en}(v)$ at a given wave number v (in cm^{-1}) when a perturbing gas at a partial density ρ_b is added into the absorption cell of sample path length ℓ containing hydrogen at a fixed base density ρ_a is given by

$$I_2(v) = I_1(v) \exp[-\alpha_{en}(v)\ell],$$

or

$$\alpha_{en}(v) = (1/\ell) \ln[I_1(v)/I_2(v)],$$

where $I_1(v)$ is the intensity transmitted by the cell with only hydrogen in the cell and $I_2(v)$ is the intensity transmitted by the binary mixture in the cell. The recorder pen deflection for infinite absorption, i.e., for zero radiation entering the spectrometer, was checked several times during an experiment. The recorder traces were reduced with the help of a standard logarithmic scale by measuring $\log_{10}[I_0(v)/I(v)]$ in the pure gas experiments, and $\log_{10}[I_1(v)/I_2(v)]$ in the mixture experiments, at intervals of 10 cm^{-1} for regions with narrow peaks or sharp dips and 20 cm^{-1} for the rest of the regions. The integrated absorption coefficients per unit path length $\int \alpha(v) dv$ and $\int \alpha_{en}(v) dv (\text{cm}^{-2})$ were obtained from the areas under the absorption profiles. The integrated absorption coefficient may be expanded in terms of density and we have for the pure gas

$$\int \alpha(v) dv = \alpha_1 a \rho_a^2 + \alpha_2 a \rho_a^3 + \dots,$$

and for binary mixture

$$\int \alpha_{en}(v) dv = \alpha_{1b}^2 a^{\rho_b} + \alpha_{2b}^2 a^{\rho_b} + \dots ,$$

In the low density approximation when only binary collisions are important

$$\int \alpha(v) dv = \alpha_1^2 a^{\rho_a} ,$$

and

$$\int \alpha_{en}(v) dv = \alpha_{1b}^2 a^{\rho_b} .$$

CHAPTER 3

Collision-Induced Vibration-Rotation

U transitions ($\Delta J = \pm 4$) in Hydrogen

Van Kranendonk's interpretation of collision-induced dipole moments as arising from two mechanisms; a short range part due to electron overlap, assumed to have an exponential dependence on intermolecular separation; and a longer range part due to quadrupole-induced dipole, and thus having R^{-4} dependence, has been sufficient up to now, and has been used almost exclusively. The quadrupole induction was chosen because it represents the first non-vanishing component in a multipole moment expansion for a cylindrically symmetric homonuclear diatomic molecule. The second non-vanishing term in the expansion is the hexadecapole moment. Selection rules for dipole transitions induced by a hexadecapole moment allow $\Delta J = \pm 4$ transitions, as well as $\Delta J = 0, \pm 2$ (as occur for quadrupolar induction).

This distinction between the two shows how such induction may be observed; because $\Delta J = 4$ transitions in H_2 may occur sufficiently separated in frequency from other branches so that they may be distinguished, i.e. the $\Delta J = 0, \pm 2$ hexadecapolar induced transitions would not be easily separated from the quadrupolar induced transitions which occur at the same frequencies and with much greater intensities.

Other mechanisms may make possible transitions with $\Delta J = \pm 4$ [see Gibbs, et al. (1974)], but in the traditional spirit of the use of multipolar expansions and because of the particular motivation it has given

this work, throughout this thesis these U transitions will be arbitrarily termed hexadecapolar-induced. Perhaps this use of a particular model may need to be extended when further theoretical developments occur. For the reason given above, and other obvious reasons, hydrogen gives the best chance for observing U transitions. Furthermore, because the transitions are expected to be weak, it was assumed that long path lengths and high gas densities would be needed. Doing the experiment at 77 K gives a gas density \sim 4 times that at room temperature and the same pressure. Other reasons favour a low temperature experiment even more - simplification of interpretation of the spectra by restricting rotational populations to $J = 0$ and 1 helps considerably, as does narrowing of lines and consequent reduction in overlap of branches of different kinds of induction.

Krypton and xenon were chosen as perturbers in mixture experiments, even though their use precludes 77 K temperature, because of their large polarizabilities and consequently expected larger induction.

The experimental apparatus described in the previous chapter was used to study the U transitions in the fundamental collision-induced infrared absorption band of hydrogen in pure H₂ at 77 K and in H₂ - Kr and H₂ - Xe mixtures at 298 K. The experimental conditions under which the spectra were obtained are summarized in Table I.

TABLE I

Summary of experimental conditions

Experiment*	Temperature (K)	Sample path length of the cell (cm)	Maximum density (amagat)	Number of densities
pure H ₂	77	194.4	700	11
H ₂ - Xe	298	195.2	300	4

*The H₂-Kr mixture experiment shows an indication of U(1) absorption.

3.1 Normal Hydrogen at 77 K

(a) Absorption Profiles

A typical spectrum of normal H₂ at a density of 637 amagat at 77 K in the spectral region 5425 - 7300 cm⁻¹ obtained with the 2 m cell is shown in Fig. 7. A characteristic peak around 5750 cm⁻¹ corresponding to the U transitions ($\Delta J = 4$) has been observed. A very interesting feature of the spectrum in this figure in the region 6100 to 7300 cm⁻¹ is that more radiation with several peaks reaches the detector in the spectrometer with the absorption cell filled with compressed hydrogen than with the evacuated cell. It was found that the amount of radiation increases with increasing gas density in the cell. We suggest that this increase in the radiation is possibly due to (i) the decrease in the reflection losses at the windows of the cell, which is more or less constant throughout the spectral region of interest here for a given density

of the gas and (ii) several emission peaks which are superimposed on the constant radiation in (i) (for details, see Chapter 5). The rest of this chapter is devoted to the presentation of the results of the U transitions.

Sample absorption profiles of normal hydrogen for gas densities 696, 637 and 454 amagat at 77 K in the spectral region 5425 to 6200 cm^{-1} are shown in Fig. 8. In Fig. 8, the positions of the transitions $U_1(1)$, $U_0(1) + Q_1(1)$ and $U_0(1) + Q_1(0)$, calculated from the constants of the free molecule (Foltz et al., 1966) are marked on the wave number axis. The peak corresponding to the $U(1)$ transitions is evident. At 77 K almost all the H_2 molecules exist in the lowest rotational states $J = 0$ and 1 and only a very small fraction ($\sim 0.1\%$) of the molecules exist in the state $J = 2$. For the first few lowest density experiments, the profiles on the recorder chart also reveal two evident absorption peaks ~ 5080 and $\sim 5300 \text{ cm}^{-1}$ (not shown in Fig. 8); the intensities were difficult to measure as the absorptions in this region were close to infinity. The first of these falls between the calculated positions of the double transitions $S_0(0) + S(1)$ (5067.3 cm^{-1}) and $S_0(1) + S_1(0)$ (5084.8 cm^{-1}) and the second corresponds to the transition $S_0(1) + S_1(1)$, whose calculated wave number is 5299.9 cm^{-1} . The occurrence of these 2 S double transitions due to the anisotropy of the polarizability of the hydrogen molecule was first observed in the pure rotational region by Kiss and Welsh (1959), and was also observed in the fundamental band by Watanabe and Welsh (1965);

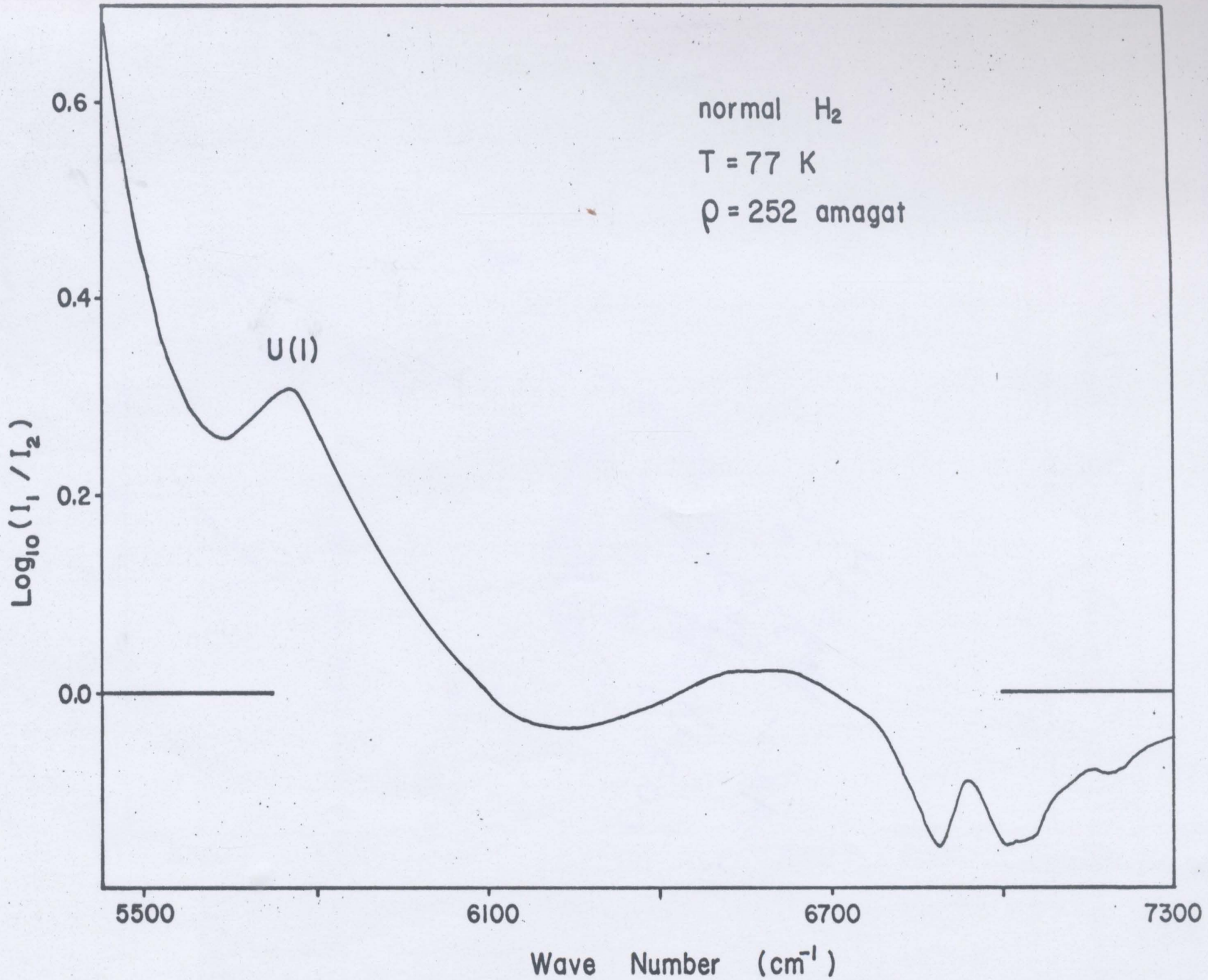


Fig. 7. Typical profile obtained at the high wave number wing of fundamental band of H₂.

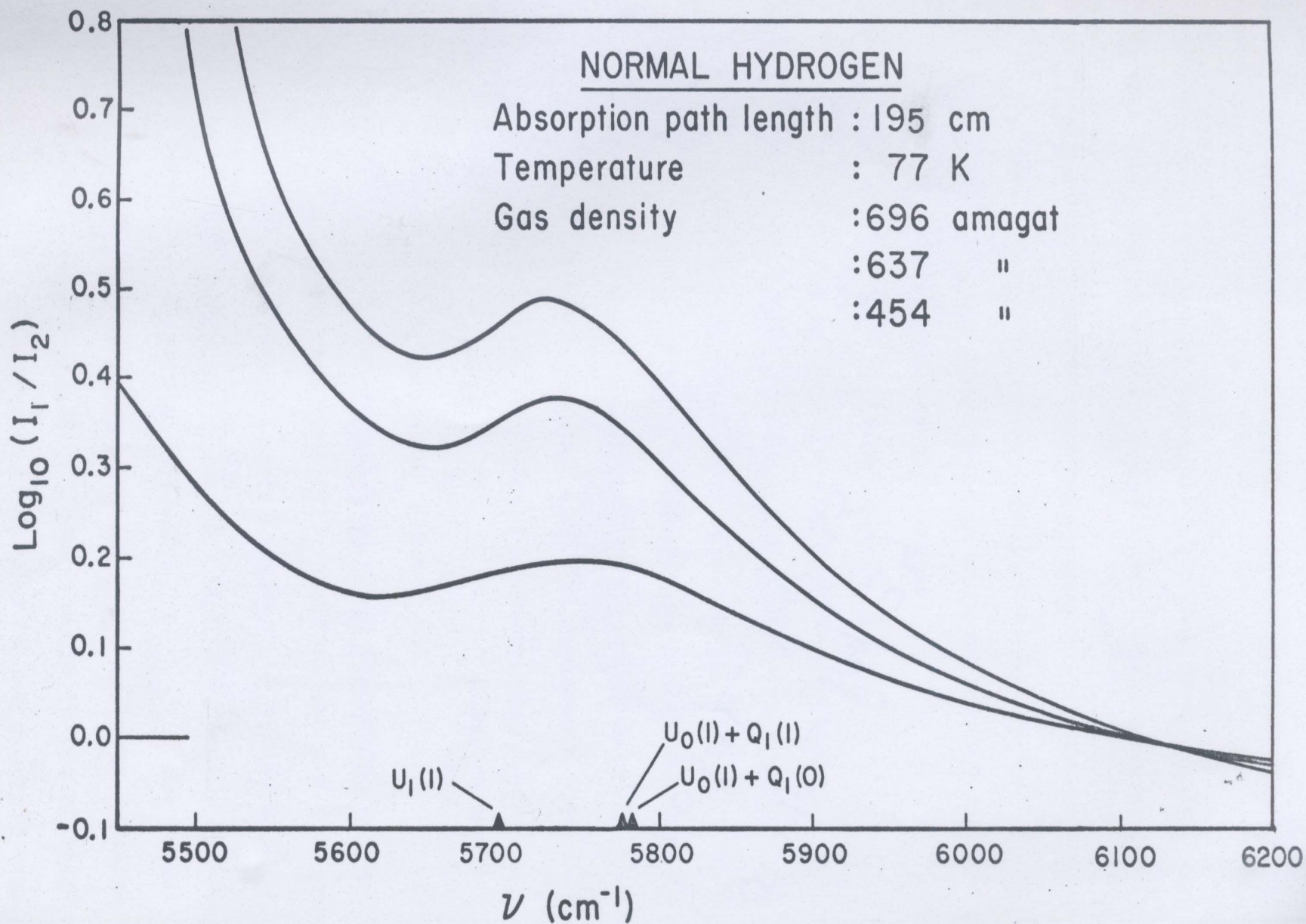


Fig. 8. Profiles of the high wave number wings of H_2 and the $U(1)$ peak.

1967).

(b) Profile Analysis: Separation of the quadrupolar transitions from the observed absorption profiles

The entire collision-induced fundamental band of hydrogen with experimental conditions used in the present work consists of the following three types of transitions:

1. Overlap Q transitions,
2. Quadrupole single and double transitions,
3. Hexadecapole single and double transitions.

In order to obtain the absorption of the hexadecapole transitions, it is necessary to subtract the absorption contribution of the transitions 1 and 2 from the observed profiles. The transitions which contribute to the intensity of the fundamental band of H_2 at 77 K and their relative positions on a wave number scale are shown in Fig. 9.

According to Van Kranendonk (1958), the Q branch intensity of a collision-induced fundamental band comes from both the overlap and quadrupolar induction effects. Therefore the two main overlap components that contribute to the intensity of the fundamental band of H_2 at 77 K are $Q_1^{\text{overlap}(0)}$ (4161.1 cm^{-1}) and $Q_1^{\text{overlap}(1)}$ (4155.2 cm^{-1}). The overlap half-width, δ_{overlap} , for normal hydrogen at 77 K was estimated to be 192 cm^{-1} by Watanabe and Welsh (1967: Table II). The intensity contribution of these overlap components to the absorption of the band in the spectral region above 5500 cm^{-1} in the present experiments is considered small and varying

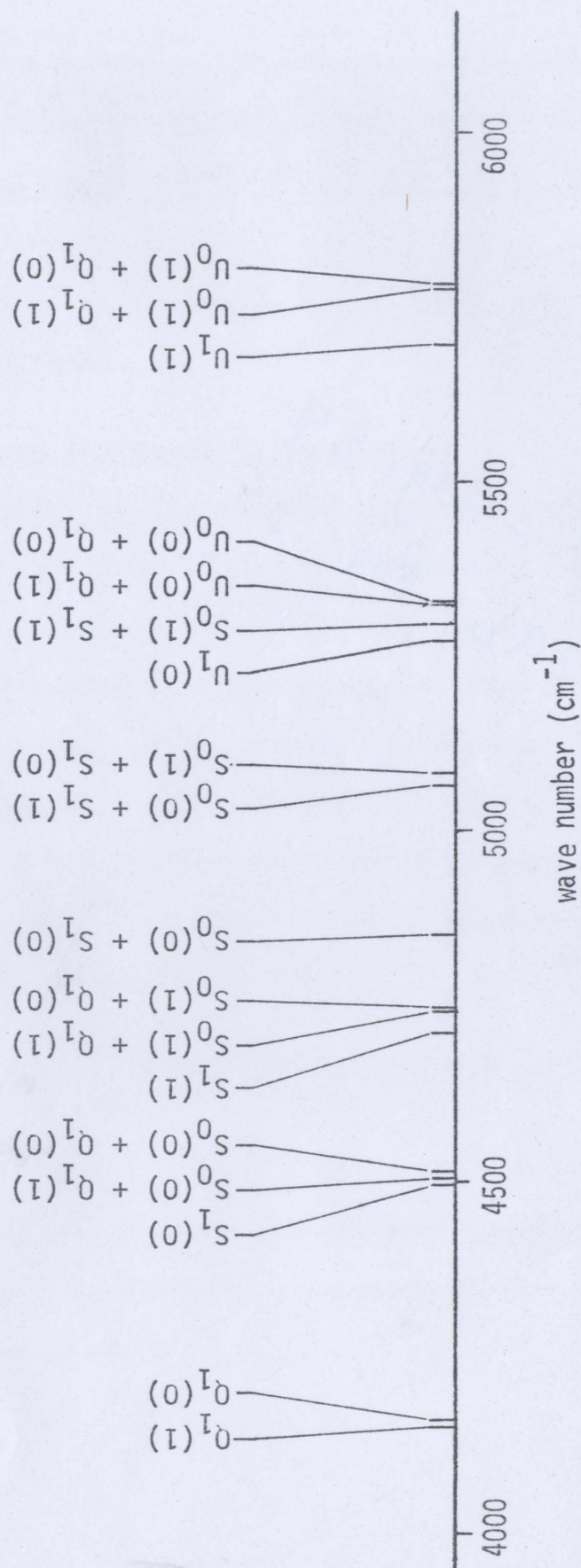


Fig. 9. Transitions in the collision-induced fundamental band of H₂ at 77 K.

slowly enough to be approximated as constant. On the basis of this, it is quite reasonable to obtain the intensity of the hexadecapolar transitions by subtracting the intensity contribution of the quadrupolar transitions from the observed absorption profiles in the region $5425 - 6075 \text{ cm}^{-1}$ by the method of profile analysis discussed in the following paragraphs.

i) Frequency Structure and Relative Intensities

The wave numbers of the transitions involving the initial rotational states $J = 0$ and 1 of the fundamental band of H_2 calculated by Foltz, Wiggins and Rank (1966), are given in Table II. Also included in this table, for the purpose of comparison, are transitions with the initial rotational state $J = 2$, even though their contribution to the intensity of the band is negligible (see below).

According to Poll (1970), the quadrupolar induction part of the integrated binary absorption coefficient of a band may be written as (see for example McKellar and Welsh, 1971)

$$\tilde{\alpha}_1^{\text{quad}} = \frac{4\pi e^2 a_0^2 N_0^2}{3\pi c} \left(\frac{a_0}{\sigma} \right)^5 J X, \quad (3-1)$$

where a_0 is the Bohr radius, $N_0 = 2.687 \times 10^{19}/\text{cm}^3$ is Loschmidt's number and σ is the Lennard-Jones range parameter. The dimensionless integral J , which is a function of the reduced temperature T^* ($= kT/\epsilon$), is given by

$$J(T^*) = 12\pi \int_0^\infty x^{-8} g_0(x) x^2 dx. \quad (3-2)$$

TABLE II

Frequencies and relative intensities of the components
of the fundamental band of H_2 at 77 K

Transition	Frequency* (cm^{-1})	Origin	Relative Intensity
$Q_1(1)$	4155.2	Overlap	—
		Quadrupolar	3.96
$Q_1(0)$	4161.1	Overlap	—
		Quadrupolar	1.22
$S_1(0)$	4497.8	Quadrupolar	8.97×10^{-2}
$S(0) S_0(0) + Q_1(1)$	4509.6	"	5.33×10^{-2}
$S_0(0) + Q_1(0)$	4515.5	"	1.59×10^{-2}
$S_1(1)$	4712.9	"	1.37×10^{-1}
$S(1) S_0(1) + Q_1(1)$	4742.3	"	9.72×10^{-2}
$S_0(1) + Q_1(0)$	4748.2	"	2.91×10^{-2}

TABLE II (continued)

	Transition	Frequency* (cm^{-1})	Origin	Relative Intensity
2S	$s_0(0) + s_1(0)$	4852.2	Quadrupolar	3.54×10^{-3}
	$s_0(0) + s_1(1)$	5067.3	"	5.73×10^{-3}
	$s_0(1) + s_1(0)$	5084.8	"	6.48×10^{-3}
	$s_0(1) + s_1(1)$	5299.9	"	1.05×10^{-2}
U(0)	$u_1(0)$	5271.6	Hexadecapolar	—
	$u_0(0) + q_1(1)$	5324.0	"	—
	$u_0(0) + q_1(0)$	5329.9	"	—
U(1)	$u_1(1)$	5696.1	"	—
	$u_0(1) + q_1(1)$	5776.9	"	—
	$u_0(1) + q_1(0)$	5782.8	"	—

TABLE II (continued)

Transition	Frequency* (cm^{-1})	Origin	Relative Intensity
<u>Transitions Involving J = 2</u>			
$Q_1(2)$	4143.4	Quadrupolar	6.86×10^{-3}
$S_0(0) + Q_1(2)$	4497.8	"	9.59×10^{-5}
$S_0(1) + Q_1(2)$	4730.4	"	1.71×10^{-4}
$S_1(2)$	4917.2	"	1.77×10^{-4}
$S_0(2) + Q_1(2)$	4957.8	"	2.68×10^{-7}
$S_0(2) + Q_1(1)$	4969.6	"	1.52×10^{-4}
$S_0(2) + Q_1(0)$	4975.5	"	6.45×10^{-7}
$S_0(0) + S_1(2)$	5271.5	"	7.90×10^{-6}
$S_0(2) + S_1(0)$	5312.2	"	2.26×10^{-5}
$S_0(1) + S_1(2)$	5504.2	"	1.63×10^{-5}
$S_0(2) + S_1(1)$	5527.3	"	1.64×10^{-5}
$S_0(2) + S_1(2)$	5731.6	"	2.26×10^{-8}

TABLE II (continued)

Transition	Frequency* (cm^{-1})	Origin	Relative Intensity
$U_0(0) + Q_1(2)$	5312.2	Hexadecapolar	—
$U_0(1) + Q_1(2)$	5765.0	"	—

*Calculated from the constants of the free molecule (Foltz *et al.*, 1966)

Its values have been tabulated by Van Kranendonk and Kiss (1959).

Here $x = R^* = R/\sigma$ is the reduced intermolecular distance and $g_0(x)$ is the low density limit of the pair distribution function of the gas. Classically, $g_0(x) = \exp(-V(x)/kT)$, where the Lennard-Jones potential $V(x) = 4\epsilon(x^{-12} - x^{-6})$ was assumed. The quantity X is given by

$$\begin{aligned} X = & \sum_{J_1} P_{J_1} P_{J_2} [C(J_1 2J_1'; 00)^2 C(J_2 0J_2'; 00)^2 \langle 0J_1 | Q_1 | v_1' J_1' \rangle^2 \langle 0J_2 | \sigma_2 | v_2' J_2' \rangle^2 \\ & + C(J_2 2J_2'; 00)^2 C(J_1 0J_1'; 00)^2 \langle 0J_2 | Q_2 | v_2' J_2' \rangle^2 \langle 0J_1 | \alpha_1 | v_1' J_1' \rangle^2 \\ & + Y] , \end{aligned} \quad (3 - 3)$$

where

$$\begin{aligned} Y = & C(J_1 2J_1'; 00)^2 C(J_2 2J_2'; 00)^2 \left[\frac{2}{9} (\langle 0J_1 | Q_1 | v_1' J_1' \rangle^2 \langle 0J_2 | \gamma_2 | v_2' J_2' \rangle^2 \right. \\ & + \langle 0J_2 | Q_2 | v_2' J_2' \rangle^2 \langle 0J_1 | \gamma_1 | v_1' J_1' \rangle^2 - \frac{4}{15} \langle 0J_1 | Q_1 | v_1' J_1' \rangle \langle 0J_2 | Q_2 | v_2' J_2' \rangle \\ & \left. + \langle 0J_1 | \gamma_1 | v_1' J_1' \rangle \langle 0J_2 | \gamma_2 | v_2' J_2' \rangle \right] . \end{aligned} \quad (3 - 4)$$

Here the subscripts 1 and 2 refer to the colliding molecules and vJ and $v'J'$ are the lower and upper vibrational and rotational quantum numbers. The Boltzmann factor $P_J (= (2J + 1)P(J))$ is defined so that $\sum P_J = 1$. [Note: $P(J) = [g_T \exp(-\beta E_J)] / \sum_J g_T (2J + 1) \exp(-\beta E_J)$, g_T being 1 and 3 for the even and odd rotational states, respectively, of H_2]. The quantities $C(JnJ'; 00)$ are Clebsch-Gordon coefficients, and $\langle vJ | Q | v'J' \rangle$, $\langle vJ | \alpha | v'J' \rangle$ and $\langle vJ | \gamma | v'J' \rangle$ are quadrupole moment, polarizability and anisotropy of the polarizability matrix elements, respectively. The Y term containing

γ is small compared to X_2 and produces double rotational transitions of the type $S(J_1) + S(J_2)$. In the calculation of the relative intensities of these transitions, the matrix elements $\langle 0J | Q | 1J' \rangle$, $\langle 0J | \alpha | 1J' \rangle$ and $\langle 0J | \gamma | 1J' \rangle$ of H_2 , calculated by Birnbaum and Poll (1969), Poll (1970), and Poll (private communication, 1974), respectively, have been used. The Boltzmann factors P_J used in the calculations are listed in Appendix AA. Finally the calculated relative intensities of the quadrupolar lines are included in Table II.

(ii) Quadrupolar line shape

Usually quadrupolar lines may be represented by the Boltzmann-modified dispersion line shape with power law tail (Kiss and Welsh, 1959; Mactaggart and Hunt, 1969). For the present profile analysis, this line shape is slightly modified and is represented by the following expressions.

$$\tilde{\alpha}^+(\nu) + A = (\tilde{\alpha}^0 + A) / [1 + (\Delta\nu/\delta)^2], \quad 0 \leq \Delta\nu \leq p\delta \quad (3 - 5a)$$

$$\tilde{\alpha}^+(\nu) + A = Q(\Delta\nu)^{-d}, \quad \Delta\nu > p\delta \quad (3 - 5b)$$

$$\tilde{\alpha}^-(\nu) + A = [\tilde{\alpha}^+(\nu) + A] \exp(-hc\Delta\nu/kT). \quad (3 - 5c)$$

Here, $\tilde{\alpha}(\nu)$ is the absorption coefficient with the frequency factor removed ($\alpha(\nu) = (1/\ell) \ln[I_0(\nu)/I(\nu)]$); $\tilde{\alpha}(\nu) = \alpha(\nu)/\nu$, and represents the transition probability at a wave number ν , $\Delta\nu = \nu - \nu_m$, ν_m being the molecular transition wave number, $\tilde{\alpha}^0 = \tilde{\alpha}(\nu_m)$ is

the transition probability at v_m , and $\tilde{\alpha}^-(\Delta v)$ and $\tilde{\alpha}^+(\Delta v)$ are absorption coefficients at wave numbers $v_m - \Delta v$ and $v_m + \Delta v$ in the low- and high-frequency wing, respectively. The half-width δ of the line is the value Δv on the high wave number side for which the transition probability is $\frac{1}{2} \tilde{\alpha}^0$. The quantity Q is determined by matching the intensities $\tilde{\alpha}^+$ in Eqs. (3 - 5a) and (3 - 5b) at the wave number $v + p\delta$. A negative constant "A" is introduced in Eqs. (3 - 5) in order to take into consideration the decrease in the reflection losses at the windows of the cell, filled with a gas. The values $p = 2.00$ and $\delta = 70 \text{ cm}^{-1}$ from the work of Mactaggart and Hunt (1969) on the collision-induced rotational spectrum of H_2 were assumed in the present analysis. This is justified on the basis that the transitions induced by the same mechanism have the same line shape (Poll, 1960).

(iii) Analysis of the Profiles

The analysis of the absorption profiles was carried out by means of a program written for the IBM 370 computer. In the computer program, for a given set of adjustable parameters, a synthetic profile which was the sum of the component profiles of the quadrupolar transitions with their calculated relative intensities is matched for the least squares fit to the experimental profile in the specified regions of the spectrum, which in the present case are from 5450 to 5540 cm^{-1} and around 6300 cm^{-1} . (The extent of the U(1) transitions is expected to be within the region

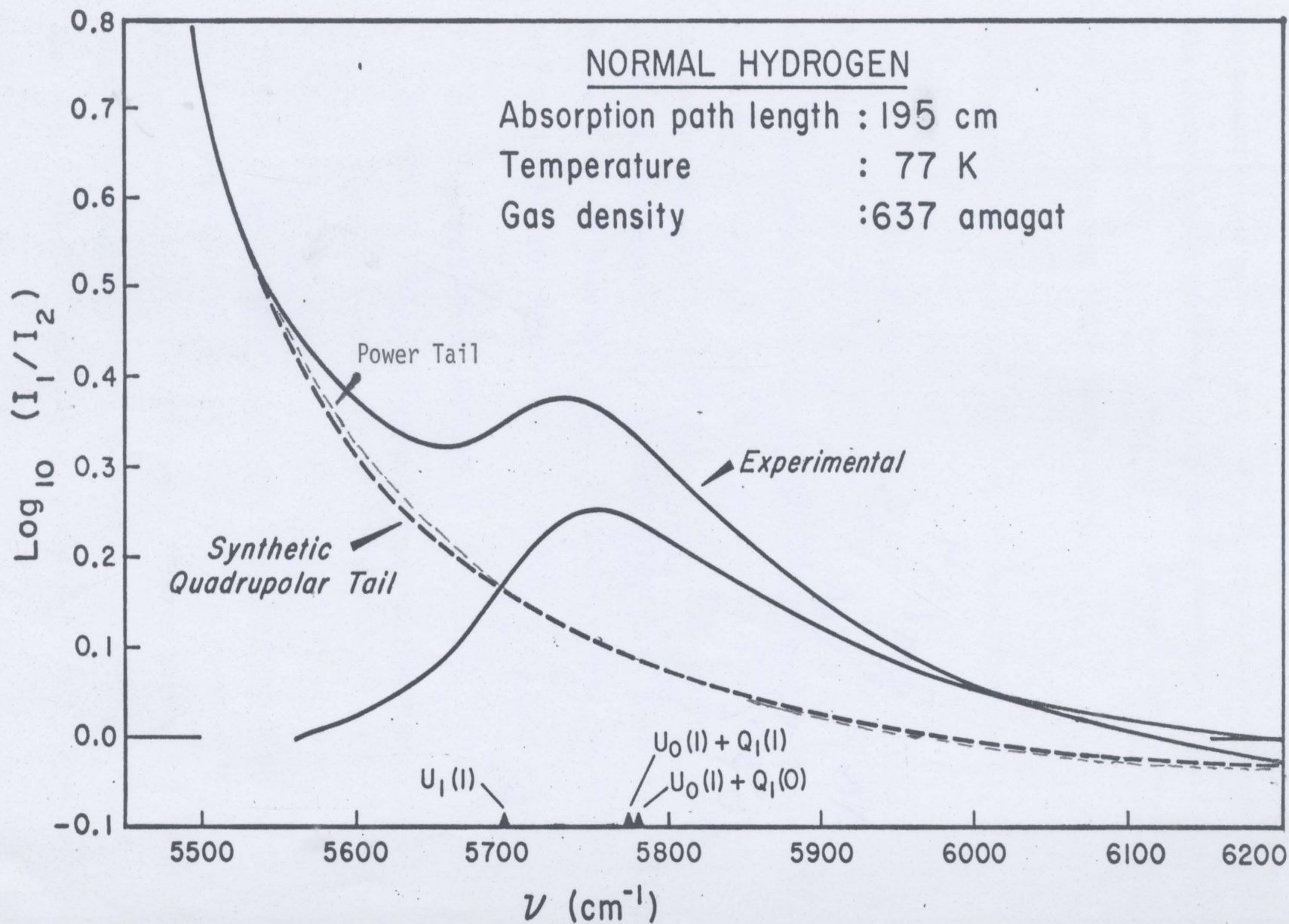
5540 to 6200 cm^{-1}).

An example of the results of the profile analysis is shown in Fig. 10. The absorption profile due to the U(1) group transitions was obtained by subtracting the synthetic quadrupolar profile from the experimental profile. The results of such subtraction is also shown in Fig. 10. In the above analysis the synthetic profile also includes the quadrupolar transitions, single as well as double, involving $J = 2$ in the initial state. As these transitions are weak (see their relative intensities in Table II) their contribution to the intensity of the band was found to be negligible.

In addition to the above method, an 'exponential tail' method was also used to separate the quadrupolar profile from the experimental profile. Following Bosomworth and Gush (1965), the high frequency wing of the quadrupolar profile may be represented by the expression.

$$\alpha(\nu) = c \exp [-\beta(\nu - \nu_0)], \quad \nu > \nu_0 + p\delta, \quad (3 - 6a)$$

where δ is the Boltzmann half-width described above and c and β are the adjusted parameters. As a matter of fact, since all the quadrupolar transitions with significant intensity occur at least several hundred wave numbers away from the U(1) group of transitions, only the 'tail' of the quadrupolar profile overlaps the latter group. A least squares fit to the regions 5450 to 5540 cm^{-1}



Fog. 10. Separation of the quadrupolar tail from the experimental profile of H_2 absorption of the fundamental band at the $U(1)$ region.

and around 6300 cm^{-1} of the profile was made with the following line form for the tail:

$$\alpha(v) + A = c \exp [-\beta(v - d)]. \quad (3 - 6b)$$

The line form given by Eq. (3 - 6b) is equivalent to

$$\ell n[\alpha(v) + A] = -\beta v + B, \quad (3 - 6c)$$

where A , β and B ($= \ell n A + d$) are adjustable parameters. Here A is again introduced to take into consideration the decrease in reflection losses at the windows of the cell filled with a gas. The synthetic exponential tail thus obtained is as good as the one obtained by the detailed method described above, and is also shown in Fig. 10 for the purpose of comparison.

(c) Derived Absorption Profiles of the U (1) Group; Binary Absorption Coefficient

Figure 11 shows the typical absorption profiles of the U (1) group transitions of normal H_2 at three different densities at 77 K. These profiles were derived by the method of profile analysis presented in Section 3.1(b). The peaks of these profiles fall at a wave number of 5750 cm^{-1} for the higher density profile, whereas the calculated wave numbers of the $U_1(1)$, $U_0(1) + Q_1(1)$, and $U_0(1) + Q_1(0)$ transitions of the free H_2 molecule are 5696.1,

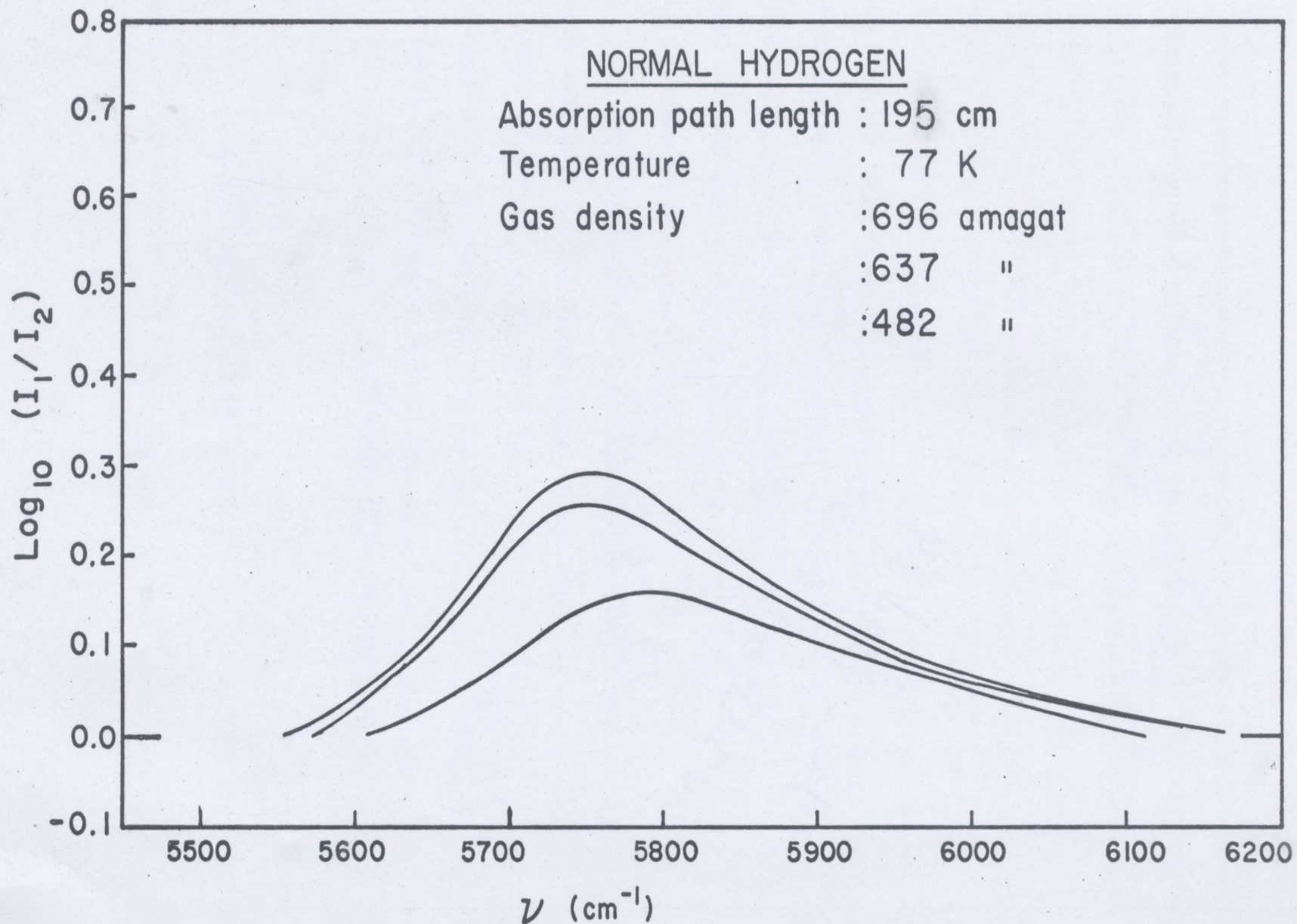


Fig. 11. The net U(1) absorption profiles of H_2 .

5776.9 and 5782.8 cm^{-1} . The half-widths of these profiles towards the high frequency side at half the peak intensity are estimated as $\sim 150 \text{ cm}^{-1}$. Since the $\Delta J = +4$ transitions are hexadecapolar in origin, the corresponding induced dipole moment varies with R^{-6} , whereas the dipole moment induced by quadrupolar induction varies with R^{-4} , and the one by overlap induction varies exponentially with R . Therefore the duration of collisions in hexadecapolar induction is shorter than that in quadrupolar induction but longer than in overlap induction. The observed half-width of the U(1) group falls between that of the quadrupole induced transitions ($\delta_{\text{quad}} = 70 \text{ cm}^{-1}$) and that of the overlap induced transitions ($\delta_{\text{overlap}} = 192 \text{ cm}^{-1}$), in agreement with expectations.

The areas under the absorption profiles of the U(1) group were measured and converted into integrated absorption coefficients $\int \tilde{\alpha}(v) dv (= \frac{1}{\lambda} \int \ln[I_o(v)/I(v)] v^{-1} dv)$. The quantities $(1/\rho^2) \int \tilde{\alpha}(v) dv$ are given for different experimental densities of hydrogen at 77 K in Table III. Usually, for an absorbing gas of density ρ_a in collision-induced absorption, the integrated absorption coefficient is given by

$$\int \tilde{\alpha}(v) dv = \tilde{\alpha}_1 \rho_a^2 + \tilde{\alpha}_2 \rho_a^2 + \dots , \quad (3 - 7)$$

where $\tilde{\alpha}_1$ is the binary absorption coefficient and $\tilde{\alpha}_2$ is the ternary

TABLE III

Integrated absorption coefficients of U(1) group

ρ (amagat)	$(1/\rho^2) \int \tilde{\alpha} dv$ (10^{-10} amagat $^{-2}$ cm $^{-1}$)
482	3.6
511	3.0
534	4.1
552	3.6
566	4.0
603	2.9
637	3.4
648	3.7
668	2.9
696	2.9
697	3.0

absorption coefficient. A plot of $(1/\rho_{H_2}^2) \int \tilde{\alpha}(\nu) d\nu$ against ρ_{H_2} is shown in Fig. 12. The points in the graph are somewhat scattered and it was not possible to obtain a value of the ternary absorption coefficient. The binary absorption coefficient is obtained from the average values of the integrated absorption coefficients using the expression $\tilde{\alpha}_1 = (1/\rho_{H_2}^2) \int \tilde{\alpha}(\nu) d\nu$. The quantity thus obtained is

$$\tilde{\alpha}_1[U_1(1), U_0(1) + Q_1(1), U_0(1) + Q_1(0)] = (3.38 \pm 0.04) \times 10^{-10} \text{ cm}^{-1} \text{ amagat}^{-2}.$$

3.2 Binary Mixtures of H₂ - Xe at 298 K

Usually the collision-induced spectrum of enhancement of absorption of a binary mixture of a symmetric diatomic gas with a monatomic foreign gas is considerably simpler than the corresponding spectrum of the pure gas because the former spectrum contains primarily single transitions. In the present work, it was considered worthwhile to investigate the collision-induced spectrum of H₂ in the U₁(1) region in the binary mixtures of hydrogen and xenon at room temperature. Xenon was chosen principally because of its high polarizability ($\alpha_{Xe} = 27.4 a_0^3$). Unfortunately, the impurity in the xenon gas just happened to have absorption with two peaks coinciding with the U₁(1) position. The profile of the impurity absorption was obtained from an experiment with xenon gas alone at a density roughly equal to the partial density of xenon in the H₂ - Xe experiment. The contribution from the impurity is more than half of the total intensity and was subtracted from the H₂ - Xe profile.

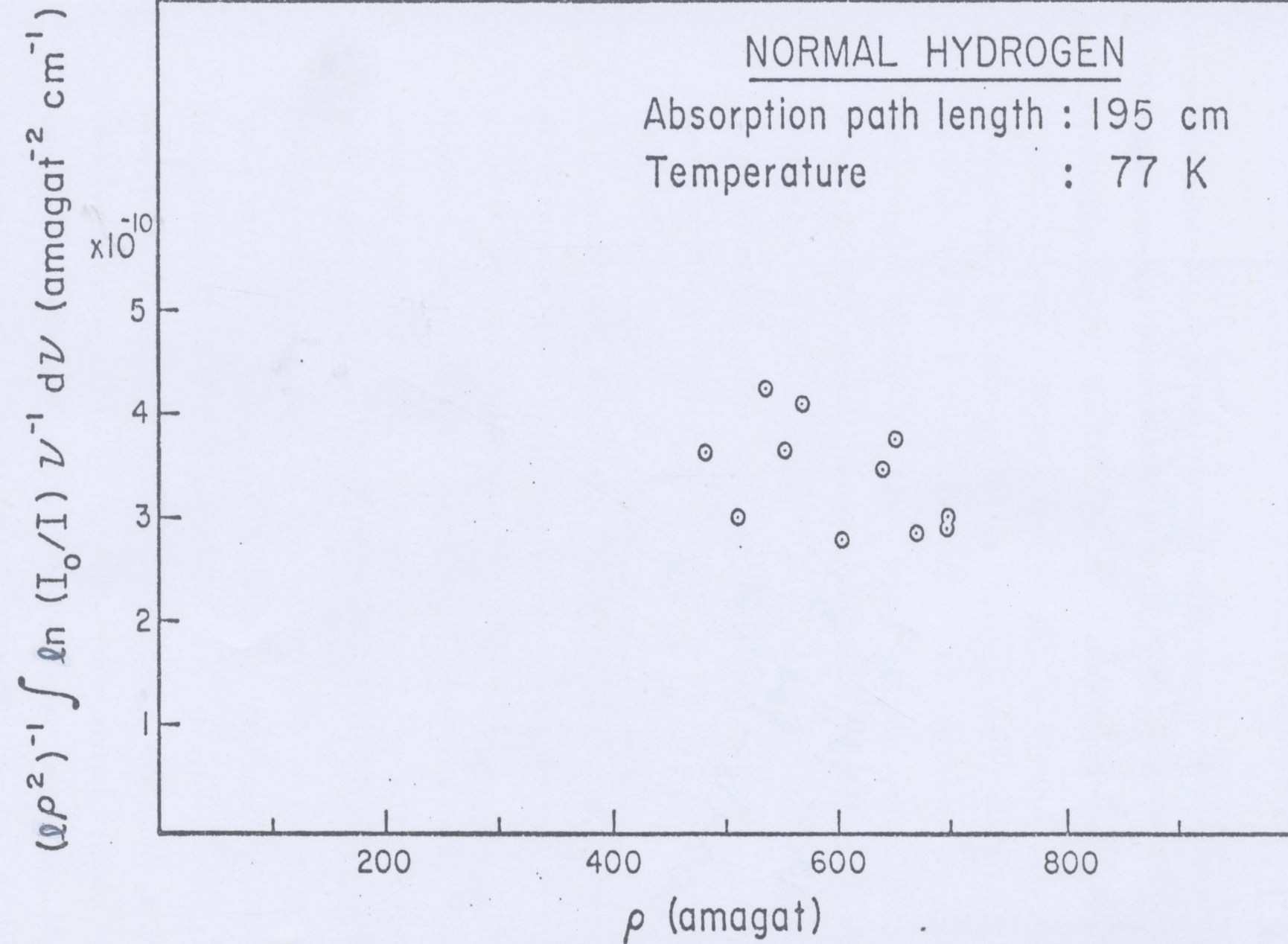


Fig. 12. The relation between integrated absorption coefficients per unit path length of the U(1) group transitions and density of H₂.

The same radiation problem mentioned earlier in the pure H_2 experiment at 77 K also occurs here. A uniform intensity corresponding to 'A' in Eqs. (3 - 5) is added through out the region. Figure 13 shows a typical profile of enhancement of absorption thus obtained in the $U(1)$ region of the fundamental band of H_2 in H_2 - Xe at 298 K. For the given profile the base density of H_2 is 31.1 amagat and the partial density of xenon is 275 amagat. To obtain profiles of enhancement of absorption the contribution of H_2 - H_2 collisions to the intensity of the band was subtracted from the recorder traces. A peak corresponding to the $U_1(1)$ transition is clearly seen around 5700 cm^{-1} .

The derived enhancement profiles of H_2 - Xe are somewhat in error because the correction applied for the impurity in the xenon gas does not take into account the effect of H_2 gas on the impurity. Moreover, the absorption intensity is not strong enough to make accurate measurements. The experiments could not be carried out at much higher densities of xenon because of its limited supply. A profile for the S wing in the region 5550 to 5900 cm^{-1} is also shown in Fig. 13. The profile of the $U_1(1)$ transitions obtained by subtracting the S wing profile from the experimental profile is also shown in the same figure. By measuring the areas of four such derived profiles of the $U_1(1)$ transition and neglecting the contribution of the ternary and higher order collisions, the approximate value of the binary absorption coefficient for H_2 - Xe mixtures

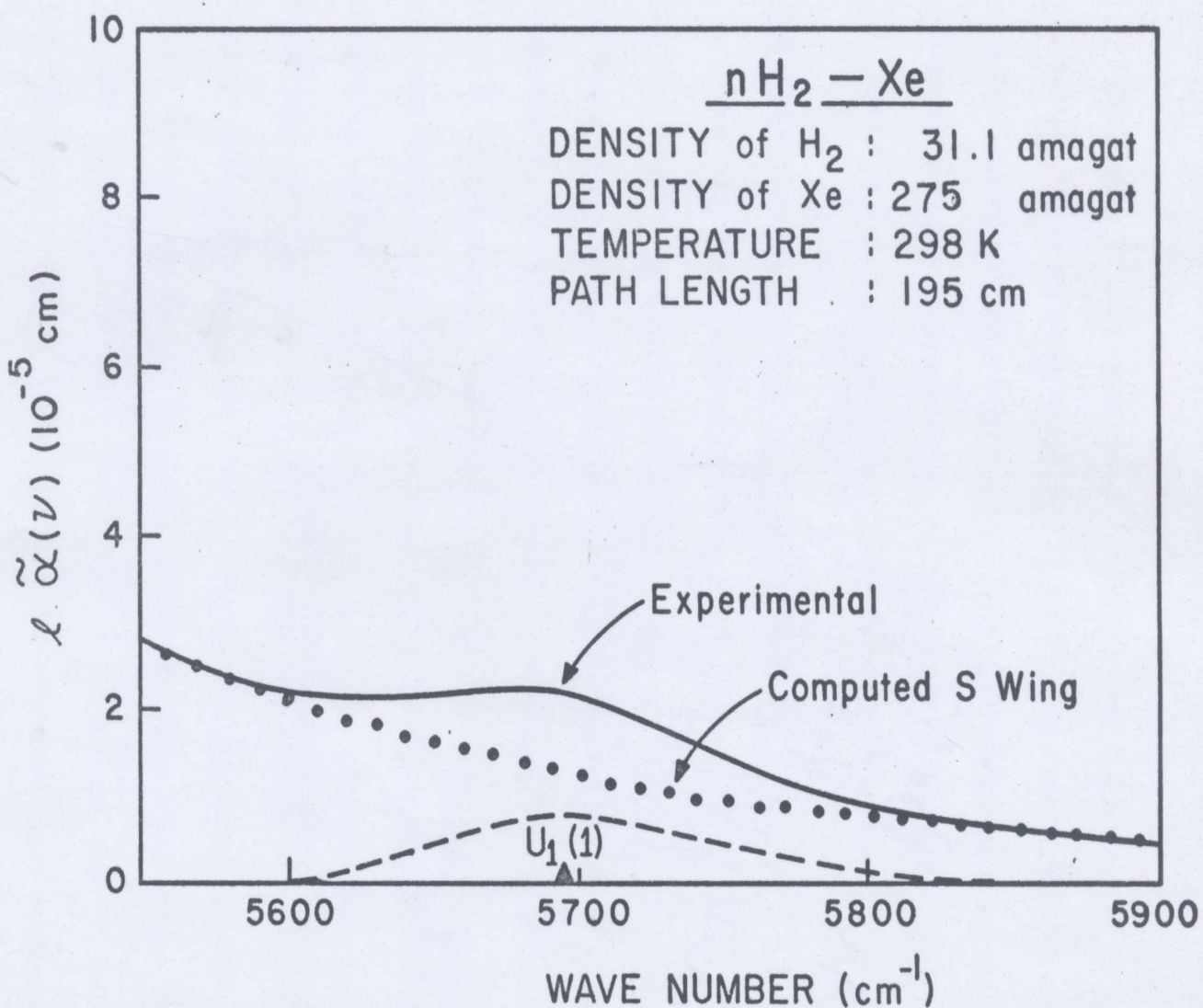


Fig. 13. Separation of the quadrupolar S wing from the experimental profile of the enhancement of $U(1)$ absorption of H_2 by Xe.

is obtained as

$$\tilde{\alpha}_1 (U_1(1)) \approx 9.7 \times 10^{-10} \text{ cm}^{-1} \text{ amagat}^{-2}.$$

Experimental evidence of U (1) transitions was also obtained in binary mixtures of hydrogen with krypton but the amount of absorption was less than that in H₂ - Xe mixtures. As the accuracy of the measurements of absorption in this case was low, the absorption profiles are not presented here.

3.3 Hexadecapole Moment Matrix Elements of H₂

The principal mechanism for the occurrence of the U transitions in the collision-induced infrared spectrum of H₂ is considered to be the hexadecapolar induction. The "level-mixing" mechanism (Van Kranendonk, 1957; Herman 1970) may contribute some small intensity to the U transitions, but no theoretical calculations in this respect are available. Triple collisions may also contribute to the intensity of absorption in the U region. In the calculations presented in the following paragraphs, we assume that experimental binary coefficient of the U(1) group transitions arises from the binary hexadecapolar induction mechanism. (see also Gibbs *et al.*, 1974).

The integrated binary absorption coefficient due to hexadecapolar induction for a given band may be expressed as (see Appendix B)

$$\tilde{\alpha}_1 (\text{hexadecapolar}) = \frac{20\pi}{9} \frac{e^2}{h} \frac{a_0^2}{c} N_0^2 \left(\frac{a_0}{\sigma} \right)^9 J_{12} X_4, \quad (3 - 8)$$

where

$$J_{12} = 12\pi \int_0^\infty x^{12} g_o(x) x^2 dx , \\ = \pi y^{-4} H_{12}(y) . \quad (3 - 9)$$

The dimensionless integral J could be obtained from the values of $H_{12}(y)$ listed by Buckingham and Pople (1955). The quantity X_4 is given by

$$X_4 = \sum P_{J_1} P_{J_2} [C(J_1 4 J_1'; 00)^2 C(J_2 0 J_2'; 00)^2 \\ x \langle 0 J_1 | H_1 | v_1' J_1' \rangle^2 \langle 0 J_2 | \alpha_2 | v_2' J_2' \rangle^2 \\ + C(J_2 4 J_2'; 00)^2 C(J_1 0 J_1'; 00)^2 \langle 0 J_2 | H_2 | 2 \\ x \langle 0 J_1 | \alpha_1 | v_1' J_1' \rangle^2 \\ + Y_4] . \quad (3 - 10)$$

Here the subscripts 1 and 2 and the quantities $x, \sigma, N_o, a_o, y, C(J n J' 1; 00)$ and $\langle v J | \alpha | v' J' \rangle$ are the same as those occurring in eq. (3 - 3) and $\langle v J | H | v' J' \rangle$ is a hexadecapole moment matrix element.

(i) From the binary absorption coefficient of $H_2 - Xe$ at 298 K

On substitution of the appropriate values for the quantities in Eq. (3 - 8), we have the value of the experimental binary absorption coefficient for the $U_1(1)$ transition in $H_2 - Xe$ equal to $386 \times 10^{-10} \langle 0 | H | 1 \rangle^2$, i.e., $\langle 0 | H | 1 \rangle \sim 0.15 ea_o^4$.

This value of $\langle 0|H|1\rangle$ is considered somewhat high. The reason for this is partly due to the uncertainty in the value of the binary absorption coefficient because of the difficulties mentioned above, and partly due to the intensity contribution to the U region by the double transitions of the type $U_0(1) + Q_1(J)$ which would arise from the triple collisions of the type $H_2 - H_2-Xe$ (see Chapter 4).

(ii) From the binary absorption coefficient of pure H_2 at 77 K

The value of experimental binary absorption coefficient of the $U(1)$ group transitions in pure H_2 at 77 K when substituted in Eq. (3 - 8) gives

$$3.4 \times 10^{-10} \text{ cm}^{-1} \text{ amagat}^{-2} = 6.46 \times 10^{-10} [28.9 \langle 0|H|0\rangle^2 + 29.4 \langle 0|H|1\rangle^2]$$

To estimate $\langle 0|H|0\rangle$ from this expression, we must have the value of $\langle 0|H|1\rangle$. Unfortunately, as mentioned above we could not obtain a reliable value of $\langle 0|H|1\rangle$ from the $H_2 - Xe$ experiments. Now we take advantage of the recent theoretical work of Karl, Obryk and Poll (1973) whose calculations show that $\langle 0|H|1\rangle \sim \frac{1}{3} \langle 0|H|0\rangle$. On substitution of this relation in Eq. (3 - 10) we obtain $\langle 0|H|0\rangle \approx 0.13 e a_0^4$. This value is in close agreement with the theoretical value ($\approx 0.10 e a_0^4$) obtained by Karl et al. (1973).

CHAPTER 4

Collision-Induced First Overtone Spectra of H₂ in H₂ - Kr and H₂-Xe Mixtures at Room Temperature

In Chapter 1, work done previously on the collision-induced first overtone band of H₂ in pure H₂ and in binary mixtures of H₂ with Ar and N₂ at different temperatures has been briefly reviewed. In the present chapter the results of the work the author has carried out on this band in binary mixtures of H₂ with Kr and Xe at room temperature will be presented. The first overtone band was studied with a 2 m absorption cell for several base densities of gaseous H₂ in the range 20.8 to 43.5 amagat. The experimental conditions under which the profiles of the enhancement of absorption were obtained are summarized in Table IV. The experimental absorption profiles of the band and the absorption coefficients will be presented in Section 4.1. A profile analysis of the band will be given in Section 4.2. A brief discussion of the experimental results will be included in Section 4.3.

TABLE IV

Summary of experiments

Mixture	Temperature (K)	Sample path length (cm)	Maximum Density of perturbing gas (amagat)	Number of mixture densities
H ₂ - Kr	298	195.3	430	31
H ₂ - Xe	298	195.3	320	17

4.1 Experimental Results:

Sample experimental profiles of enhancement of absorption of the induced first overtone band of hydrogen obtained in H_2 - Kr and H_2 - Xe mixtures at room temperature are shown in Figs. 14 and 15, respectively. For the three profiles in Fig. 14, the base density of hydrogen is 43.5 amagat and the partial densities of krypton are 423, 325 and 232 amagat, and for those in Fig. 15, these are 20.8 amagat for H_2 , and 318, 288, and 263 amagat for xenon. It was not possible to obtain results at higher densities with available amounts of the perturbing gases and within the pressure limits of the apparatus. The positions of the single transitions $O_2(2)$, $Q_2(J)$ with $J = 1, 2$ and 3 , and $S_2(J)$ with $J = 0$ to 3 , marked on the wave number axis, were calculated from the constants of the free molecule. One striking feature of the enhancement absorption profiles is the absence of the overlap dip in the Q branch, which is rather characteristically present in the fundamental band of H_2 in H_2 - Kr and H_2 - Xe mixtures at 298 K (cf. Reddy and Lee 1968; Varghese and Reddy 1969). The single transitions $S_2(J)$ for $J = 0$ to 2 in H_2 -Xe are distinct; $S_2(3)$ for H_2 - Xe is below the zero line. (See discussion below). The Q_2 branch occurs as a single peak, although at room temperature it consists of three quadrupolar components $Q_2(J)$ with $J = 1, 2$ and 3 (the quadrupolar component $Q_2(0)$ is forbidden). On both ends of the spectrum, the high and low wave number wings, we actually get more radiation than the background. It increases with the gas density, stronger on the high wave number side and is stronger for

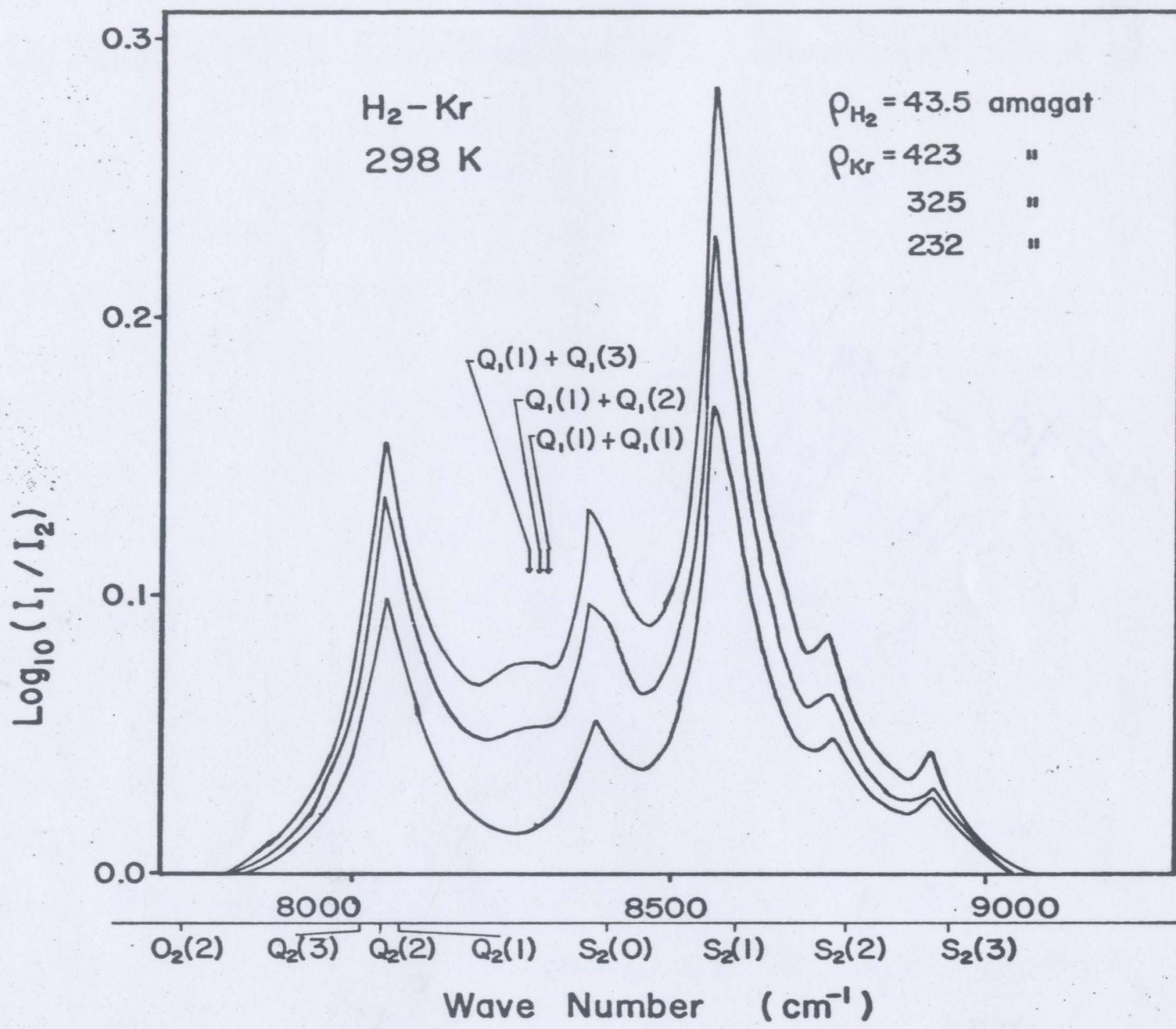


Fig. 14. Profiles of the enhancement of absorption of the first overtone band of H_2 by Kr.

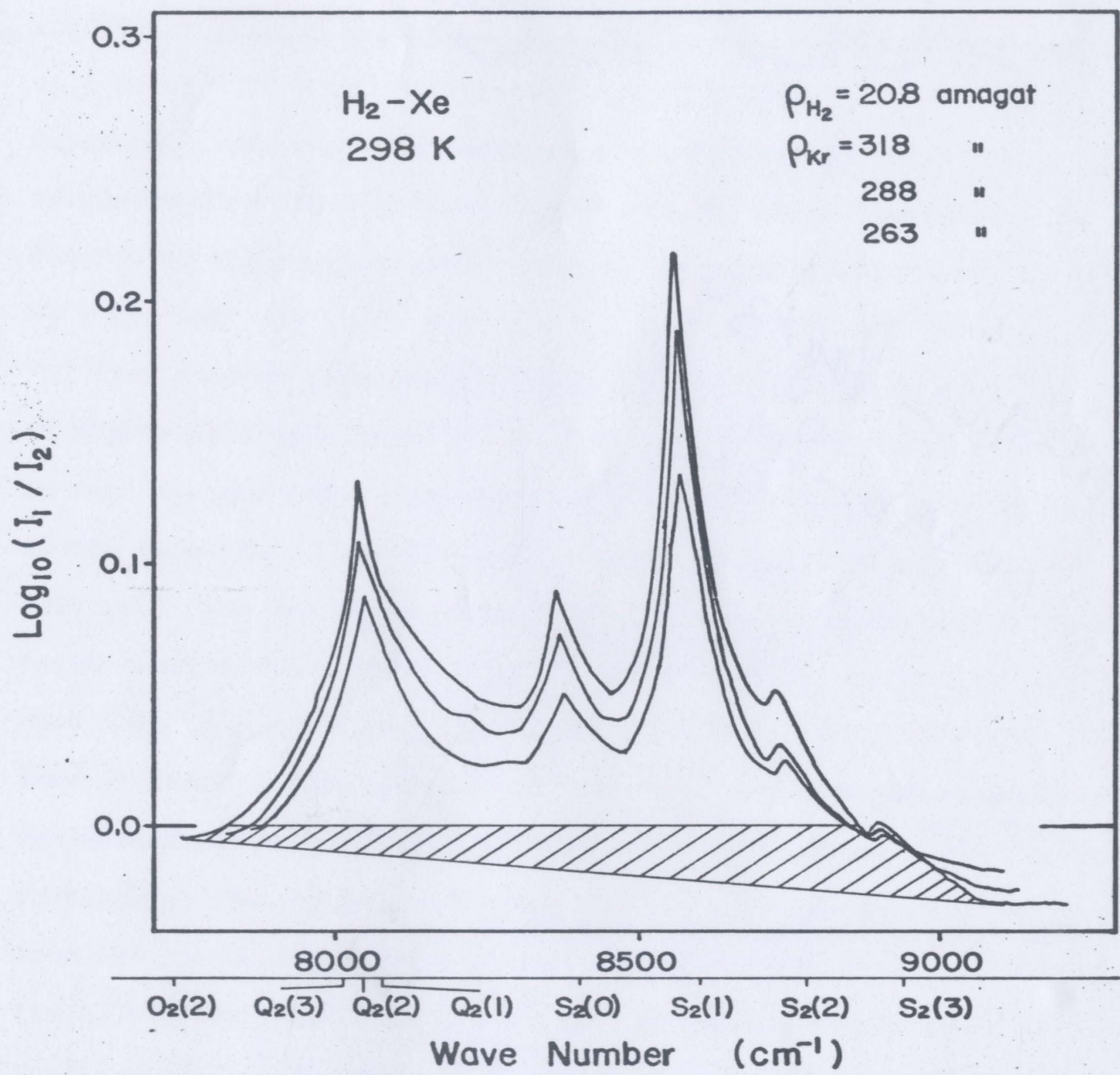


Fig. 15. Profiles of the enhancement of absorption of the first overtone of H_2 by Xe.

the H_2 - Xe mixture. This radiation was actually much stronger than what is shown here, as the amplifier gain was adjusted during the successive density experiments to assume the intensity remained constant at a point (7400 cm^{-1}) free of molecular absorption. Another important feature of the profiles is that there is considerable shift of quadrupolar lines to lower wave numbers, which increases with the density of the foreign gas. These shifts are as large as -23 cm^{-1} for H_2 - Kr and -35 cm^{-1} for H_2 - Xe (see section 4.2 below).

Yet another interesting feature of the absorption profiles is that, at higher densities both in H_2 - Kr and H_2 - Xe, double transitions in two H_2 molecules are evident, possibly arising from triple collisions of the type H_2 - H_2 - Kr or H_2 - H_2 - Xe. The absorption peak around 8250 cm^{-1} for the higher density profiles in Figs. 14 and 15 corresponds to the double transitions $Q_1(J) + Q_1(J)$ (note: $Q_1(1) + Q_1(1) : 8310.5\text{ cm}^{-1}$; $Q_1(1) + Q_1(2) : 8298.7\text{ cm}^{-1}$; $Q_1(1) + Q_1(3) : 8281.1\text{ cm}^{-1}$). Some of these double transitions are shown by the arrows. The reader is reminded that the profiles of enhancement of absorption were obtained by subtracting the intensity contribution of the base density H_2 gas from the recorder traces. It must be pointed out here that Mactaggart (1971) has observed similar but more pronounced double transitions in the profiles of the enhancement of absorption of the first overtone band of H_2 in H_2 - Ar mixtures at high total densities around 1000 amagat and was able to do a more exhaustive study of the single and double transitions. He suggested that a possible mechanism for the double transitions is the trapping of two or more H_2 molecules in a temporary cage of argon.

molecules. Because of the limited range of foreign gas densities used in the present work, it was not possible to do a thorough investigation of the double transitions.

The integrated absorption coefficient of the enhancements, $\int \alpha_{en}(v) dv = (1/\ell) \int \ln(I_1(v)/I_2(v)) dv$, for the mixtures were calculated by numerical integration of the areas under the experimental profiles. The areas under the zero line were also estimated by assuming that the amount of radiation is linearly varying with the wave number as shown in Fig. 15. The quantities $(1/\rho_a \rho_b) \int \alpha_{en}(v) dv$ are listed in Table V, with the corresponding experimental conditions, and were also plotted against ρ_b in Figs. 16 and 17. Considering the binary and ternary collisions, one can represent $\int \alpha_{en}(v) dv$ by the relation,

$$\int \alpha_{en}(v) dv = \alpha_{1b} \rho_a \rho_b + \alpha_{2b} \rho_a \rho_b^2 + \alpha'_{2a} \rho_a \rho_b^2 .$$

As also observed by Mactaggart (1971), the absorption intensity is very sensitive to the base density of the hydrogen gas. This effect can be seen in Fig. 17, in which the base densities were as much as 30% different. Under this circumstance an extrapolation to the zero density limit of ρ_b for the binary absorption coefficient without considering the $\rho_a \rho_b^2$ term would be misleading. Again experiments with smaller ρ_a , and thus necessarily greater ρ_b , were restricted by the gas supply and pressure limit of the cell.

4.2 Analysis of the Profiles of Enhancement of Absorption

In Chapter 3, equation (3 - 1) was used to calculate the relative intensities of the quadrupolar lines of the fundamental band of H₂. The same equation (cf. Poll, 1970) is valid for the overtone bands as

TABLE V

Absorption coefficients of $H_2 + Kr$ and $H_2 + Xe$

ρ_a (amagat)	ρ_b (amagat)	$\frac{1}{\rho_a \rho_b} \int \alpha(v) dv$ ($\times 10^{-5} \text{ cm}^{-2} \text{ amagat}^{-2}$)
$H_2 + Kr$		
38.9	207	5.9
	309	7.0
	330	7.2
	346	7.2
40.2	72.6	5.4
	117	5.8
	160	6.1
	208	6.2
	237	6.4
	267	6.5
	291	6.7
43.5	157	5.5
	232	6.0
	285	6.4
	325	7.0
	354	7.4
	379	7.4
	401	7.3
	423	7.1

TABLE V (continued)

ρ_a (amagat)	ρ_b (amagat)	$\frac{1}{\rho_a \rho_b} \int \alpha(v) dv$ ($\times 10^{-5}$ cm $^{-2}$ amagat $^{-2}$)
$H_2 + Kr$		
34.2	57.1	4.9
	170	5.9
	245	5.9
	319	7.3
	382	7.5
	427	6.5
42.3	56.5	7.0
	99.0	6.8
	143	6.5
	186	6.3
	218	6.2
	250	6.6
$H_2 + Xe$		
20.8	164	4.0
	243	6.1
	263	8.2
	278	9.9
	288	10
	297	11

TABLE V (continued)

ρ_a (amagat)	ρ_b (amagat)	$\frac{1}{\rho_a \rho_b} \int \alpha(v) dv$ ($\times 10^{-5}$ cm $^{-2}$ amagat $^{-2}$)
H_2 -Xe		
20.8	306	11
	312	11
	318	12
28.0	189	3.4
	243	5.8
	260	9.9
	270	12
	281	14
	290	15
	297	16
	303	16
	309	15

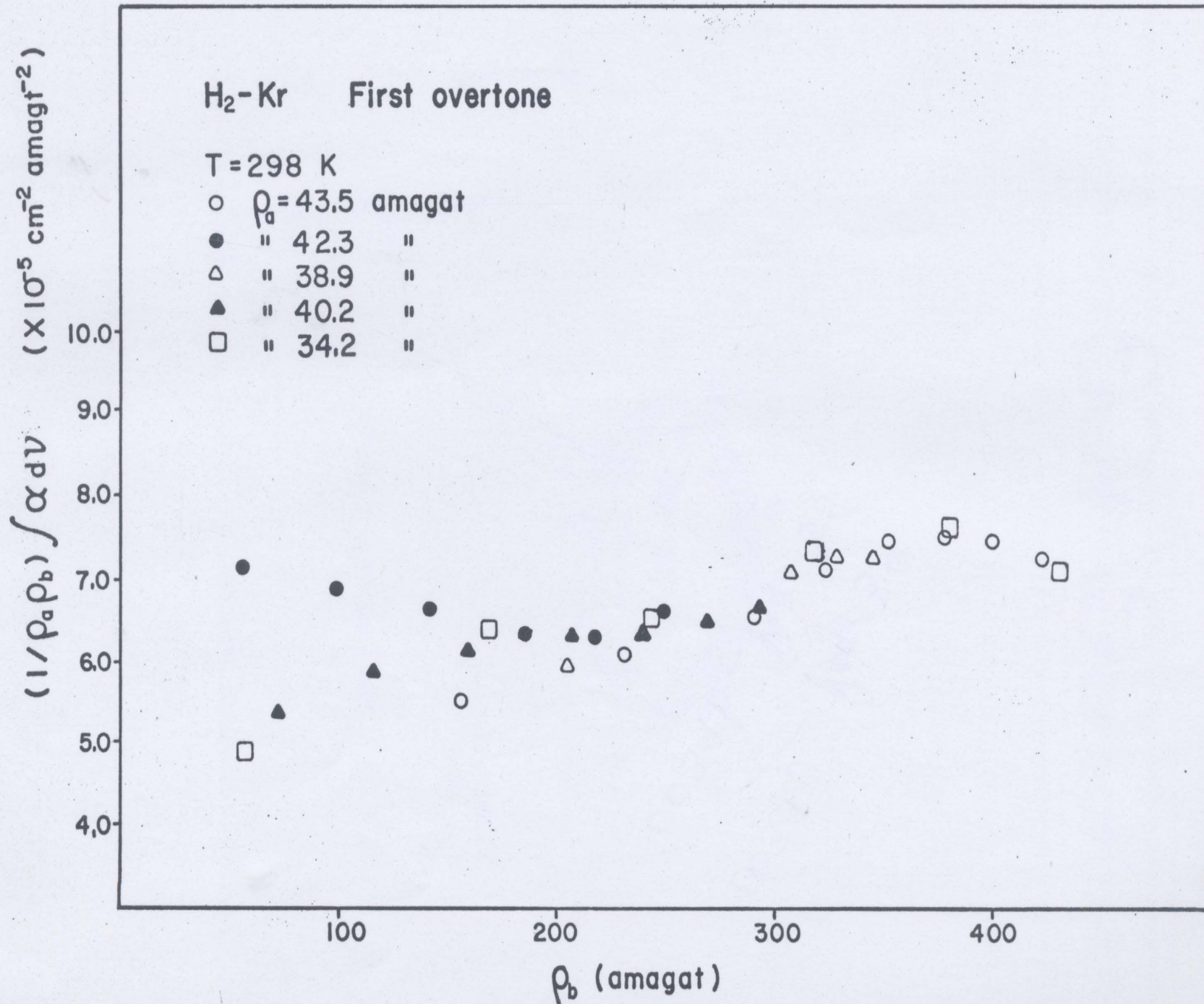


Fig. 16. The relation between the enhancements in the integrated absorption coefficients and $\rho_a \rho_b$ for H_2 - Kr.

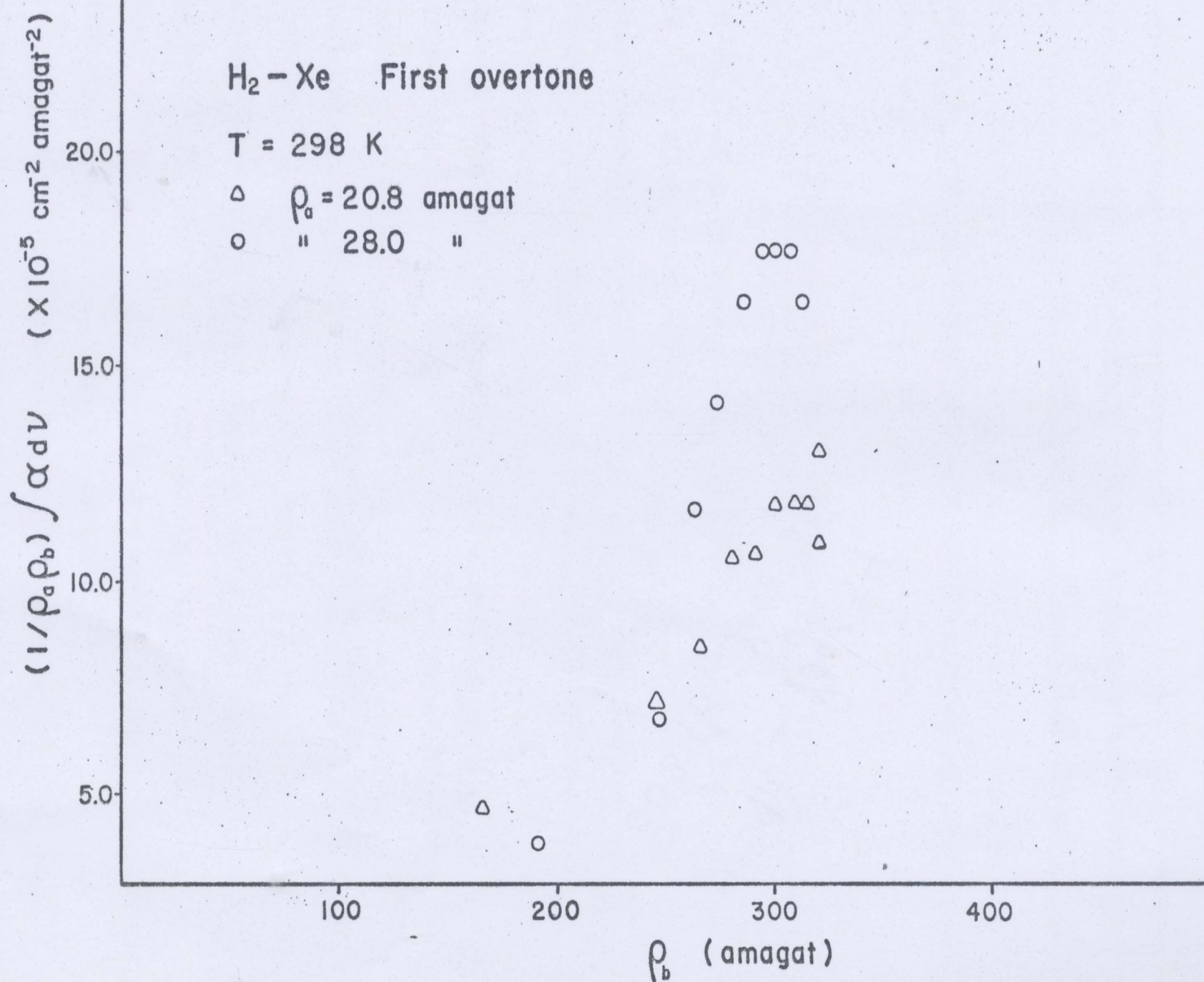


Fig. 17. The relation between the enhancements in the integrated absorption coefficients and ρ_a and ρ_b for $H_2 - Xe$.

well. The equation is written as

$$\tilde{\alpha}_1(\text{quad}) = \frac{4\pi^2 e^2 a_0^5 N_0^2}{3 \hbar c} \left(\frac{a_0}{\sigma} \right)^5 J x, \quad (4 - 1)$$

where x is now simplified for the single transitions of the overtone band in $H_2 - Kr$ and $H_2 - Xe$ mixtures as follows:

$$x = \sum P_{J_1} C(J_1 2 J_1' ; 00)^2 \langle 0 J_1 | Q_1 | v_1' J_1' \rangle^2 \alpha_2^2. \quad (4 - 2)$$

It is noted that the quadrupole moment Q_2 of krypton and xenon [see Eq. (3 - 3)] is zero and their polarizabilities α_2 are constants. The other quantities in Eqs. (4 - 1) and (4 - 2) were defined earlier in Chapter 3. The quadrupole matrix elements $\langle 0 J | Q | 2J' \rangle$ of H_2 for the transitions $Q_2(1)$, $Q_2(2)$ and $S_2(J)$ with $J = 0$ to 2 were directly obtained from Birnbaum and Poll (1969) and those for the transitions $Q_2(3)$, $S_2(3)$, $O_2(2)$ and $O_2(3)$ were calculated by the method given by Tipping and Herman (1970). These calculations are included as an appendix. All these matrix elements are tabulated in Table VI. The normalized Boltzmann factors P_J for H_2 at 298 K are given in Appendix A. The intensities of the quadrupolar lines relative to the $S_2(1)$ line obtained from Eq. (4 - 1) are given in Table VII. Also included in this table are the wave numbers of these lines, calculated from the constants of the free H_2 molecule.

In order to calculate the theoretical band profile, each component of the single-transition quadrupolar line was broadened with a Boltzmann-

TABLE VI

Matrix elements of the quadrupolar moment of H₂ for its 1st overtone band
(Birnbaum and Poll, 1970)

J	$\langle 0J Q 2J - 2 \rangle$	$\langle 0J Q 2J \rangle$	$\langle 0J Q 2J + 2 \rangle$
0		- 0.01121	- 0.01166
1		- 0.01125	- 0.01184
2	- 0.01052*	- 0.01132	- 0.01194
3	- 0.00990*	- 0.01146*	- 0.01196*

* Calculated by the method given by Tipping and Herman (1970).

TABLE VII

Relative intensities of the single-transition quadrupolar
lines of H_2 in the first overtone region at 298 K

Transition	Calculated wave number	Relative intensity
$O_2(3)$	7488.2	0.037
$O_2(2)$	7732.6	0.045
$Q_2(3)$	8017.2	0.051
$Q_2(2)$	8052.0	0.075
$Q_2(1)$	8075.3	0.060
$Q_2(0)$	8087.0	0
$S_2(0)$	8406.3	0.323
$S_2(1)$	8604.1	1.000
$S_2(2)$	8784.9	0.149
$S_2(3)$	8946.6	0.100

modified dispersion line shape (Kiss and Welsh, 1959). Provision was made to incorporate frequency shifts of the component lines. Thus the line shape is represented as,

$$\tilde{\alpha}^+(v) = \tilde{\alpha}^0(v_o') [1 + (v - v_o')/\delta]^2 , \quad v \geq v_o' , \quad (4 - 3)$$

$$\tilde{\alpha}^-(v) = \tilde{\alpha}^+(v) \exp(-hc \Delta v/KT) , \quad v < v_o' , \quad (4 - 4)$$

where $\tilde{\alpha}(v)$ is the absorption coefficient free from the frequency factor v , i.e., $\tilde{\alpha}(v) = \alpha(v)/v$, $[\alpha(v) = (2.303/\lambda) \log_{10} (I_1(v)/I_2(v))]$. The quantity $v_o' = v_m + \Delta v_o$ is the shifted wave number for the transition, v_m being the wave number of the transition of the free molecule and Δv_o being the shift in wave number. $\tilde{\alpha}^0(v_o')$ is the transition probability at the peak position v_o' of the line and $\tilde{\alpha}^-(v)$ and $\tilde{\alpha}^+(v)$ are transition probabilities at wave numbers $v_o' - \Delta v$ and $v_o' + \Delta v$ in the low- and high-frequency wing, respectively.

Profiles of the enhancement of absorption were analysed by means of a programme written for the IBM 370 computer. At a given density all the quadrupolar single-transition components were assumed to have the same half-width δ . In the computer programme the parameters δ , the frequency shift Δv_o , the peak intensity $\tilde{\alpha}^0(v_o')$ (the peak intensities of all lines were expressed in terms of the intensity of the $S_2(1)$ line) were left as adjustable parameters. The criterion for the best fit of the calculated profile to the experimental profile in any specified spectral region was that the sum of the squares of the deviations between the calculated and experimental profiles in that region be a minimum. The

spectral region $8100 - 8500 \text{ cm}^{-1}$ had to be excluded for the fit because double transitions of the type $Q_1(J) + Q_1(J)$ are evident from the experimental profiles. Furthermore, both high and low frequency wings could not be fitted because the observed absorption coefficient drops through zero and actually becomes negative. This kind of observation was mentioned in both Chapter 3 and earlier in this chapter, and will be further discussed in Chapter 5. Reasonable fit of the calculated profile to the experimental profile was obtained in the region around 8000 cm^{-1} (region of $Q_2(J)$ transitions) and between 8500 to 8700 cm^{-1} . Examples of the profile analysis for $H_2 - Kr$ and $H_2 - Xe$ mixtures are shown in Figs. 18 and 19.

4.3 Results of the Profile Analysis

(i) Frequency Shifts

The frequency shifts of the quadrupolar lines of the first overtone band of H_2 in $H_2 - Kr$ and $H_2 - Xe$ binary mixtures in the range of densities used in the present investigation were found to be negative and density-dependent (Tables VIII and IX). The shifts obtained are probably somewhat smaller than the actual shifts because of the neglect of the intensity contribution of the double transitions of the form $Q_1(J) + S_1(0)$ and $Q_2(J) + S_0(1)$, to the band in the calculated profile. Here double transitions are expected to fall near $S_2(1)$ line on the high frequency side. In Figs. 20 and 21, the frequency shifts ($\text{in } \text{cm}^{-1}$) were plotted as functions of the density of the perturbing gas, krypton or xenon. In both cases, the

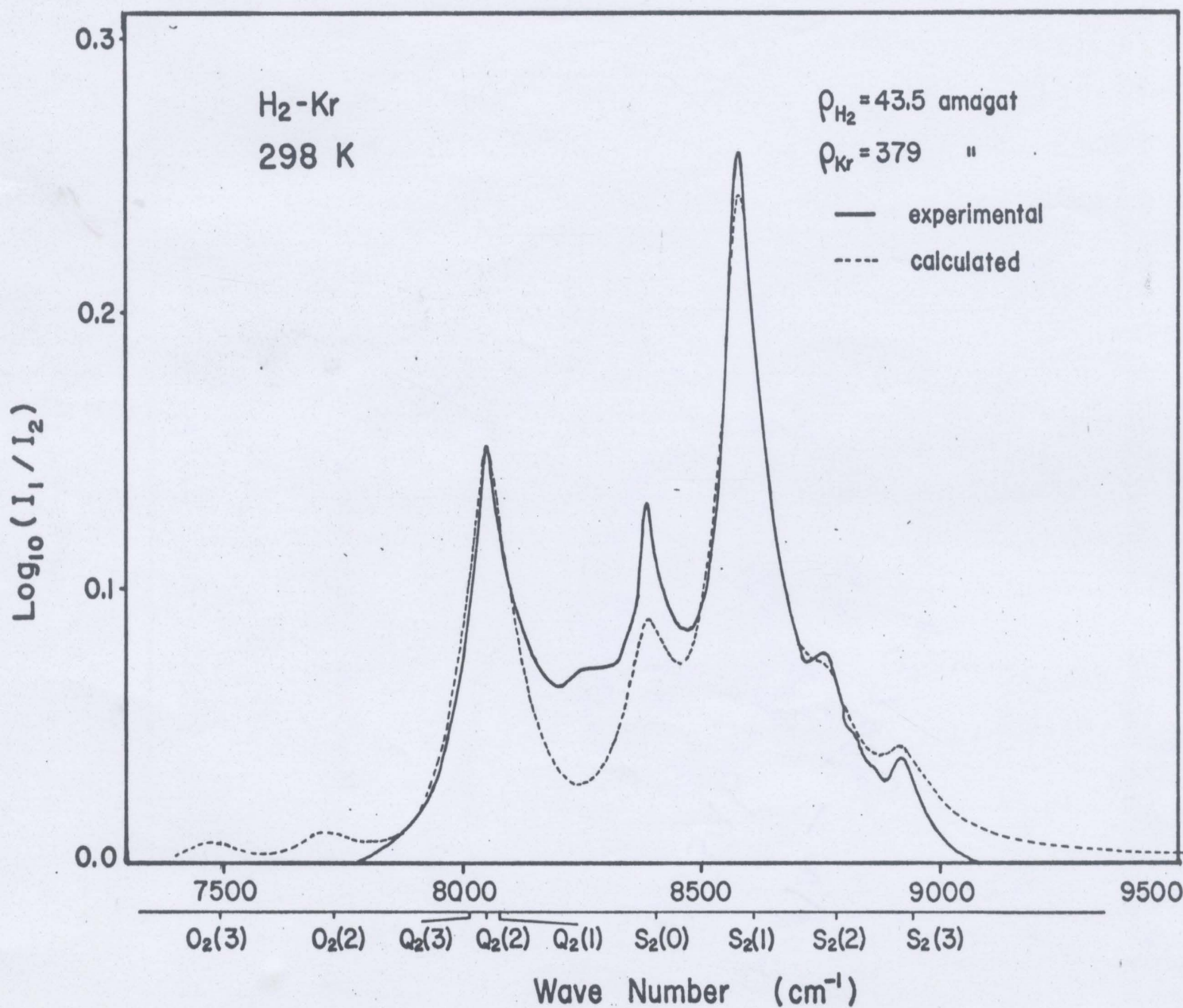


Fig. 18. Analysis of the enhancement of the first-overtone band of H₂ by Kr.

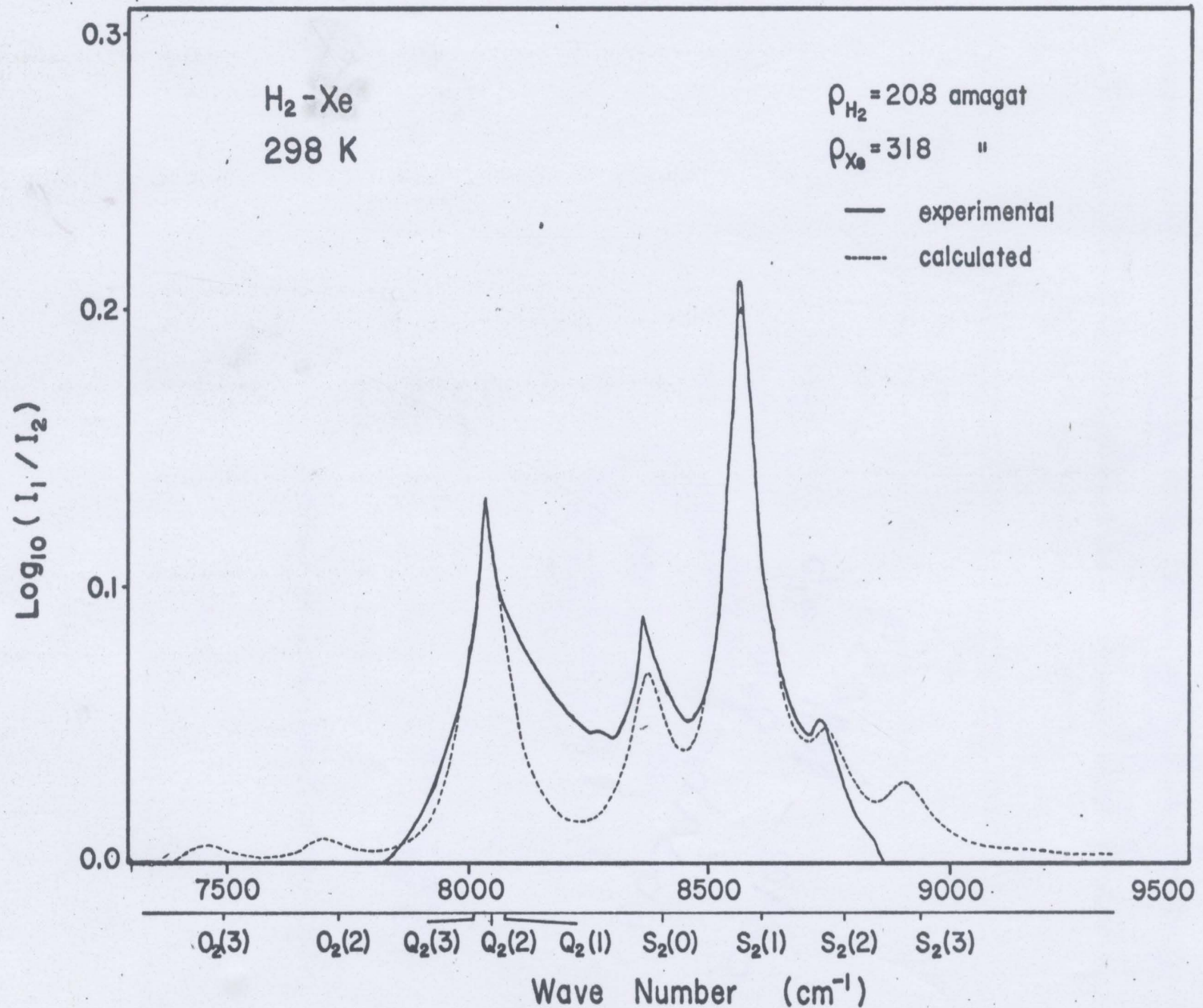


Fig. 19. Analysis of the enhancement of the first overtone band of H_2 by Xe.

TABLE VIII

Data of density versus half-width δ and frequency shift $\Delta\nu_0$
for the quadrupolar components of the first overtone band
of H_2 in H_2 -Kr mixtures at 298 K

ρ_a (amagat)	ρ_b (amagat)	δ (cm^{-1})	$\Delta\nu_0$ (cm^{-1})
43.5	157	61.7	-14
	232	64.1	-18
	285	66.5	-20
	325	71.6	-22
	354	71.7	-22
	379	72.8	-23
	401	73.8	-22
	423	74.5	-23
42.3	56.5	61.8	-12
	99.0	62.3	-13
	143	64.6	-13
	186	63.0	-16
	218	62.7	-17
	250	66.2	-19
38.9	207	61.7	-16
	309	67.9	-20
	330	70.5	-21
	346	72.8	-22

TABLE VIII (continued)

ρ_a (amagat)	ρ_b (amagat)	δ (cm^{-1})	$\Delta\nu_0$ (cm^{-1})
40.2	72.6	59.9	-11
	117	63.3	-14
	160	61.6	-14
	208	63.8	-18
	237	65.7	-18
	267	67.4	-18
	291	66.4	-19
34.2	57	57.8	-11
	170	63.6	-15
	245	64.4	-18
	319	71.4	-23
	382	86.2	-21
	427	75.8	-23

TABLE IX

Data of density versus half-width δ and frequency shift $\Delta\nu_0$
for the quadrupolar components of the first overtone band
of H_2 in H_2 -Xe mixtures at 298 K

ρ_a (amagat)	ρ_b (amagat)	δ (cm^{-1})	$\Delta\nu_0$ (cm^{-1})
20.8	164	45.0	-14
	243	54.4	-20
	263	50.7	-25
	288	50.2	-31
	297	52.7	-33
	306	52.1	-35
	312	52.1	-35
	318	54.1	-35
28.0	189	48.8	-16
	243	54.4	-20
	260	59.3	-25
	270	61.8	-30
	281	62.7	-33
	290	65.3	-32
	297	72.8	-35
	303	72.8	-35
	309	65.3	-34

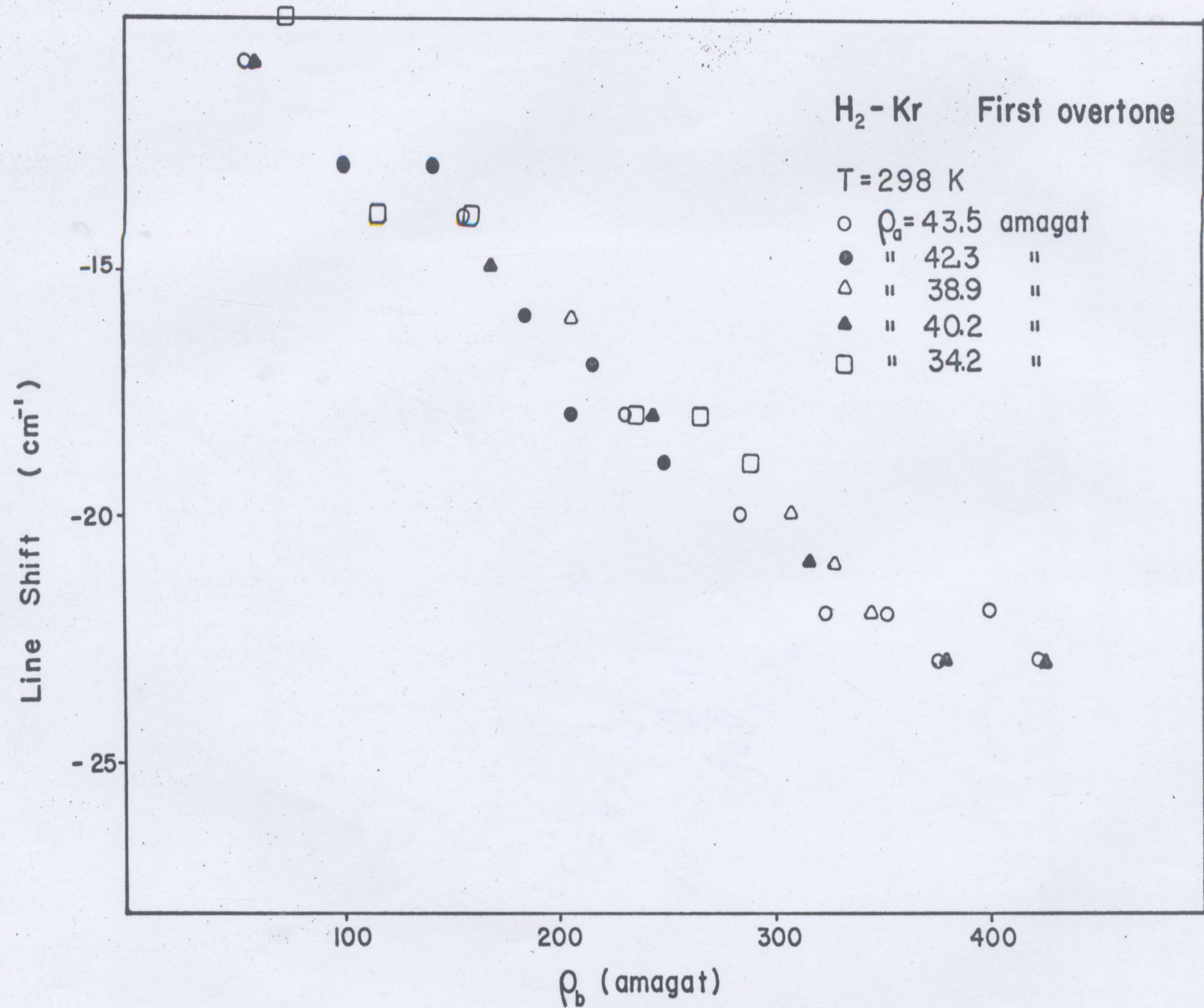


Fig. 20. The relation between the overtone quadrupolar line shift and the perturbing gas density ρ_b in $H_2 - Kr$.

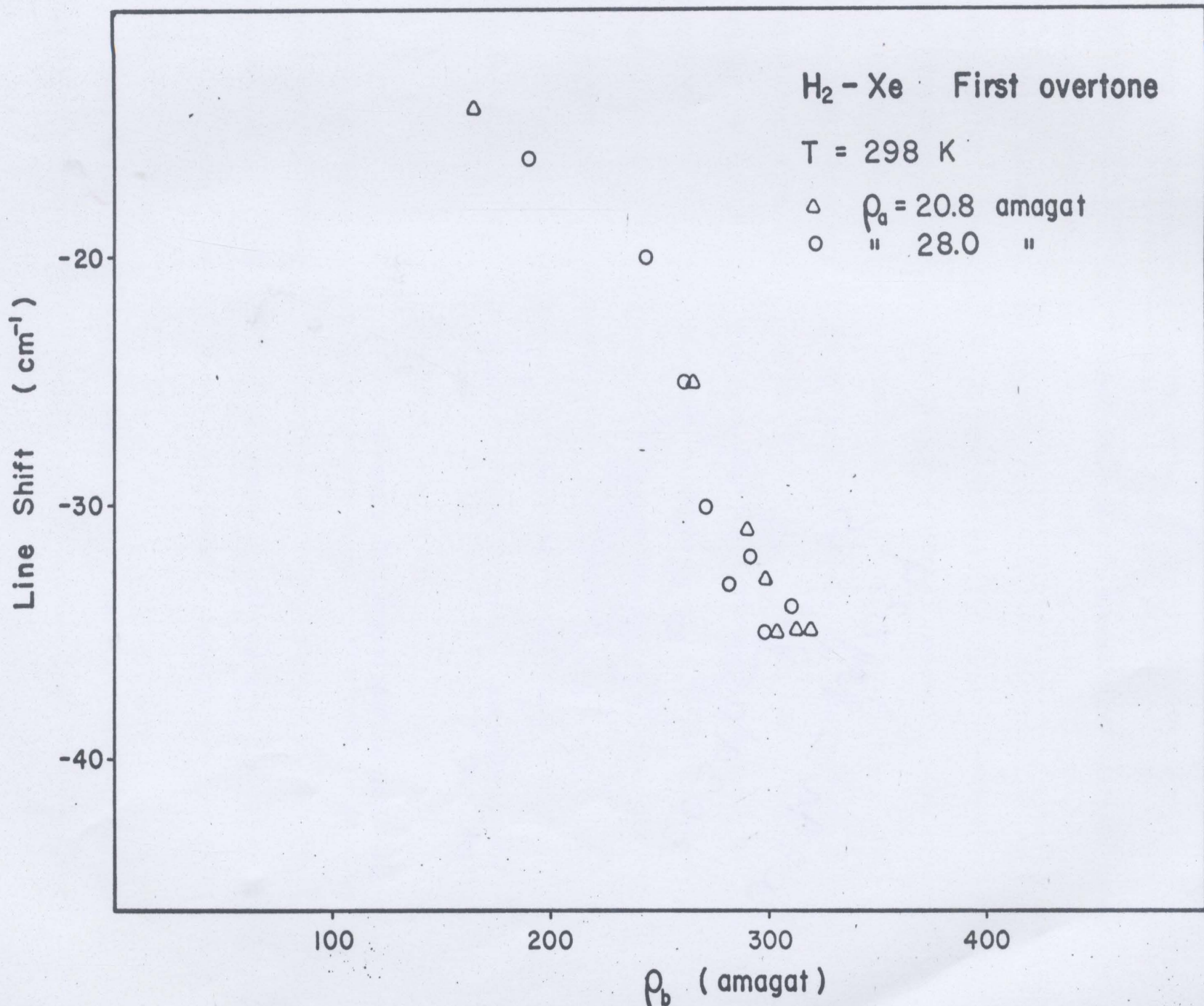


Fig. 21. The relation between the overtone quadrupolar line shift and the perturbing gas density ρ_b in $H_2 - Xe$.

observed shifts decrease at first and then level off with increasing density of the perturbing gas. Similar shifts were observed for the induced fundamental band of H₂ with argon, krypton and xenon as perturbing gases (cf. Mactaggart 1971; also see Varghese; Ghosh and Reddy, 1972). In both the fundamental and the first overtone bands the frequency shifts, within the experimental accuracy, were observed to be the same for all the quadrupolar lines within a band. This means that the observed shifts are due mainly to a perturbation in the vibrational frequency ω_e of the H₂ molecule during collisions with the foreign gas molecules. The frequency shifts of the quadrupolar components of the first overtone band obtained in the present work are slightly more than twice the shifts observed for the corresponding components of the fundamental band (Mactaggart, 1971).

The frequency shifts $\Delta\nu_o$ of the quadrupolar lines could be expressed in a density expansion by the relation

$$\Delta\nu_o = a_o + ap + bp^2 , \quad (4 - 5)$$

where ρ is the density of the perturbing gas. For both krypton and xenon the coefficient a is negative and coefficient b is positive, qualitatively. Determination of numerical values for these parameters is not warranted because of the considerable uncertainty caused by the effect of double transitions.

May, Degen, Stryland and Welsh (1961) and May, Varghese, Stryland and Welsh (1964) observed density shifts of the Q₁(J) lines in the

Raman spectrum of hydrogen gas compressed to densities up to 800 amagat.

According to them the linear coefficient a can be represented by the relation

$$a = K_{\text{rep}} I_1 - K_{\text{att}} I_2 , \quad (4 - 6)$$

where K_{rep} and K_{att} are positive constants representing the frequency shift due to repulsive and attractive intermolecular forces, respectively, and I_1 , I_2 are temperature dependent integrals. The negative values of a obtained for $\text{H}_2 - \text{Kr}$ and $\text{H}_2 - \text{Xe}$ in the present work show that the attractive forces predominate over the repulsive forces for these binary mixtures at room temperature, as expected.

Improvement of the interpretation of the frequency shifts could be obtained by extending the analysis to include double transitions induced in ternary collisions. Experimentally, extending the ranges of temperatures and densities with different perturbers would be useful.

(ii) Line Widths

The line widths, δ , determined as adjustable parameters in the synthetic profiles, are also listed in Table VIII, and IX and were plotted in Figures 22 and 23 as functions of the perturbing gas density. These

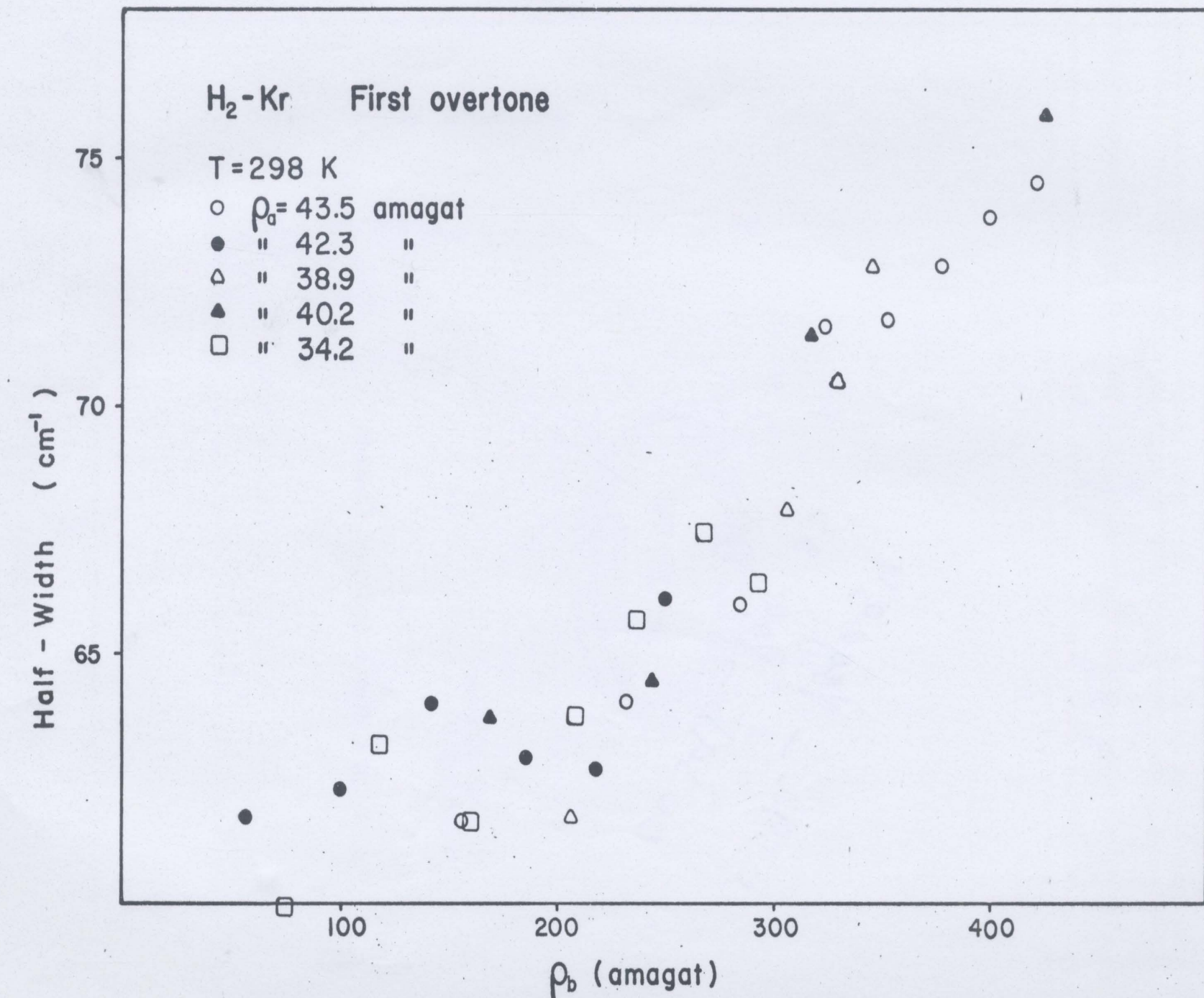


Fig. 22. The relation between half-width and ρ_b for the first overtone band in H_2 - Kr mixtures.

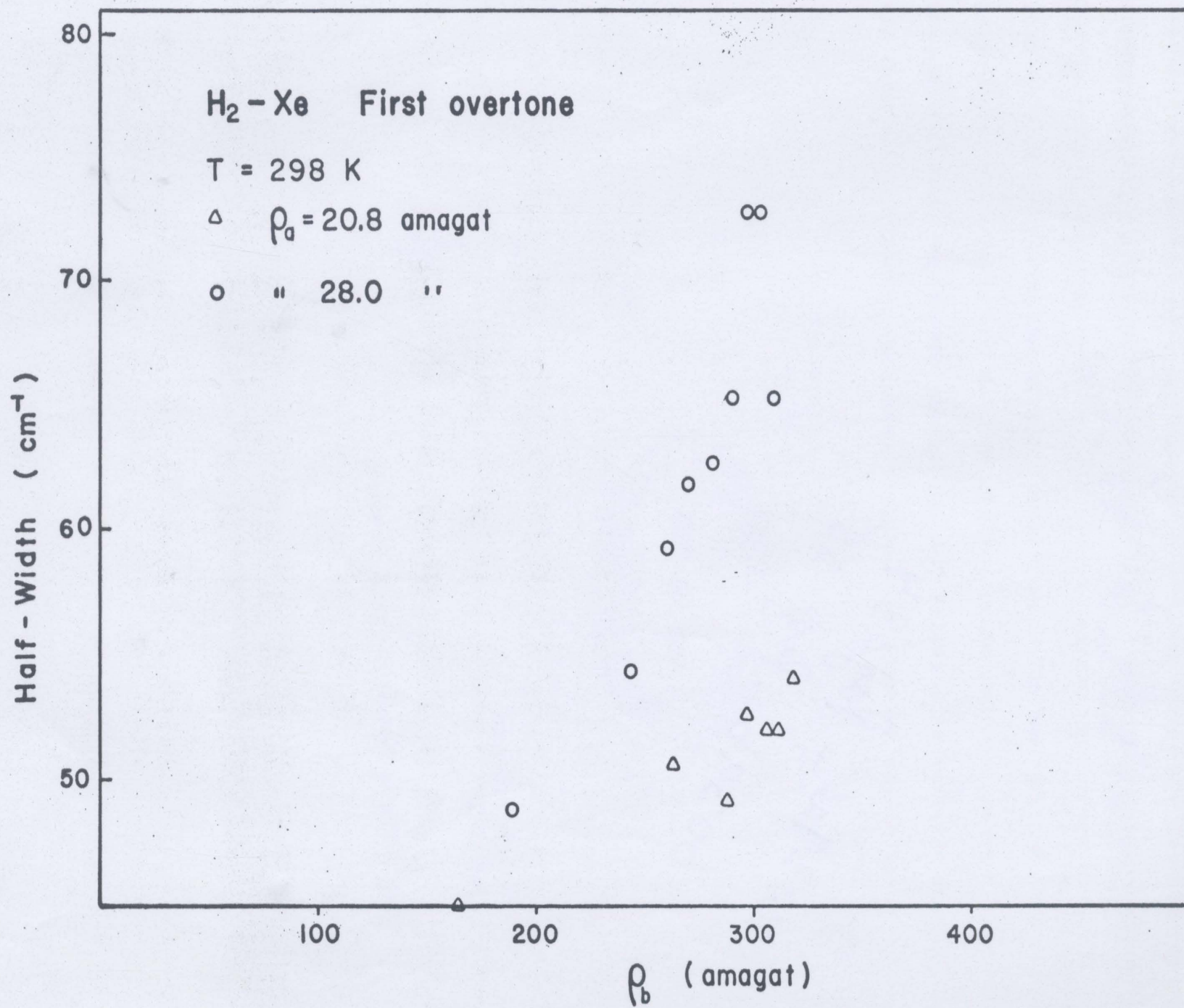


Fig. 23. The relation between half-width and ρ_b for the first overtone band in $H_2 - Xe$ mixtures.

"widths" are probably properly considered as a manifestation of the double transitions $Q_1(J) + S_1(0)$ and $Q_2(J) + S_0(1)$, situated near $S_2(1)$ but not resolved from it, and due to ternary collisions, rather than as real widths of the single transitions. The ambiguities in determining the widths, as well as shifts, could only be removed by new theoretical work explicitly accounting for relative intensities of single and double transitions, including induction by ternary collisions.

CHAPTER 5

Apparent Collision-Induced Emission in Hydrogen

5.1 Experimental Observations

In all the experiments mentioned earlier in this thesis, one very peculiar phenomenon always happened in the regions where there were no strong molecular absorptions, that actually more signal reached the detector with the gas in the absorption cell than without. In one case the weak $S_2(3)$ transition of the $H_2 - Xe$ mixture (Chapter 4) was actually below the zero line. Had we not changed the amplifier gain as mentioned in Chapter 4, a greater part of the $H_2 - Xe$ spectrum and even some of that of the $H_2 - Kr$ spectrum would have been under the zero line.

This phenomenon was observed to a very small extent in $H_2 - Ar$ mixtures, and not at all in mixtures of neon and helium with hydrogen. Furthermore experiments with ~ 330 amagat of pure Kr and Xe showed small effect.

Consistent results were obtained with different monochromators, two different amplifier systems, and PbS detectors operated at both room- and liquid nitrogen temperatures. The possibility of the radiation from the detector to the cell caused by the detector looking at the colder cell, is eliminated by the use of detector operated at 77 K. In this case it also eliminated the possibility of the detector being cooled and thus more sensitive, say, by more absorption in the first pass region of the monochromator. Besides, the filter in front of the monochromator also cuts

off all the first pass radiation, which is visible light in this case. The linearity of response of the detector and amplifier system was also checked.

Under the same experimental conditions, the discrepancy is greater at the high wave number side than at the low wave number side of the first overtone band, and it is slowly and more or less regularly increasing with wave number. (No experiment with comparable gas density was done at the low wave number side of the fundamental band.) One most peculiar feature is that in the region between 6800 to 7400 cm^{-1} a few broad peaks could be seen. These peaks do not occur in pure Kr and Xe experiments. The differences were greater for H₂ - Xe than H₂ - Kr and both were increasing with density. In pure H₂ experiments at 77 K the peaks became quite distinct and their intensities were large enough to make measurements. Fig. 7 of Chapter 3 showed the spectrum with the U-line and wing of the fundamental band of pure H₂ at 77 K. The graph is plotted with $\log_{10}(I_0/I)$ against the wave number. The intensity difference is actually slightly greater than the absorption of the U transitions. This part of the spectrum is again shown in Fig. 24 at three different experimental gas densities. Three broad peaks can easily be seen, with the middle peak broader than the others, and perhaps looking as if it consists of two neighbouring peaks, at intermediate densities. The peaks occur at ~ 6875 , 7030 , 7090 , and 7230 cm^{-1} and the half-width is estimated as $\sim 70 \text{ cm}^{-1}$; the peaks appear to merge and become less distinct at the higher densities. The density fluctuation of the gas at higher densities, causing random noise could have caused some

apparent smearing.

In the plotting of the graph we have interpreted the intensity with $\log_{10}(I/I_0)$ in the usual way of treating an absorption intensity, in this case a negative absorption. Another way of interpreting the intensity is to measure the net intensity, $(I - I_0)$, in arbitrary units. The result of this plotting is shown in Fig. 25. The profiles are similar in general appearance to those in Fig. 24.

The areas under Fig. 24, $\int \log_{10}(I/I_0)dv$, and under Fig. 25, $\int (I - I_0)dv$ were measured and tabulated in Table X and XI, respectively, with the corresponding gas density, and were plotted in Figs. 26, and 27 respectively. The results perhaps favour

$$\int \log_{10}(I/I_0)dv \propto \rho^2 \dots \quad (5 - 1)$$

The results of the least square fit of this equation is plotted with solid line in Fig. 26.

It should be noted here, that because the extent of the spectra are not known, the area measurements were made between $6800 - 7340 \text{ cm}^{-1}$, arbitrarily chosen. They do not represent integrated coefficient (or net intensity) of a band.

These radiation peaks still occur in an experiment with P.E. 203 - 1104 filter in front of the light source, i.e., after cutting off all the radiation above $\sim 8500 \text{ cm}^{-1}$ (right after first overtone) from entering the absorption cell. No filter, that cuts off the first overtone but transmits the radiation region, nor filter that transmits the first overtone but cuts off the radiation region were available.

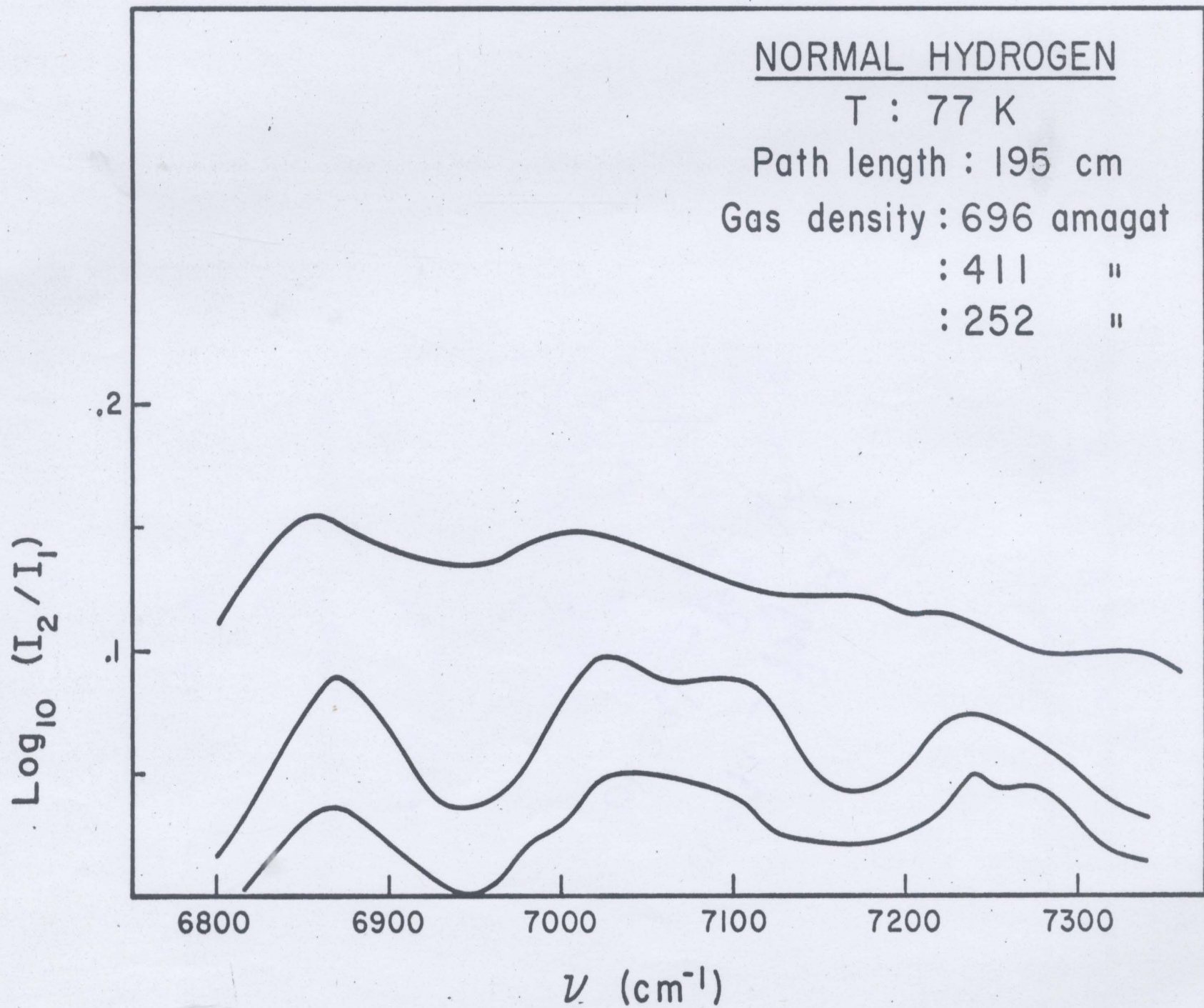


Fig. 24. Profiles of part of the apparent collision-induced emission spectrum of H_2 .

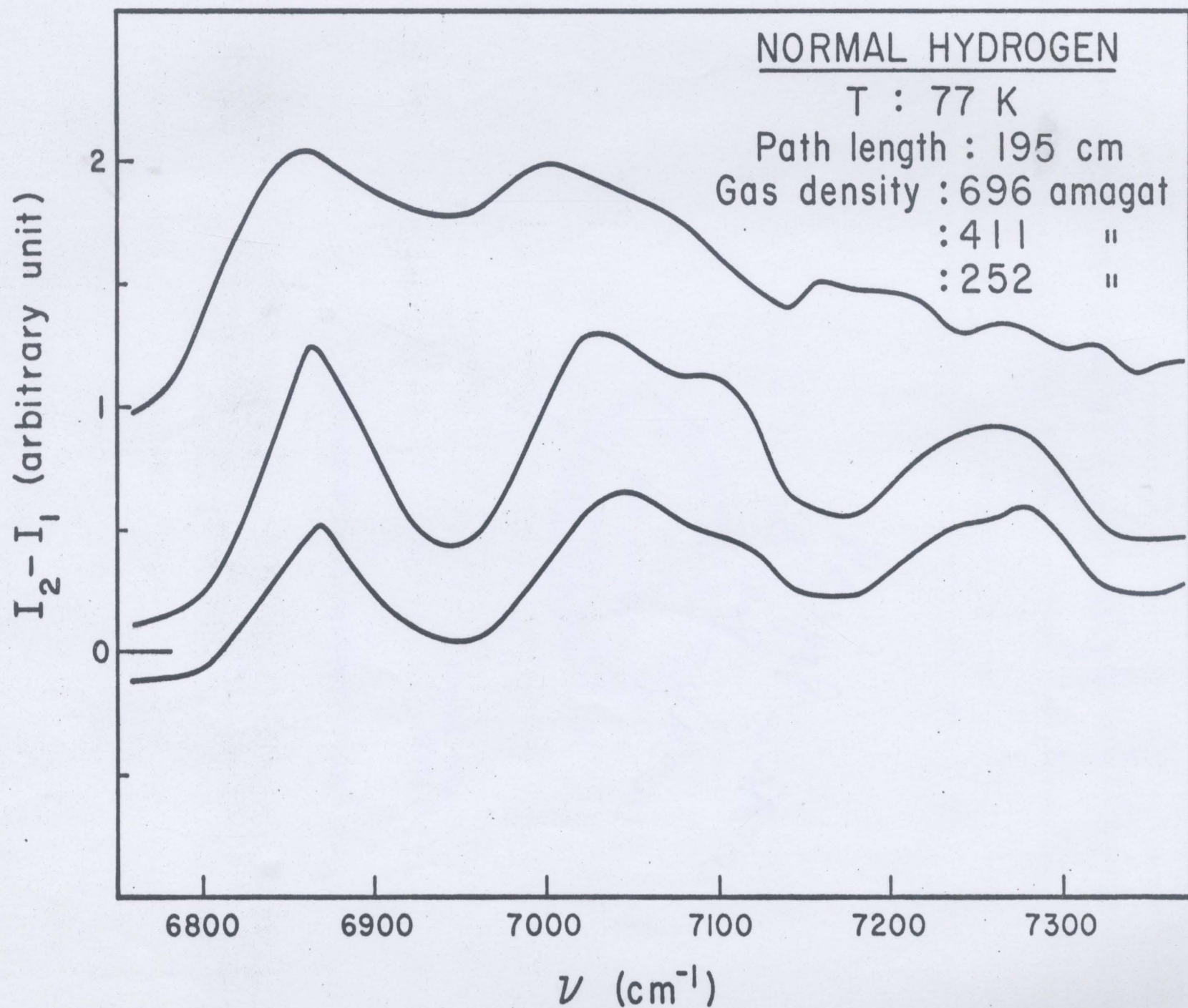


Fig. 25. Profiles of part of the apparent collision-induced emission spectrum of H₂.

TABLE X

Integrated radiation coefficient of H₂ at 77 K

ρ (amagat)	$\int \log_{10}(I/I_0)dv \text{ (cm}^{-1}\text{)}$
252	15.3
363	34.5
398	39.6
411	34.0
454	43.1
482	50.2
511	49.8
534	60.7
552	66.2
566	85.2
603	85.3
637	116.9
648	108.4
668	116.9
696	112.7
697	112.7

TABLE XI

Integrated net radiation intensity of H₂ at 77 K

ρ (amagat)	$\sum(I - I_0)\Delta\nu$ (arbitrary unit)
252	195
363	424
398	595
411	463
454	616
482	590
511	720
534	720
552	808
566	597
603	780
637	936
648	780
668	936
696	990
697	990

NORMAL HYDROGEN

T : 77 K

Path length : 195 cm

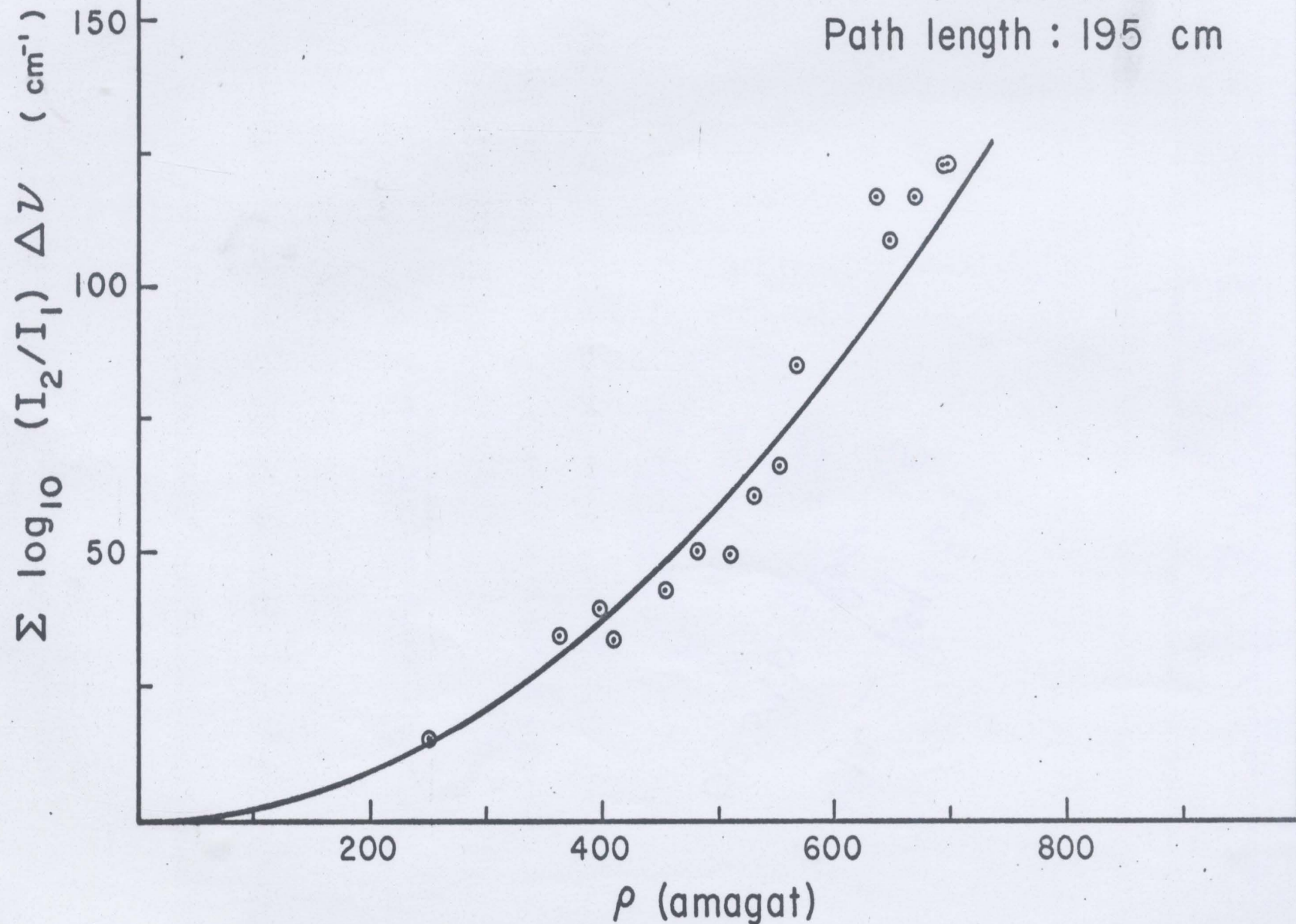


Fig. 26. The relation between the apparent integrated emission intensity and the density.
Solid line: $\sum \log_{10} (I_2/I_1) \Delta\nu = \alpha \rho^2$, least squares fit to the data.

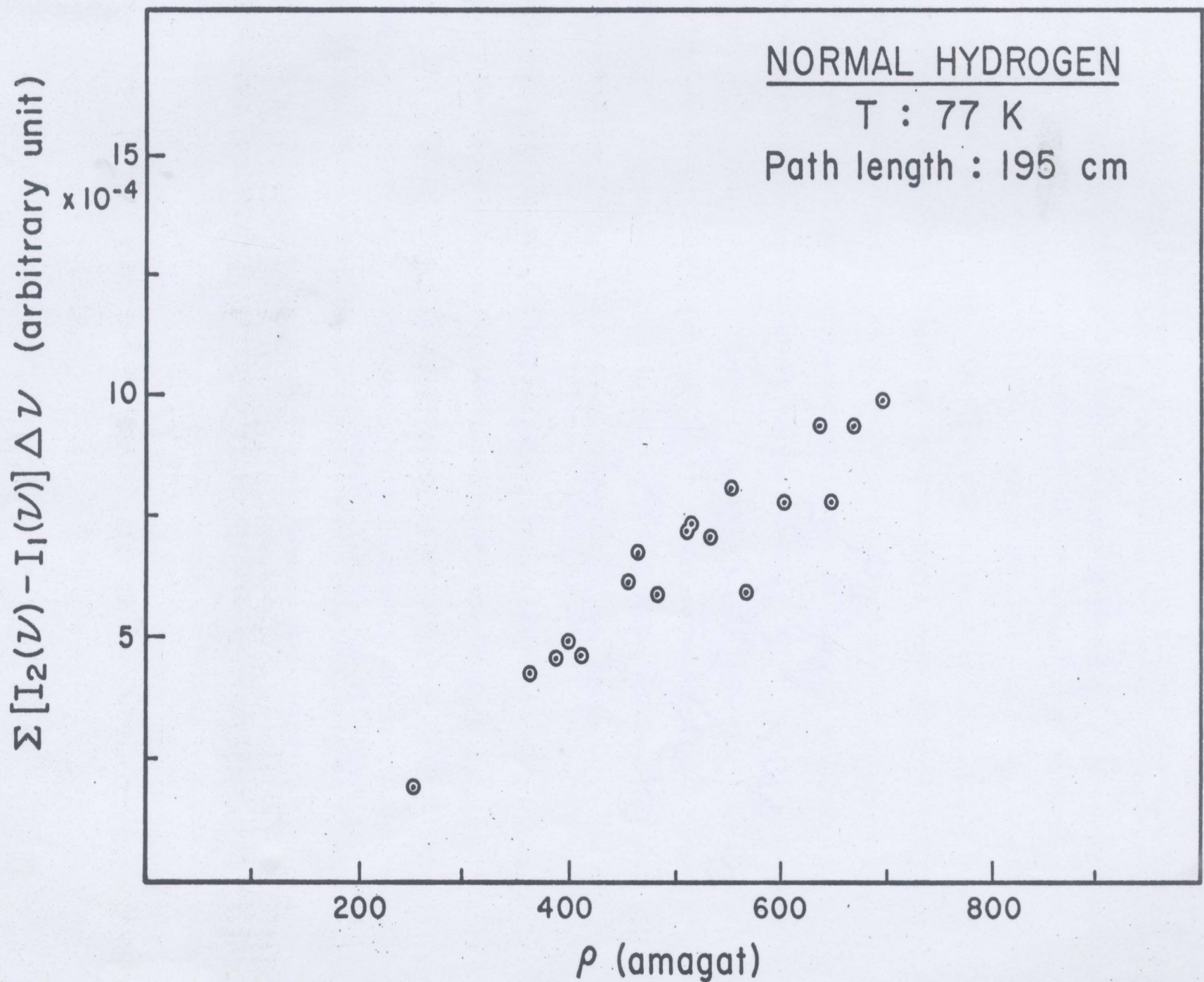


Fig. 27. The relation between the integrated net intensity of apparent emission and density.

Another experiment was made to observe the signal at 180° from the direction of the incident light. Reflected light from the windows in the absorption cell was the main signal when the cell was evacuated. When the gas was admitted to the cell, less signal ($\sim 10\%$) less) reached the detector, as expected because of reduction in reflection loss at the inner surface. No radiation peaks or negative peaks were observed corresponding to the region where the peaks occur in the transmission experiments.

A series of experiments was also made to find any peak in the low wave number side of the fundamental band with pure H_2 at 77 K. No consistent result was found because impurity in the H_2 gas happens to have very strong and broad absorption in the suspected region between 3000 to 3500 cm^{-1} . Although purification was attempted by passing the gas through low temperature traps, the results were still not definite.

5.2 Speculations on the Causes of the Phenomenon

(i) Changes in Reflectivity at the Window Surfaces

When the absorption cell is filled with high density gas, the index of refraction is increased, so the reflectivity at the inner surfaces of the windows of the absorption cell decreases from that when it was evacuated. The decrease in reflection loss at these surfaces will cause an increase in signal in spectral regions where no absorption occurs. Most spectroscopic studies with low pressure gases justifiably ignore the small correction that should be applied to account for this, but it obviously must be considered here.

For normal incidence, assuming a wave incident from a non-absorbing medium (μ') on an absorbing medium of refractive index $\mu - iK$, the reflectivity is

$$R = \frac{(\mu' - \mu)^2 + K^2}{(\mu' + \mu)^2 + K^2}.$$

An order of magnitude estimate of the contribution of anomalous dispersion owing to the adjacent collision-induced absorptions in hydrogen shows it is negligible, leaving

$$R = \left(\frac{\mu' - \mu}{\mu' + \mu} \right)^2.$$

At 1.5μ sapphire has a refractive index of 1.75, giving loss due to two windows of 15% in an evacuated cell. Hydrogen gas at a density of 500 amagat is estimated to have $\mu = 1.08$, giving reflection loss at two windows of 10%, so that the increase is $\sim 5\%$ in transmission intensity. This correction of course depends on the composition and density of gases in the cell, but cannot account for signal increases which reached as much as 35%, and is $\sim 20\%$ throughout the region between the U(1) transitions and the first overtone band with ~ 660 amagat of H_2 .

(ii) Radiative Emission from Hydrogen

Spectra taken in the region between the U(1) transitions and the first overtone band show considerable intensity increases, apparently including peaks, in mixtures of $H_2 - Kr$ and $H_2 - Xe$, but smaller increases

in the same region of spectra of the pure perturbing gases and without peaks. A possible implication is that collision-induced emission from hydrogen is the source of the extra intensity, and that since it is a very small effect, it is only apparent in spectral regions where absorption is absent, or very weak. (It does not seem any more plausible to blame an impurity for the effect, because emission would still be required.) Although this postulated emission evidently occurs throughout the spectral regions from below the fundamental band to frequencies above the first overtone, the observation of apparent peaks in the region between the $U(1)$ transitions and the first overtone encourages particular speculation about that part of the spectrum.

The breadth of the peaks is consistent with the speculative collision-induced emission explanation. In fact the $\sim 70 \text{ cm}^{-1}$ widths are consistent with widths of quadrupole-induced absorption widths at 77 K. The apparent ρ^2 dependence of integrated intensity may not necessarily be taken as evidence for the postulated mechanism, since the density dependence of the over-all process must include both the population of the upper states and non-radiative processes for de-excitation of those upper states as well as the emission process itself. It is known from direct measurements using stimulated Raman scattering (Ducuing et al. 1970, Audibert et al. 1974) that the vibrational relaxation time for H_2 for our experimental density and temperature ranges may be of the order of 10 μsec . This long time allows $\sim 10^7$ collisions and suggests that collision-induced emission is possible in principle. Experiments with filters limiting the spectral input to the cell are consistent with

speculation that these peaks correspond to emission from levels with $v = 2$ to $v = 0$ lower levels. This assumes population of the upper levels by collision-induced absorption. Several possible complicating factors would make even tentative specific assignments of the peaks unwise. Some of these are as follows:

1. Peak positions may not correspond to band origins,
2. Density dependent frequency shifts may occur,
3. Double transitions are probable,
4. Upper state J levels are not known (though one would anticipate $J = 0$ and 1 dominant, since rotational relaxation would be expected to be much faster than vibrational relaxation),
5. Two or more transitions might overlap one another, and
6. Location of the peaks experimentally is somewhat uncertain because of their weakness and breadth, and noise due to density fluctuation of the gas in the cell.

If the possibility of radiative emission were accepted, then one might further speculate on the relative importance of spontaneous and stimulated emission. A quick reaction, and probably the correct one is that stimulated emission is very improbable with the relatively weak intensity of the source in these experiments. However, the geometry of the experiment certainly favours stimulated emission somewhat. Since the apparatus is designed for absorption experiments, the cell is long (2 m) and of small aperture (0.5 x 1.0 cm.) Thus a small fraction of isotropically emitted spontaneous emission could be collected and passed through the monochromator to the detector. On the other hand, this geometry favours stimulated emission in the sense that such emission is directed along the same direction as the

stimulating radiation, i.e., along the light guide within the cell, in the same way that it is intended to be used for absorption studies. Nevertheless, qualitative arguments and order-of-magnitude estimates lead one back to the conclusion that the spontaneous process is more likely. In this connection it is interesting to note the proposal for a collision-induced laser using H_2 - Xe mixtures but pumped by an electron beam, (Christiansen and Greenfield, 1973).

Then the question becomes - Is it possible to see the spontaneous process? Again only an order-of-magnitude estimate is possible (Courtesy of Prof. J. D. Poll). If one assumes that all depopulation of the upper states is radiative, and that transition probabilities are the same for the absorbing and emitting transitions (J dependence would actually make them somewhat different), and considers that geometry of the cell and collecting optics, then one concludes that the integrated intensity of emission in one band might be of the order of $10^{-5} - 10^{-6}$ times the integrated absorption for the same band. This seems to agree roughly with observations.

An experiment intended to provide more information about this last question was suggested by the idea that population of optically excited states will decrease exponentially along the length of the cell, following Beer's law. Thus observation of stimulated radiation would be favoured by the long cell, since the stimulating radiation would not be absorbed and would traverse the cell without attenuation, in fact with increasing intensity. On the other hand spontaneously emitted light, isotropically emitted, would be stronger in the backward direction, for a cell long

enough and absorption strong enough to give an appreciable gradient in excited state population along the length of the cell. Accordingly, radiation emerging from the cell was observed in the direction at 180° from the incident beam. No peaks were observed in this spectrum; the intensity decreased by $\sim 10\%$, which is about the same as calculated by considering the reflection from all four windows, with and without gas in the cell.

In summary, in certain spectral regions more radiation reaches the detector when gas fills the cell than when it is evacuated, decreased window reflection doesn't seem to explain the difference, and the discrepancy is speculated to be accounted for by collision-induced emission.

APPENDIX A

Normalized Boltzmann factors for normal hydrogen at different temperatures

The normalized Boltzmann factor P_J is defined (Poll, 1970) as

$$\begin{aligned} P_J &= (2J+1) P(J) \\ &= Z^{-1} g_J (2J+1) \exp(-E_J/kT) . \end{aligned} \quad (A-1)$$

It is normalized such that

$$\sum_J P_J = 1, \quad (A-2)$$

where $E_J = J(J+1)B_0 hc$ and $B_0 = 60.9 \text{ cm}^{-1}$ is the rotational constant of H_2 in the ground vibrational state. $g_J = 1, 3$ for J even, odd and Z is the rotational partition function.

For normal hydrogen, the ortho-para ratio is constant and equal to that at room temperature, $\sum_{\text{odd } J} P_J \text{ (room temperature)} : \sum_{\text{even } J} P_J \text{ (room temperature)} = 3:1$.

TABLE A

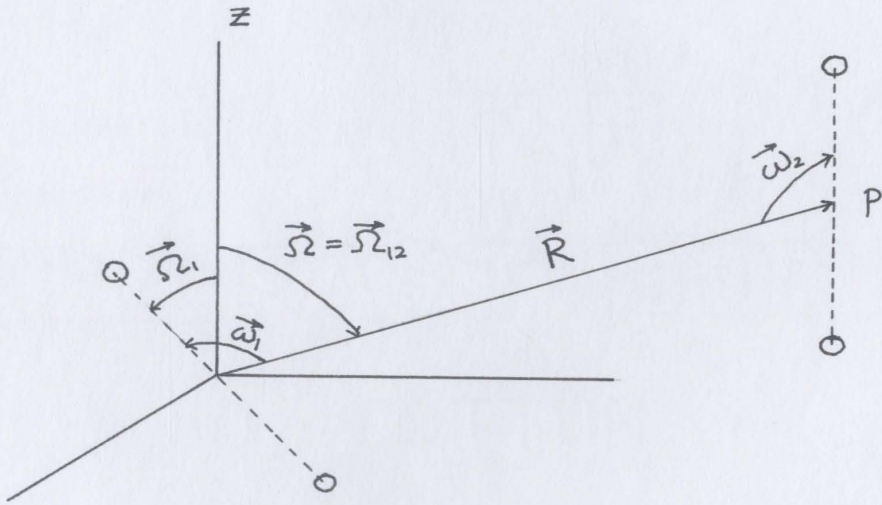
Normalized Boltzmann factors for normal hydrogen

T	J	P _J
77 K	0	0.249
	1	0.750
	2	0.001
	3	—
298 K	0	0.133
	1	0.667
	2	0.114
	3	0.082
	4	0.003
	5	—

APPENDIX B

Binary absorption coefficient due to electrostatic-induction
between two homonuclear diatomic molecules*

Using the first two non-vanishing terms in a multipole expansion, the electrostatic field at a point P, a position $\vec{R}(R, \vec{\Omega}_1)$ away from the center of mass of a homonuclear diatomic molecule can be obtained in a space-fixed coordinate system as



$$\begin{aligned}
 E_{\kappa} &= \frac{4\pi\sqrt{3}}{\sqrt{7}} \sum \frac{Q}{R} Y_{2m}(\Omega_1) Y_{3-m+\kappa}(\Omega) C(213; -m\kappa) (-)^m \\
 &+ \frac{4\pi\sqrt{5}}{\sqrt{11}} \sum \frac{H}{R} Y_{4m}(\Omega_1) Y_{5-m+\kappa}(\Omega) C(415; -m\kappa) (-)^m . \quad (B-1)
 \end{aligned}$$

*An extra term (hexadecapolar term) is simply added to the notes from Poll (1974).

Here Q and H are quadrupole and hexadecapole moments of the molecule, respectively. If a second molecule with polarizability α is placed at the point P , it will be polarized and the induced dipole moment is

$$\mu_{\kappa}^{(1)} = E_{\kappa}^{(1)} \alpha_{\kappa}^{(2)} . \quad (B-2)$$

The α is most conveniently expressed in a coordinate system with z -axis pointed along the internuclear axis of the second molecule. In this coordinate system the spherical components of α are

$$(-)^v \alpha_v = -\alpha\sqrt{3} C(110; v-v) + \gamma \sqrt{\frac{2}{3}} C(112; v-v) \quad (B-3)$$

where α is the isotropic part of the polarizability and γ is the anisotropy of the polarizability. If one transforms eq. (B-1) to the new coordinate system, substitutes into eq. (B-2), then returns to the original system, then the dipole moment components are

$$\begin{aligned} \mu_{\kappa}^{(1)} &= 4\pi \frac{Q_1}{R^4} \sum_{\nu\kappa'\mu j} (-)^{\kappa'+\mu} \sqrt{\frac{3}{7}} \left(\frac{4\pi}{2j+1}\right)^{\frac{1}{2}} C(213; -\mu\kappa') C(11j; \kappa'-\kappa) \\ &\quad \times Y_{2\mu} (\vec{\Omega}_1) C(11j; v-v) (-)^v \alpha_v \\ &\quad \times Y_j \kappa-\kappa' (\vec{\Omega}_2) Y_{3 \kappa'-\mu} (\vec{\Omega}_{12}) \\ &+ 4\pi \frac{H_1}{R^6} \sum_{\nu\kappa'\mu j} (-)^{\kappa'+\mu} \sqrt{\frac{5}{11}} \left(\frac{4\pi}{2j+1}\right)^{\frac{1}{2}} C(415; -\mu\kappa') C(11j; \kappa'-\kappa) \\ &\quad \times Y_{4\mu} (\vec{\Omega}_1) C(11j; v-v) (-)^v \alpha_v \\ &\quad \times Y_j \kappa-\kappa' (\vec{\Omega}_2) Y_{5 \kappa'-\mu} (\vec{\Omega}_{12}) . \end{aligned} \quad (B-4)$$

Using the Clebsch-Gordan relations

$$C(110; \nu-\nu) = (-)^{1-\nu} \left(\frac{1}{3}\right)^{\frac{1}{2}}$$

$$C(112; \nu-\nu) = (-1)^{1-\nu} \sqrt{\frac{1}{6}} (3\nu^2 - 2) , \quad (B-5)$$

and $\sum_{\nu} C(112; \nu-\nu)^2 = 1$, summing over ν and specializing the original coordinate system so that its z -axis points along \vec{R} (intermolecular direction), i.e. $\vec{\Omega}_{12} = 0$, $\vec{\Omega}_1 = \vec{\omega}_1$, $\vec{\Omega}_2 = \vec{\omega}_2$, then

$$\begin{aligned} \mu_{\kappa}^{(1)} &= 4\pi \frac{\alpha_2 Q_1}{R^4} \sqrt{3} (-)^{\kappa} C(213; -\kappa\kappa) Y_{2\kappa} (\vec{\omega}_1) Y_{00} (\vec{\omega}_2) \\ &\quad + 4\pi \frac{\gamma_2 Q_1}{R^4} \sqrt{\frac{2}{5}} \sum_{\mu} C(213; -\mu\mu) C(112; \mu-\kappa) Y_{2\mu} (\vec{\omega}_1) \\ &\quad \times Y_{2\kappa-\mu} (\vec{\omega}_2) \\ &\quad + 4\pi \sqrt{5} \frac{\alpha_2 H_1}{R^6} (-)^{\kappa} C(415; -\kappa\kappa) Y_{4\kappa} (\vec{\omega}_1) Y_{00} (\vec{\omega}_2) \\ &\quad + 4\pi \sqrt{\frac{2}{5}} \frac{\gamma_2 H_1}{R^6} \sum_{\mu} C(415; -\mu\mu) C(112; \mu-\kappa) Y_{4\mu} (\vec{\omega}_1) \\ &\quad \times Y_{2\kappa-\mu} (\vec{\omega}_2) . \end{aligned} \quad (B-6)$$

Similarly for $\mu_{\kappa}^{(2)}$, by just interchanging the subscripts 1 and 2. For the total $\vec{\mu} = \vec{\mu}^{(1)} + \vec{\mu}^{(2)}$, we have in terms of coefficients D_{κ} ,

$$\mu_{\kappa} = 4\pi \sum_{\substack{\lambda_1 \mu_1 \\ \lambda_2 \mu_2}} D_{\kappa} (\lambda_1 \mu_1 \lambda_2 \mu_2; R) Y_{\lambda_1 \mu_1} (\vec{\omega}_1) Y_{\lambda_2 \mu_2} (\vec{\omega}_2) , \quad (B-7)$$

and so comparing this to (B-4) we have

$$\begin{aligned}
 D_{\kappa} (2 \kappa 00) &= \frac{\alpha_2 Q_1}{R^4} \sqrt{3} (-)^{\kappa} C(213; -\kappa\kappa) \\
 D_{\kappa} (00 2 \kappa) &= \frac{\alpha_1 Q_2}{R^4} \sqrt{3} (-)^{\kappa} C(213; -\kappa\kappa) \\
 D_{\kappa} (2 \mu 2 \kappa-\mu) &= \frac{\gamma_2 Q_1}{R^4} \sqrt{\frac{2}{5}} C(213; -\mu\mu) C(112; \mu-\kappa) \\
 D_{\kappa} (2 \kappa-\mu 2 \mu) &= - \frac{\gamma_1 Q_2}{R^4} \sqrt{\frac{2}{5}} C(213; -\mu\mu) C(112; \mu-\kappa) \\
 D_{\kappa} (4 \kappa 00) &= \frac{\alpha_2 H_1}{R^4} \sqrt{5} (-)^{\kappa} C(415; -\kappa\kappa) \\
 D_{\kappa} (00 4 \kappa) &= - \frac{\alpha_1 H_2}{R^4} \sqrt{5} (-)^{\kappa} C(415; -\kappa\kappa) \\
 D_{\kappa} (4 \kappa 2 \kappa-\mu) &= \frac{\gamma_2 H_1}{R^6} \sqrt{\frac{2}{5}} C(415; \mu\mu) C(112; \mu-\kappa) \\
 D_{\kappa} (2 \kappa-\mu 4 \kappa) &= - \frac{\gamma_1 H_2}{R^6} \sqrt{\frac{2}{5}} C(415; \mu\mu) C(112; \mu-\kappa) \quad (B-8)
 \end{aligned}$$

where κ and μ can take values 0, ± 1 .

Substituting into the binary absorption coefficient

$$\begin{aligned}
 \tilde{\alpha}_1 &= \int d\nu \frac{\alpha(\nu)}{\nu} \begin{pmatrix} n_O \\ n_1 \end{pmatrix} \begin{pmatrix} n_O \\ n_2 \end{pmatrix} = \frac{4\pi^2 e^2 a_O^5 n_O^2}{3\hbar C} \sum_{\lambda_1 \lambda_2} \sum_{J_1 J_2} P_{J_1} P_{J_2} C(J_1 \lambda_1 J_1'; 00)^2 \\
 &\times C(J_2 \lambda_2 J_2'; 00)^2 \int_0^\infty |B(\lambda_1 \lambda_2 L\Lambda)|^2 g(R) \\
 &\times 4\pi R^2 dR, \quad (B-9)
 \end{aligned}$$

where

$$B(\lambda_1 \lambda_2 L\Lambda) = | v_1 J_1 | < v_2 J_2 | A(\lambda_1 \lambda_2 L\Lambda) | v_2' J_2' > | v_1' J_1' > \quad (B-10)$$

and

$$A(\lambda_1 \lambda_2 L\Lambda) = \left(\frac{2L+1}{3} \right)^{\frac{1}{2}} \sum_{\kappa \mu_1 \mu_2} D_{\kappa} (\lambda_1 \mu_1 \lambda_2 \mu_2) \\ \times C(\Lambda L 1; \kappa 0) C(\lambda_1 \lambda_2 \Lambda; \mu_1 \mu_2) \quad (B-11)$$

leads to the solution in Chapter 3 (equation 3 - 8) in which the Clebsch-Gordan coefficients (Rose, 1957) are

$$C(J 0 J'; 00)^2 = \delta_{JJ'} \\ C(J 2 J-2; 00)^2 = \frac{3J(J-1)}{2(2J-1)(2J+1)} \\ C(J 2 J; 00)^2 = \frac{J(J+1)}{(2J-1)(2J+3)} \\ C(J 2 J+2; 00)^2 = \frac{3(J+1)(J+2)}{2(2J+1)(2J+3)} \\ C(J 4 J-4; 00)^2 = \frac{35J(J-3)(J-2)(J-1)}{3(2J-5)(2J-3)(2J-1)(2J+1)} \\ C(J 4 J-2; 00)^2 = \frac{5J(J-2)(J-1)(J+1)}{2(2J-5)(2J-1)(2J+1)(2J+3)} \\ C(J 4 J; 00)^2 = \frac{9J(J-1)(J+1)(J+2)}{4(2J-3)(2J-1)(2J+3)(2J+5)} \\ C(J 4 J+2; 00)^2 = \frac{5J(J+1)(J+2)(J+3)}{2(2J-1)(2J+1)(2J+3)(2J+7)} \\ C(J 4 J+4; 00)^2 = \frac{35(J+1)(J+2)(J+3)(J+4)}{8(2J+1)(2J+3)(2J+5)(2J+7)} . \quad (B-12)$$

APPENDIX C

Quadrupole-moment matrix elements of H₂ in supplement to the matrix elements given by Birnbaum and Poll (1969)*

Herman et al. (1970) have developed analytic expressions for vibration-rotation wave functions for gound electronic state diatomic molecules having an arbitrary internuclear potential expressed as a power series about the equilibrium separation. Using these wave functions, the matrix elements for $\Delta v = 2$ can be expressed (Tipping and Herman, 1970) as

$$\langle 2J' | Q | 0J \rangle^2 = \langle 20 | Q | 00 \rangle^2 F_0^2(m) , \quad (C-1)$$

where $F_0^2(m)$ is a complicated expression, but can be written in short as

$$F_0^2(m) = 1 + mA + m^2B , \quad (C-2)$$

where $m = \frac{J'(J'+1) - J(J+1)}{2}$, A and B are J dependent constants; eq. (C-1) can be rewritten as

$$\langle 2J' | Q | 0J \rangle = \langle 20 | Q | 00 \rangle [1 + mA + m^2B]^{\frac{1}{2}} . \quad (C-3)$$

Instead of doing complicated calculations, A and B may be obtained by fitting matrix elements from Birnbaum and Poll (1969) to (C-3), and extrapolating to obtain $\langle 03 | Q | 25 \rangle$, $\langle 02 | Q | 20 \rangle$ and $\langle 03 | Q | 21 \rangle$. Matrix elements computed by this extrapolation were found to agree within 1% with results using A, B and $F_0^2(m)$ calculated by the method of Herman et al. (1970) with Q expressed in term of power series of $\frac{r-r_e}{r_e}$. This expression

*Method suggested by R. H. Tipping.

does not work for the Q-branch, as m would always equal 0, so

$\langle 03 \mid Q \mid 23 \rangle$ was obtained instead by means of extrapolation with

$$\langle 2J \mid Q \mid 0J \rangle = \langle 20 \mid Q \mid 00 \rangle [1 + J(J+1)A] . \quad (C-4)$$

ACKNOWLEDGMENTS

I would like to express my grateful thanks to Professor S. P. Reddy, Chairman of the Supervisory Committee, for his support throughout the course of this work and his suggestion of the first overtone experiments.

My gratitude is due to Professor S. W. Breckon, Head of the Department of Physics, and Professor C. W. Cho, for their continued interest in this research. Thanks are also due to faculty members of the Physics Department who have helped in this research, in particular, to Dr. M. J. Clouter for helpful conversations about the thermodynamics property, and ortho-para conversion of H₂, and Dr. R. Tipping for discussion on the first overtone quadrupole moment matrix elements.

Conversations with Dr. A. R. McKellar of NRC and his early supply of his notes from Poll have been helpful. I would like to thank him for his courtesy.

All but the mixtures experiments in this thesis were carried out in collaboration with Dr. N. H. Rich; my thanks to him and for his continued interest and initiation of the radiation gain problem, and many valuable conversations with him.

Technical assistance of Messrs. P. Robinson and L. Feltham of the Technical Services, and T. White of the Machine Shop of the Department of Physics are gratefully acknowledged.

Finally, I acknowledge the financial assistance of Memorial University of Newfoundland in the form of a University fellowship, and also Dr. Reddy's NRC grant #A-2440, which have supported me during my graduate studies.

REFERENCES

- Audibert, M.M., Joffrin, C., and Ducuing, J. 1974. Chem. Phys. Letters 25, 158.
- Birnbaum, A. and Poll, J.D. 1969. J. Atmos. Sci. 26, 943.
- Bosomworth, D.R. and Gush, H.P. 1965. Can. J. Phys. 43, 751.
- Buckingham, A.D. and Pople, J.A. 1955. Trans. Far. Soc. 51, 1173.
- Chang, K.S. 1971. M.Sc. Thesis, Memorial University of Newfoundland, St. John's, Newfoundland.
- Christiansen, W.H. and Greenfield, E. 1973. Appl. Phys. Letters 23, 623.
- Crawford, M.F., Welsh, H.L., and Locke, J.L. 1949. Phys. Rev. 75, 1607.
- Delgarno, A., Allison, A.C., and Browne, J.C. 1969. J. Atmos. Sci. 26, 946.
- Dean, J.W. 1961. National Bureau of Standards Technical Note 120 (U.S. Department of Commerce, Washington, D.C., U.S.A.)
- Ducuing, J., Joffrin, C., and Coffinet, J.P. 1970. Opt. Comm. 2, 245.
- Foltz, J.V., Rank, D.H., and Wiggins, T.A. 1966. J. Mol. Spectrosc. 21, 203.
- Gibbs, P.W., Gray, C.G., Hunt, J.L., Reddy, S.P., Tipping, R.H., and Chang, K.S. 1974. Phys. Rev. Letters 33, 256.
- Goodwin, R.D., Diller, D.E., Roder, H.M., and Weber, L.A. 1963. J. Res. Natl. Bur. Standards 67A, 173.
- Hare, W.F. and Welsh, H.L. 1958. Can. J. Phys. 36, 88.
- Herman, R.M. 1970. J. Chem. Phys. 52, 2040.
- Herman, R.M., Tipping, R.H., and Short, S. 1970. J. Chem. Phys. 53, 595.
- Humphreys, C.J. 1953. J. Opt. Soc. Amer. 43, 1027.
- Karl, G. and Poll, J.D. 1967. J. Chem. Phys. 46, 2944.
- Karl, G., Obryk, E., and Poll, J.D. 1973. Can. J. Phys. 51, 2216.
- Kiss, Z.J. and Welsh, H.L. 1959. Can. J. Phys. 37, 1249.

- McKellar, A.R.W. and Welsh, H.L. 1971. Proc. Roy. Soc. (London) A 322, 421.
- Mactaggart, J.W. 1971. Ph.D. Thesis, University of Toronto, Toronto, Ontario.
- Mactaggart, J.W. and Hunt, J.L. 1969. Can. J. Phys. 47, 65.
- May, A.D., Degen, V., Stryland, J.C., and Welsh, H.L. 1961. Can. J. Phys. 39, 1769.
- May, A.D., Varghese, G., Stryland, J.C., and Welsh, H.L. 1964. Can. J. Phys. 42, 1058.
- Michels, A., Wassenaar, T., and Louwerse, P. 1954. Physica 20, 99.
- Plyler, E.K., Gilar, N.M., and Wiggins, T.A. 1952. J. Res. Natl. Bur. Standards 48, 221.
- Plyler, E.K., Blaine, L.R., and Tidwell, E.D. 1955. J. Res. Natl. Bur. Standards 55, 279.
- Poll, J.D. 1960. Ph.D. Thesis, University of Toronto, Toronto, Ontario.
- Poll, J.D. 1970. Proc. I.A.U. Symposium No. 40 on Planetary Atmospheres, Marfa, Texas; October, 1969 (Dordrecht, Reidel).
- Poll, J.D. 1974. Private communication.
- Reddy, S.P. and Chang, K.S. 1973. J. Mol. Spectrosc. 47, 22.
- Reddy, S.P. and Kuo, C.Z. 1971. J. Mol. Spectrosc. 37, 327.
- Reddy, S.P. and Lee, W.F. 1968. Can. J. Phys. 46, 1373.
- Sleator, W.W. and Phelps, E.R. 1925. Astrophys. J. 62, 28.
- Rose, M.E. 1957. Elementary Theory of Angular Momentum (John Wiley and Sons, New York).
- Tipping, R.H. and Herman, R.M. 1970. J. Mol. Spectrosc. 36, 404.
- Trappeniers, N.J., Wassenaar, T., and Wolkers, G.J. 1966. Physica 32, 1503.
- Van Kranendonk, J. 1957. Physica 23, 825.
- Van Kranendonk, J. 1958. Physica 24, 347.
- Van Kranendonk, J. and Kiss, Z.J. 1959. Can. J. Phys. 37, 1187.

- Varghese, G., Ghosh, S.N., and Reddy, S.P. 1972. J. Mol. Spectrosc. 41, 291.
- Varghese, G. and Reddy, S.P. 1969. Can. J. Phys. 47. 2745.
- Watanabe, A. 1971. Can. J. Phys. 49, 1320.
- Watanabe, A., Hunt, J.L., and Welsh, H.L. 1971. Can. J. Phys. 49, 860.
- Watanabe, A. and Welsh, H.L. 1965. Can. J. Phys. 43, 818.
- Watanabe, A. and Welsh, H.L. 1967. Can. J. Phys. 45, 2859.
- Welsh, H.L. 1972. MTP International Reviews of Science. Physical Chemistry, Vol 3; Spectroscopy (Butterworths, London).
- Welsh, H.L., Crawford, M.F., MacDonald, J.C.F., and Chisholm, D.A. 1951. Phys. Rev. 83, 1264.
- Welsh, H.L., Crawford, M.F., and Locke, J.L. 1949. Phys. Rev. 76, 580.
- Zaide^l, A.N. Prokof'ev, V.K., Raiskii, S.M., Slavnyi, V.A., and Shreider, E.Ya. 1970. Tables of Spectral Lines. (IFI/Plenum, New York-London).

PUBLICATIONS

PREVIOUS COPYRIGHTED MATERIALS NOT MICROFILMED

Collision-Induced Fundamental Band of H₂ in H₂-He and H₂-Ne
Mixtures at Different Temperatures.

S. Paddi Reddy and K.S. Chang

Journal of Molecular Spectroscopy, Volume 47, no. 1, July 1973

New Rotational Transition in the Hydrogen Molecule.

P.W. Gibbs, C.G. Gray, J.L. Hunt, S. Paddi Reddy, R.H. Tipping
and K.S. Chang

Physical Review Letters, Volume 33, no. 5, July 29, 1974

Collision-Induced Fundamental Band of H₂ in H₂-He and H₂-Ne Mixtures at Different Temperatures

S. PADDI REDDY AND K. S. CHANG

Department of Physics, Memorial University of Newfoundland, St. John's, Newfoundland, Canada

Reprinted from JOURNAL OF MOLECULAR SPECTROSCOPY, Volume 47, No. 1, July 1973
Copyright © 1973 by Academic Press, Inc. Printed in U.S.A.

Collision-Induced Fundamental Band of H₂ in H₂-He and H₂-Ne Mixtures at Different Temperatures ¹

S. PADDI REDDY AND K. S. CHANG

Department of Physics, Memorial University of Newfoundland, St. John's, Newfoundland, Canada

The collision-induced fundamental infrared absorption band of hydrogen in binary mixtures H₂-He and H₂-Ne at 77, 195, 273, and 298 K has been studied with absorption path lengths of 27 and 105 cm for gas densities up to 530 amagat for several base densities of hydrogen. In each of these mixtures the enhancement absorption profiles show, in addition to the usual splitting of the Q branch into the main Q_P and Q_R components, a splitting of the S(1) line into the S_P(1) and S_R(1) components at all the experimental temperatures and a secondary splitting of the main Q_P component into the Q_P(3) and Q_R(3) components at 273 and 298 K. The profiles of H₂-He at 77 K also show a splitting of the S(0) line into S_P(0) and S_R(0). Integrated absorption coefficients were measured and binary and ternary absorption coefficients were derived. Van Kranendonk's theory of the 'exponential-4' model for the induced dipole moment was applied to the experimental binary absorption coefficients. The quadrupolar parts of these coefficients were calculated from the known molecular parameters and were then subtracted from the experimental values to obtain the overlap parts. The overlap parameters λ and ρ , giving respectively the magnitude and range of the overlap moment, were determined for each of the mixtures by obtaining the best fit of the calculated overlap part of the binary absorption coefficient as a function of temperature to the experimental values of the overlap parts. The values of λ , ρ , and $\mu(\sigma)$ (the overlap induced dipole moment at the Lennard-Jones intermolecular diameter σ) are as follows:

Mixture	λ	ρ	$\mu(\sigma)$
H ₂ -He	5.6×10^{-3}	0.24 Å	$2.92 \times 10^{-2} ea_0$
H ₂ -Ne	9.0×10^{-3}	0.29 Å	$4.85 \times 10^{-2} ea_0$

INTRODUCTION

An isolated homonuclear diatomic molecule in its electronic ground state has no permanent electric dipole moment on account of the symmetry of its charge configuration. Consequently, unlike a polar molecule, it has no electric dipole absorption at its rotational or vibrational frequencies. However, an electric dipole moment can be induced in two or more colliding molecules by intermolecular forces because of an asymmetric distortion of the electron charge distribution during collisions. This induced dipole moment is modulated by the rotation, vibration, and relative translational motion of the colliding molecules and causes the phenomenon of collision-induced absorption in which normally forbidden molecular transitions occur. Broad and diffuse

¹ This research was supported in part by a grant (S. P. R.) from the National Research Council of Canada.

bands arising from collision-induced absorption were first observed in compressed oxygen and nitrogen by Crawford, Welsh, and Locke (1) and in compressed hydrogen by Welsh, Crawford, and Locke (2) in the regions of their fundamental vibrational frequencies. The collision-induced fundamental band of gaseous hydrogen has been studied over wide ranges of pressure and temperature and its general characteristics are mostly well understood [cf. Varghese and Reddy (3) and Varghese, Ghosh, and Reddy (4) and the references therein].

The general theory of the collision-induced absorption of the fundamental band of homonuclear diatomic gases has been given by Van Kranendonk (5, 6) who used the so-called 'exponential-4' model for the dipole moment induced by a colliding pair of molecules and the Lennard-Jones 12-6 potential for the intermolecular potential of the pair. According to the 'exponential-4' model the dipole moment induced in a colliding pair of molecules is considered to be the sum of two additive moments, each of them being a distinct function of the intermolecular separation R . One is the isotropic short-range electron overlap moment and is given by

$$\begin{aligned}\mu_{\text{overlap}}(R) &= \mu_0 \exp(-R/\rho) \\ &= \mu(\sigma) \exp[-(R - \sigma)/\rho] \\ &= \lambda e\sigma \exp[-(R - \sigma)/\rho].\end{aligned}\quad (1)$$

In this model the overlap dipole moment is characterized by the parameters μ_0 and ρ or $\mu(\sigma)$ and ρ or λ and ρ . In Eqs. (1) $\lambda = (\mu_0/e\sigma) \exp(-\sigma/\rho) = \mu(\sigma)/e\sigma$ is a dimensionless quantity which represents the magnitude of the overlap moment when the intermolecular separation is σ [corresponding to the Lennard-Jones intermolecular potential $V(\sigma) = 0$], ρ is the range of the overlap moment and e is the electronic charge. The second moment is the anisotropic long-range moment resulting from the polarization of one molecule by the quadrupole field of the other and may be represented by

$$\mu_{\text{quad}}(R) \propto [(Q_1' \alpha_2)^2 + (\alpha_1' Q_2)^2]/R^4. \quad (2)$$

Here Q_1' and α_1' are respectively the derivatives of the quadrupole moment and polarizability of molecule 1 with respect to its internuclear distance, and Q_2 and α_2 are the quadrupole moment and polarizability of molecule 2. The short-range moment contributes to the intensity of the broad Q lines (i.e., Q_{overlap}) ($\Delta J = 0$) and the long-range moment produces the $S(\Delta J = +2)$, Q (i.e., Q_Q ; $\Delta J = 0$), and $0(\Delta J = -2)$ lines. The quadrupolar induction part of the binary absorption coefficient of a given collision-induced band can be calculated from the theory in terms of known molecular constants of the colliding pairs. The parameters λ and ρ can be determined by fitting the theoretical binary absorption coefficient as a function of temperature to the experimental values of the binary absorption coefficient at several temperatures. For the pure hydrogen gas, this procedure was carried out by Hunt (7) [see also Van Kranendonk and Kiss (8)] for the experimental values of the binary absorption coefficients at 195 and 300 K and the values of λ and ρ were determined for the H₂-H₂ pair. However, prior to the present work, this type of fit has not been attempted for the binary mixtures of H₂ with foreign gases because of the inadequacy of the accurate values of the binary absorption coefficients over a wide temperature range.

The present investigation was designed to obtain reasonably accurate values of the binary absorption coefficients of the fundamental band of H₂ in H₂-He and H₂-Ne at four different temperatures in the range 77-298 K and to estimate the overlap parameters λ [and, hence, $\mu(\sigma)$] and ρ for these two mixtures. The present work on H₂-He at 195 K and 298 K and on H₂-Ne at 298 K is complimentary to the work of the previous investigators at McLennan Laboratory, University of Toronto [Chisholm and Welsh (9), Hare and Welsh (10), and Hunt (7)] and to that of Reddy and Lee (11) in our laboratory, respectively. Since the polarizabilities [α_2 in Eq. (2)] of He and Ne are small and their quadrupole moments [Q_2 in Eq. (2)] are zero, the main contribution to the absorption coefficients comes from the overlap parts (the reader will find later in this paper that the overlap part in these two mixtures contributes 84 to 97% to the total binary absorption coefficient in the temperature range 77-298 K). Moreover, since H₂, He, and Ne remain gaseous down to very low temperatures, the two binary mixtures under consideration provide a unique opportunity to study the behavior of the distortions of the electron clouds of the H₂-He and H₂-Ne pairs over a wide range of temperatures. Actually, the band was studied in the two mixtures for gas pressures up to 200 atm at 77, 195, 273, and 298 K. Integrated absorption coefficients were measured and the binary and ternary absorption coefficients were determined. The quadrupolar parts of the binary absorption coefficients were calculated from the theory (6) in terms of the molecular constants of the gases. In these calculations the matrix elements of the quadrupole moment of H₂ between the vibrational states $v = 0$ and 1, $\langle 0J|Q|1J' \rangle$ which have been found to be sensitive to the initial and final rotational quantum numbers J and J' of a transition [Karl and Poll (12) and Birnbaum and Poll (13)] were used. The overlap parts of the binary absorption coefficients were then obtained by subtracting the quadrupolar parts from the experimental values. The parameters λ , $\mu(\sigma)$, and ρ were determined for each of the mixtures by obtaining the best fit of the theoretical overlap parts of the binary absorption coefficients as a function of temperature to the experimental values of the overlap parts.

EXPERIMENTAL

Two transmission-type absorption cells were used to study the fundamental band of H₂ in binary mixtures of hydrogen with helium and neon. The first of these was used to study the band at 298, 273, and 195 K for gas densities up to 250 amagat. It was constructed of a stainless steel tube with a central bore of diameter 0.75 in. and a wall thickness 0.13 in. It has a sample path length 105 cm and was provided with a stainless steel light guide of rectangular cross-section 1 cm \times 0.5 cm. It was fitted with polished synthetic sapphire windows 1 in. in diameter and 0.5 cm thick. For the experiments at low temperatures the cell was provided with a cylindrical jacket, 3.4 in. in diameter and made of galvanized tin sheet, to contain the coolants. The jacket was insulated by a 2-in. layer of styrofoam. Frosting on the windows was prevented by providing a vacuum chamber at each end of the cell. These vacuum chambers were constructed of plexiglass and provided with quartz windows. The coolants used with the cell were ice (273 K) and dry ice-alcohol mixture (195 K).

The second cell which was used to study the band at liquid nitrogen temperature (77 K) for gas densities up to 540 amagat has a sample path length 27 cm at room

temperature. It was constructed of a stainless steel cylinder 3.2 in. in diameter with a central bore having a diameter 0.75 in. The details of the light guide and the windows of the cell are similar to those described for the first cell. The vacuum chamber at each end of the cell was made of stainless steel extension fitted with a plexiglass tubing to which a sapphire window was sealed. Frosting on the outer windows was prevented by passing current in the heating coils attached to the plexiglass tubings.

A water-cooled tungsten filament lamp with a sapphire window, prepared from a standard General Electric 750 W projection bulb filament, served as the source of infrared radiation. A Perkin-Elmer Model 112 single-beam double-pass spectrometer equipped with a LiF prism was used to record the spectrum of the band at 195, 273, and 298 K with the 105 cm absorption cell. To obtain the spectrum at 77 K with the second absorption cell, a Perkin-Elmer Model 112 G single-beam double-pass spectrometer in the first order of a Bausch and Lomb grating with 300 lines/mm blazed at 3.0 μ was used. An uncooled PbS detector was used with both spectrometers. The slits of the prism and grating spectrometers maintained respectively at 50 and 160 μ gave spectral resolutions of ~ 4.0 cm⁻¹ and 1.6 cm⁻¹, respectively, at the position of $Q(0)$ (4161 cm⁻¹) of the fundamental band of H₂. The spectral region was calibrated with the emission lines of mercury (14, 15) and neon (16) and the absorption peaks of atmospheric water vapor (15, 17) and 1-, 2-, 4-trichlorobenzene (18). The low- and high-frequency wings of the hydrogen fundamental band are overlapped by strong atmospheric water-vapor absorption. The effect of this absorption was reduced considerably by flushing the entire optical path outside the absorption cells with carefully dried air.

The procedure to obtain profiles of enhancement of absorption of the fundamental band of H₂ in binary mixtures of hydrogen with helium and neon was similar to the one described by Reddy and Lee (11). 'Ultra-High Pure' hydrogen and research grade neon, both supplied by Matheson of Canada, and commercial grade helium, supplied by Canadian Liquid Air, were used in the experiments. All the gases were further purified by slowly passing them through a liquid nitrogen trap. In a given experiment the base density of hydrogen was kept constant and the enhancement of absorption of the fundamental band was studied for a series of pressures of the binary gas mixtures of hydrogen with helium or neon. For the experiments with the 105 cm cell two thermal compressors were used to develop the required pressures of helium and neon and for those with the 26.7 cm cell a mercury-column gas compressor was used instead.

The densities of hydrogen at 298, 273, and 195 K were obtained from its isothermal data given by Michels *et al.* (19). Its densities at 77 K for pressures up to 100 atm were taken directly from Dean (20) and those for pressures above 100 atm were deduced from the equation of state for H₂ whose virial coefficients at 77 K were calculated by a least-square polynomial fit of each of the coefficients as a function of temperature (19). The densities of helium at 298 and 273 K were obtained from Michels and Wouters (21). Its densities at 195 and 77 K for pressures up to 100 atm were taken from Mann (22) and those for pressures above 100 atm were extrapolated using the virial equation of state of gases (23) whose coefficients were determined from the available isothermal data up to 100 atm. The densities of neon at 298 and 273 K were taken from Michels *et al.* (24) and those at 195 and 77 K were determined from the data given by Timmerhaus (25). For a given experiment the base density ρ_a of hydrogen was directly obtained from its isothermal data and the partial densities ρ_b of helium or neon in a

binary mixture with hydrogen were obtained by the interpolation method described by Reddy and Cho (26).

The enhancement in the absorption coefficient per unit path length $\alpha_{en}(\nu)$ at a given wave number ν in cm^{-1} due to the addition of a perturbing gas at a density ρ_b into the absorption cell of sample path length l containing hydrogen at a fixed base density ρ_a is given by

$$\alpha_{en}(\nu) = (1/l) \ln [I_1(\nu)/I_2(\nu)], \quad (3)$$

(i.e., $I_2(\nu) = I_1(\nu) \exp[-\alpha_{en}(\nu)l]$), where $I_1(\nu)$ is the intensity transmitted by the absorbing gas in the cell and $I_2(\nu)$ is the intensity transmitted by the binary gas mixture in the cell. For each experiment background recorder traces were taken with a known base pressure of hydrogen in the cell. The pen deflection for infinite absorption, i.e., for zero radiation entering the spectrometer, was checked several times during the experiment. The recorder traces were reduced with the help of a standard logarithmic scale by measuring $\log_{10}[I_1(\nu)/I_2(\nu)]$ at intervals of 5 cm^{-1} in the regions of the band-origin and the $S(1)$ line and at intervals of 10 cm^{-1} in the rest of the spectral region of the band. For some experiments $I_1(\nu)$ and $I_2(\nu)$ were read directly from each trace of enhancement and the values of $\log_{10}(I_1/I_2)$ were derived later. The integrated absorption coefficients of the band per unit sample path length $\int \alpha_{en}(\nu) d\nu$ in cm^{-2} were obtained from the areas under the profiles of the enhancement of absorption.

EXPERIMENTAL RESULTS

For experiments with each perturbing gas He or Ne, several base densities of gaseous H_2 in the range 11 to 60 amagat were used. The experimental conditions under which the profiles of the enhancement of absorption were obtained are summarized in Table I. First, the experimental profiles of the band are presented, their features are discussed, and then the binary and ternary absorption coefficients of the band are derived.

TABLE I
SUMMARY OF EXPERIMENTAL CONDITIONS

Mixture	Temperature (K)	Sample path length of the cell (cm)	Maximum density of the perturbing gas (amagat)	Number of mixture densities
$\text{H}_2\text{-He}$	298	105.2	160	24
$\text{H}_2\text{-He}$	273	105.2	240	37
$\text{H}_2\text{-He}$	195	105.0	210	16
$\text{H}_2\text{-He}$	77	26.6	450	14
$\text{H}_2\text{-Ne}$	298	105.2	90	17
$\text{H}_2\text{-Ne}$	273	105.2	100	15
$\text{H}_2\text{-Ne}$	195	105.0	180	16
$\text{H}_2\text{-Ne}$	77	26.6	510	18

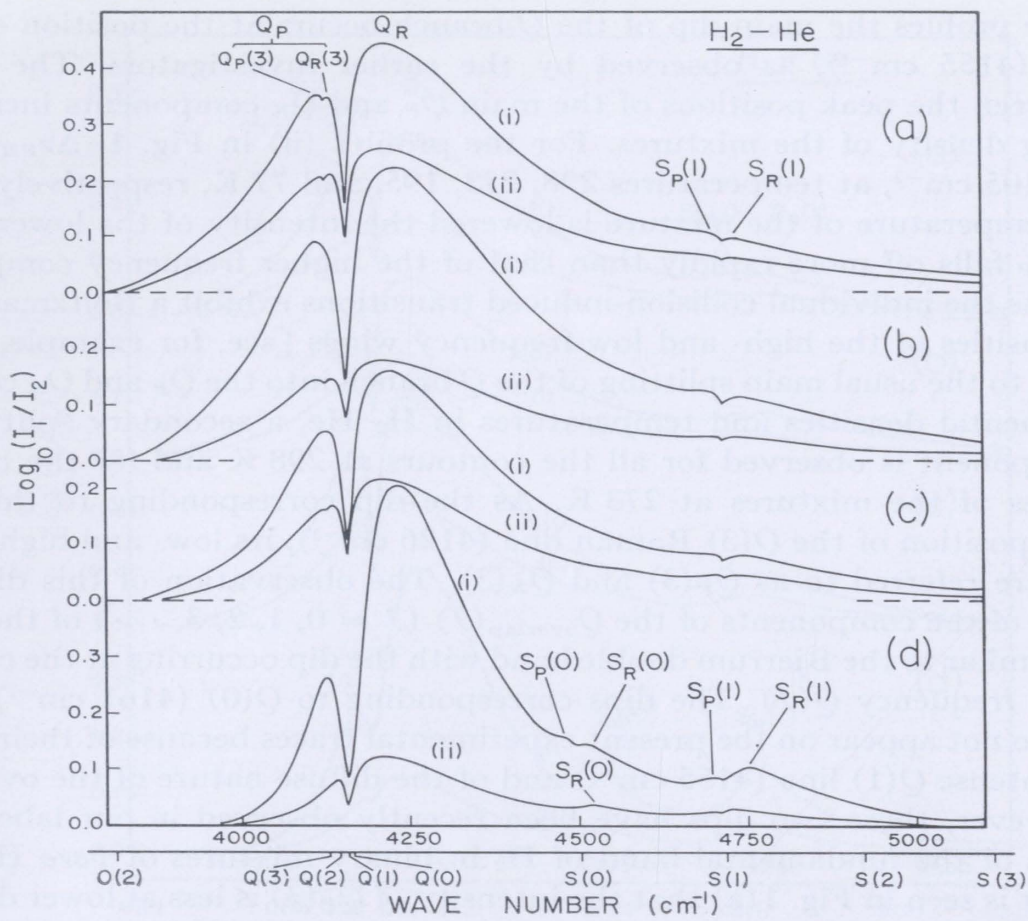


FIG. 1. Profiles of the enhancement of absorption of the collision-induced fundamental band of H₂ in H₂-He mixtures:

	<i>T</i> (K)	<i>l</i> (cm)	ρ_{H_2} (amagat)	ρ_{He} for (i) (amagat)	ρ_{He} for (ii) (amagat)
(a)	298	105.2	18.7	138	79
(b)	273	105.2	13.1	232	85
(c)	195	105.0	14.4	207	111
(d)	77	26.6	59.3	450	104

Profiles of the Enhancement of Absorption

Profiles of H₂-He Mixtures

Examples of typical sets of enhancement absorption profiles of the band obtained in H₂-He mixtures at 298, 273, and 195 K with the 105 cm cell and at 77 K with the 27 cm cell are presented in Fig. 1. At each temperature values of log₁₀(I₁/I₂) are plotted against wave number (cm⁻¹) for two representative total densities of the mixture with a fixed base density of hydrogen. The positions of the transitions O(2), Q(*J*), and S(*J*) with *J* = 0 to 3, calculated from the constants of molecular hydrogen obtained from the high resolution Raman data of the low pressure gas (26), are marked on the wave number axis.

In all these profiles the main dip of the Q -branch occurs at the position of the $Q(1)$ Raman line (4155 cm^{-1}), as observed by the earlier investigators. The separation $\Delta\nu_{PR}^{\max}$ between the peak positions of the main Q_P and Q_R components increases with the increasing density of the mixtures. For the profiles (ii) in Fig. 1, $\Delta\nu_{PR}^{\max}$ are 90, 120, 90, and 105 cm^{-1} , at temperatures 298, 273, 195, and 77 K, respectively. It is seen that as the temperature of the mixture is lowered the intensity of the lower frequency component Q_P falls off more rapidly than that of the higher frequency component Q_R . This is because the individual collision-induced transitions exhibit a Boltzmann relation between intensities of the high- and low-frequency wings [see, for example, Ref. (4)].

In addition to the usual main splitting of the Q branch into the Q_P and Q_R components at all experimental densities and temperatures in $\text{H}_2\text{-He}$, a secondary splitting of the main Q_P component is observed for all the contours at 298 K and for the contours at lower densities of the mixtures at 273 K. As the dip corresponding to this splitting occurs at the position of the $Q(3)$ Raman line (4126 cm^{-1}), its low- and high-frequency components are referred to as $Q_P(3)$ and $Q_R(3)$. The observation of this dip suggests that each one of the components of the $Q_{\text{Overlap}}(J)$ ($J = 0, 1, 2, 3, \dots$) of the Q branch has a profile similar to the Bjerrum double band with the dip occurring at the corresponding molecular frequency $Q(J)$. The dips corresponding to $Q(0)$ (4161 cm^{-1}) and $Q(2)$ (4143 cm^{-1}) do not appear on the present experimental traces because of their proximity to the more intense $Q(1)$ line (4155 cm^{-1}) and of the diffuse nature of the overlap components. However, these two dips have been recently observed in our laboratory (4) in the profiles of the fundamental band of H_2 in binary mixtures of *para* H_2 with Ar, Kr, and Xe. It is seen in Fig. 1(a) that the intensity of $Q_P(3)$ is less at lower density and more at higher density than the corresponding intensity of $Q_R(3)$. This can be explained on the basis of the increase in the peak separations of the individual $Q_P(J)$ and $Q_R(J)$ components with increasing density of the mixture. For the contours at 273 K [Fig. 1(b)] the splitting of the $Q_{\text{Overlap}}(3)$ component into $Q_P(3)$ and $Q_R(3)$ disappears as the density of the mixture is increased.

The striking feature of the $S(1)$ line at all the four experimental temperatures is its splitting into the low- and high-frequency components $S_P(1)$ and $S_R(1)$ with the minimum occurring at the position of the calculated $S(1)$ Raman line (4713 cm^{-1}). This splitting of the profiles at lower densities at 77 K is not well pronounced; at lower densities the $S_R(1)$ peak occurs at positions about $35\text{--}40\text{ cm}^{-1}$ higher than that of the $S(1)$ Raman line with no indication of $S_P(1)$ peak.

For the profiles of $\text{H}_2\text{-He}$ at higher densities in the experiments at 77 K, there is a clear indication of the splitting of the $S(0)$ line into $S_P(0)$ and $S_R(0)$ components with the minimum between them occurring at the position of the calculated $S(0)$ Raman line (4498 cm^{-1}). This is the first time that such a dip has been observed for the $S(0)$ line of the collision-induced fundamental band of gaseous hydrogen.

Profiles of $\text{H}_2\text{-Ne Mixtures}$

Representative sets of enhancement absorption profiles of the H_2 fundamental band obtained in $\text{H}_2\text{-Ne}$ mixtures at 298, 273, and 195 K with the 105 cm cell and at 77 K with the 27 cm cell are given in Fig. 2. The behavior of the main splitting of the Q branch into Q_P and Q_R in $\text{H}_2\text{-Ne}$ mixtures at all the four experimental temperatures is

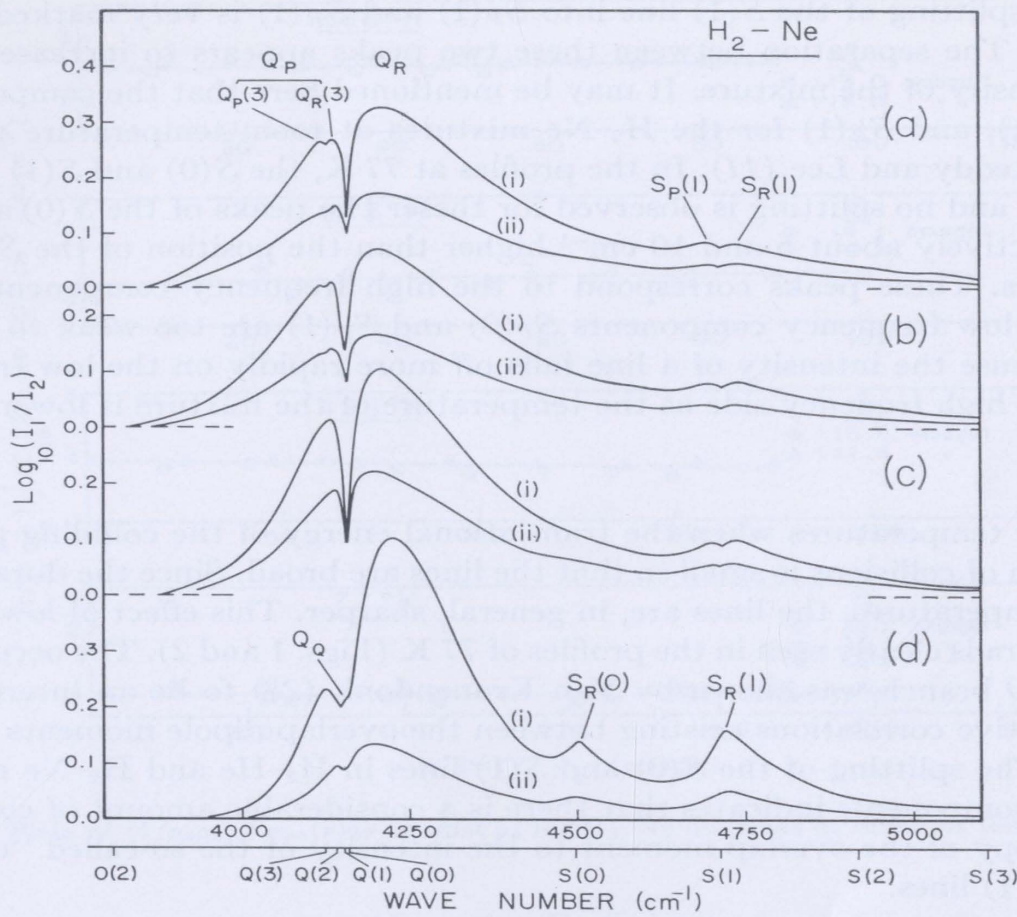


FIG. 2. Profiles of the enhancement of absorption of the collision-induced fundamental band of H₂ in H₂-Ne mixtures:

	<i>T</i> (K)	<i>l</i> (cm)	ρ_{H_2} (amagat)	ρ_{Ne} for (i) (amagat)	ρ_{Ne} for (ii) (amagat)
(a)	298	105.2	15.0	89	47
(b)	273	105.2	14.1	100	52
(c)	195	105.0	13.8	149	80
(d)	77	26.6	36.2	445	109

similar to that discussed previously for the H₂-He mixtures. For the experimental profiles (ii) in Fig. 2, the separations $\Delta\nu_{PR}^{\max}$ are 85, 80, 85, and 100 cm⁻¹ and at temperatures 298, 273, 195, and 77 K, respectively. One additional feature of the *Q* branch in H₂-Ne mixtures at 77 K is the appearance of the (quadrupolar) *Q*_Q component at high densities of the mixture. At 77 K, only the two lowest rotational states *J* = 0 (para H₂) and *J* = 1 (ortho H₂) are populated. For the enhancement absorption profiles of the band in binary mixtures of hydrogen with monoatomic perturbing gases, only single transitions can occur for the *Q*_Q components as well as for the *S* lines. Since the quadrupolar single transition *J* = 0 → *J'* = 0 is forbidden, the only quadrupolar component that occurs at 77 K is *Q*_Q(1).

The splitting in the main *Q*_P component of the *Q* branch into *Q*_P(3) and *Q*_R(3) is also observed for the profiles of H₂-Ne at 298 and 273 K for higher densities of the mix-

tures. The splitting of the $S(1)$ line into $S_P(1)$ and $S_R(1)$ is very marked at 298, 273, and 195 K. The separation between these two peaks appears to increase with the increasing density of the mixture. It may be mentioned here that the components $Q_P(3)$, $Q_R(3)$, $S_P(1)$, and $S_R(1)$ for the H_2 -Ne mixtures at room temperature were first observed by Reddy and Lee (11). In the profiles at 77 K, the $S(0)$ and $S(1)$ lines are well pronounced and no splitting is observed for these. The peaks of the $S(0)$ and $S(1)$ lines occur respectively about 5 and 10 cm^{-1} higher than the position of the $S(0)$ and $S(2)$ Raman lines. These peaks correspond to the high frequency components $S_R(0)$ and $S_R(1)$. The low frequency components $S_P(0)$ and $S_P(1)$ are too weak to be observed. This is because the intensity of a line falls off more rapidly on the low frequency side than on the high frequency side as the temperature of the mixture is lowered.

Discussion

At higher temperatures when the translational energy of the colliding pairs is large, the duration of collisions is small so that the lines are broad. Since the duration is larger at lower temperatures, the lines are, in general, sharper. This effect of low temperature on the spectra is clearly seen in the profiles of 77 K (Figs. 1 and 2). The occurrence of the dip in the Q branch was shown by Van Kranendonk (28) to be an interference effect due to negative correlations existing between the overlap dipole moments in successive collisions. The splitting of the $S(0)$ and $S(1)$ lines in H_2 -He and H_2 -Ne mixtures into S_P and S_R components indicates that there is a considerable amount of contribution of the anisotropy of the overlap moment to the intensity of the so-called "quadrupolar" $S(0)$ and $S(1)$ lines.

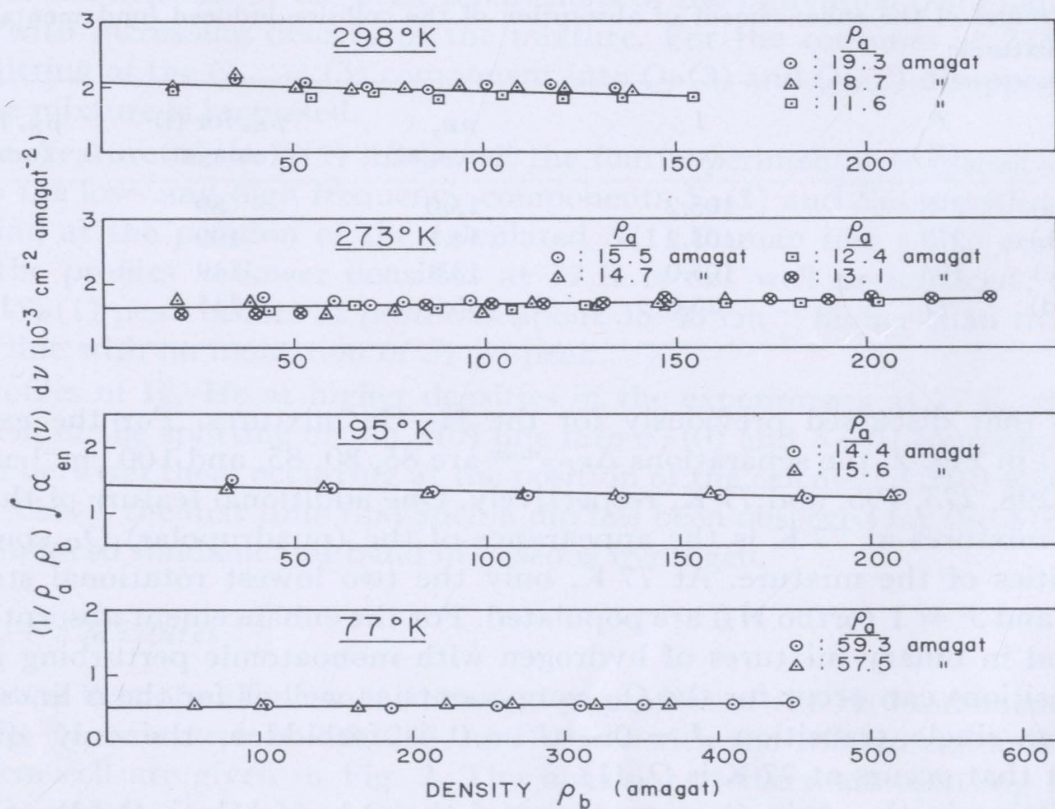


FIG. 3. Plots of $(1/\rho_a\rho_b)\int \alpha_{en}(\nu)d\nu$ against ρ_b for H_2 -He mixtures at different temperatures.

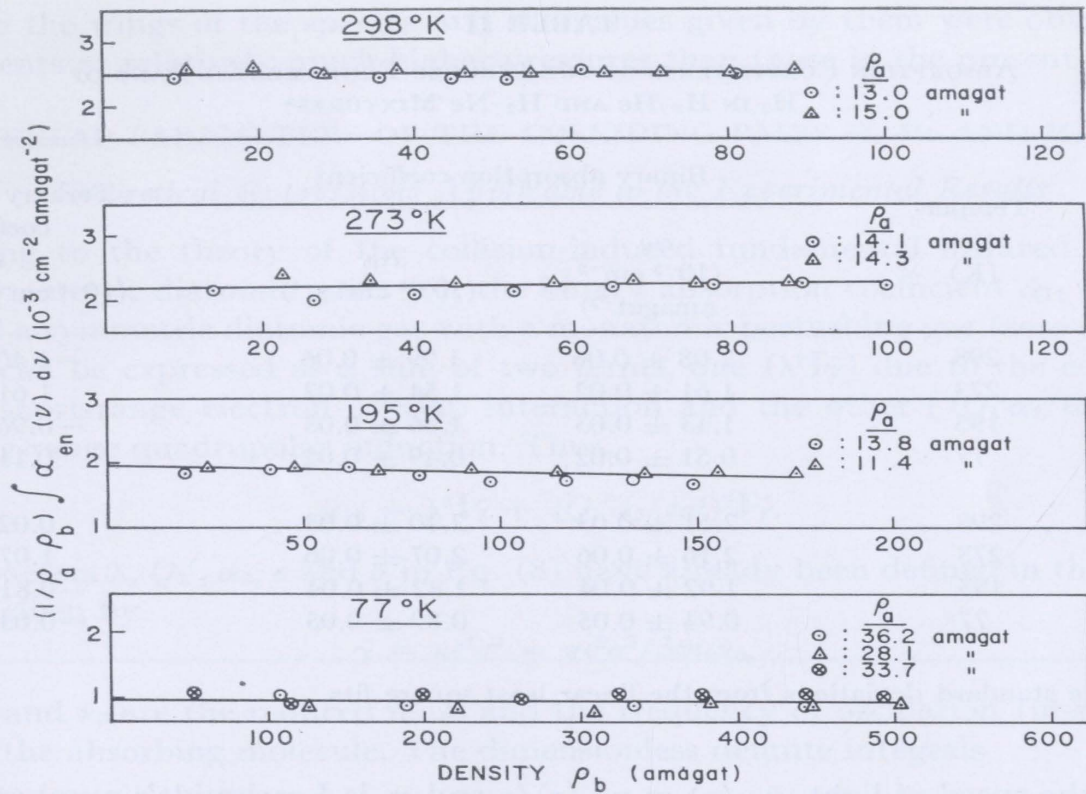


FIG. 4. Plots of $(1/\rho_a \rho_b) \int \alpha_{en}(\nu) d\nu$ against ρ_b for H₂-Ne mixtures at different temperatures.

Absorption Coefficients

The values of $\int \alpha_{en}(\nu) d\nu$ (cm⁻²) obtained for the profiles of the enhancement of absorption of the band in H₂-He and H₂-Ne mixtures at all the experimental temperatures were found to satisfy the relation

$$\int \alpha_{en}(\nu) d\nu = \alpha_{1b} \rho_a \rho_b + \alpha_{2b} \rho_a \rho_b^2, \quad (4)$$

where ρ_a and ρ_b are the partial densities of hydrogen and the perturbing gas in a mixture, respectively, and α_{1b} and α_{2b} are the binary and ternary absorption coefficients, respectively. Plots of $(1/\rho_a \rho_b) \int \alpha_{en}(\nu) d\nu$ versus ρ_b for H₂-He and H₂-Ne are shown in Figs. 3 and 4, respectively. The intercepts and the slopes of the straight lines obtained give the binary and ternary absorption coefficients, respectively. The values of these coefficients obtained by a least-square fit of the experimental data are given in Table II. It is noted that the ternary absorption coefficients for H₂-He and H₂-Ne are very small compared to their binary absorption coefficients. Therefore, most of the intensity of the induced absorption in these mixtures at moderate densities arises from the binary collisions. For the purpose of comparison with the theory the integrated absorption coefficients can be represented by the expression

$$c \int \tilde{\alpha}_{en}(\nu) d\nu = \tilde{\alpha}_{1b} \rho_a \rho_b n_0^3 + \tilde{\alpha}_{2b} \rho_a \rho_b n_0^3, \quad (5)$$

TABLE II
ABSORPTION COEFFICIENTS OF THE INDUCED FUNDAMENTAL BAND OF
 H_2 IN H_2 -He AND H_2 -Ne MIXTURES^a

Mixture	Temper- ature (K)	Binary absorption coefficient		Ternary absorption coefficient α_{2b} ($10^{-6} \text{ cm}^{-2} \text{ amagat}^{-3}$)
		α_{1b} (10^{-3} cm^{-2} amagat $^{-2}$)	$\tilde{\alpha}_{1b}$ ($10^{-35} \text{ cm}^6 \text{ s}^{-1}$)	
H_2 -He	298	2.08 ± 0.06	1.99 ± 0.06	-1.40 ± 0.64
H_2 -He	273	1.61 ± 0.02	1.54 ± 0.02	1.61 ± 0.15
H_2 -He	195	1.43 ± 0.03	1.36 ± 0.03	-0.96 ± 0.22
H_2 -He	77	0.51 ± 0.02	0.49 ± 0.02	0.11 ± 0.05
H_2 -Ne	298	2.51 ± 0.03	2.40 ± 0.03	0.02 ± 0.52
H_2 -Ne	273	2.16 ± 0.06	2.07 ± 0.06	1.07 ± 0.99
H_2 -Ne	195	1.92 ± 0.04	1.82 ± 0.04	-0.81 ± 0.37
H_2 -Ne	77	0.94 ± 0.05	0.89 ± 0.05	-0.03 ± 0.14

^a Errors are standard deviations from the linear least-square fits.

where c is the speed of light, $\tilde{\alpha}_{en}(\nu) = \alpha_{en}(\nu)/\nu$ and n_0 is Loschmidt's number (number of molecules per cm^3 at STP: $2.687 \times 10^{19} \text{ cm}^{-3}$). The experimental absorption coefficients α_{1b} ($\text{cm}^{-2} \text{ amagat}^{-2}$) and α_{2b} ($\text{cm}^{-2} \text{ amagat}^{-3}$) are related to the new coefficients $\tilde{\alpha}_{1b}$ ($\text{cm}^6 \text{ s}^{-1}$) and $\tilde{\alpha}_{2b}$ ($\text{cm}^9 \text{ s}^{-1}$), respectively, by

$$\tilde{\alpha}_{1b} = (c/n_0^2)\alpha_{1b}/\bar{\nu}; \quad \tilde{\alpha}_{2b} = (c/n_0^3)\alpha_{2b}/\bar{\nu}, \quad (6)$$

where $\bar{\nu}$, the effective band center, is given by

$$\bar{\nu} = \int \alpha_{en}(\nu) d\nu / \int \alpha_{en}(\nu) \nu^{-1} d\nu. \quad (7)$$

The new binary and ternary coefficients $\tilde{\alpha}_{1b}$ and $\tilde{\alpha}_{2b}$ represent the transition probabilities induced in collisions of types *a-b* and *b-a-b*, respectively. The average values of $\bar{\nu}$ for H_2 -He and H_2 -Ne at 298, 273, 195, and 77 K are 4335, 4388, 4354, and 4373 cm^{-1} , respectively. The values of $\tilde{\alpha}_{1b}$ ($\text{cm}^6 \text{ s}^{-1}$) for H_2 -He and H_2 -Ne are also included in Table II.

The values of the binary absorption coefficients in H_2 -He at 298 and 195 K obtained in the present work are considerably higher, and that at 77 K is considerably lower than the corresponding values obtained by earlier researchers [Refs. (7, 9, 10)]. To check the consistency of the experimental results of the present work, we measured the absorption of the induced fundamental band of H_2 in the pure gas at room temperature and obtained a value of $(2.44 \pm 0.02) \times 10^{-3} \text{ cm}^{-2} \text{ amagat}^{-2}$ for the binary absorption coefficient which was in close agreement with the values obtained in Refs. (9, 10, 7). The discrepancy between the values obtained in the present work and those obtained by the earlier researchers for H_2 -He may be attributed to the following facts: The earlier researchers might have experienced considerable uncertainty in determining the ab-

sorption in the wings of the spectra and the values given by them were obtained from measurements at relatively much higher pressures than those in the present work.

OVERLAP PARAMETERS OF THE COLLIDING PAIRS H₂-He AND H₂-Ne

Theoretical Expressions Applicable to the Experimental Results

According to the theory of the collision-induced fundamental infrared absorption band of symmetric diatomic gases (6), the binary absorption coefficient $\tilde{\alpha}_{1b}$ of a binary mixture of a symmetric diatomic gas with a monatomic perturbing gas (zero quadrupole moment) can be expressed as a sum of two terms, one ($\lambda^2 \mathbf{I}\tilde{\gamma}$) due to the contribution from the short-range electron overlap interaction and the other [$(Q_1' \alpha_2 / e\sigma^4)^2 \mathbf{J}\tilde{\gamma}$] due to the long-range quadrupolar induction. Thus,

$$\tilde{\alpha}_{1b} = \lambda^2 \mathbf{I}\tilde{\gamma} + (Q_1' \alpha_2 / e\sigma^4)^2 \mathbf{J}\tilde{\gamma}. \quad (8)$$

The parameters λ , Q_1' , α_2 , e and σ in Eq. (8) have already been defined in the introduction. $\tilde{\gamma}$ is given by

$$\tilde{\gamma} = \kappa e^2 \sigma^3 = \pi e^2 \sigma^3 / 3m_0 \nu_0, \quad (9)$$

where m_0 and ν_0 are the reduced mass and the frequency of oscillation (in s^{-1}), respectively, of the absorbing molecule. The dimensionless definite integrals

$$\mathbf{I} = 4\pi \int_0^\infty \exp[-2(x-1)\sigma/\rho] g_0(x) x^2 dx \quad (10)$$

and

$$\mathbf{J} = 12\pi \int_0^\infty x^{-8} g_0(x) x^2 dx, \quad (11)$$

where $x = R^* = R/\sigma$, R being the intermolecular separation and $g_0(x)$ is the low density limit of the pair distribution function. At higher temperatures, $g_0(x)$ is equal to the classical value, $\exp[-V(x)/kT]$. At intermediate temperatures, $g_0(x)$ may be expanded as an asymptotic series in powers of Planck's constant h . The resulting expressions for \mathbf{I} and \mathbf{J} are

$$\mathbf{I} = \mathbf{I}_{c1} - \Lambda^{*2} \mathbf{I}^{(2)} + \Lambda^{*4} \mathbf{I}^{(4)} + \dots, \quad (12)$$

and

$$\mathbf{J} = \mathbf{J}_{c1} - \Lambda^{*4} \mathbf{J}^{(2)} + \Lambda^{*4} \mathbf{J}^{(4)} + \dots, \quad (13)$$

where $\mathbf{I}^{(2)}$, $\mathbf{I}^{(4)}$, $\mathbf{J}^{(2)}$, and $\mathbf{J}^{(4)}$ are the quantum corrections, and

$$\Lambda^* = (h^2 / 2m_{00} \epsilon \sigma^2)^{\frac{1}{2}} \quad (14)$$

is the reduced mean de Broglie wavelength. Here m_{00} is the reduced mass of the colliding pairs of molecules and ϵ is the depth of the Lennard-Jones intermolecular potential.

Calculation of the Quadrupolar Parts ($\tilde{\alpha}_{1b,quad}$) of the Binary Absorption Coefficients

Recent theoretical calculations of Karl and Poll (12) and Birnbaum and Poll (13) indicate that the matrix elements of the quadrupole moment between different vibrational states of H₂, $\langle vJ | Q | v'J' \rangle$, are sensitive to the values of J and J' . Consequently,

TABLE III
MOLECULAR CONSTANTS FOR H₂-He AND H₂-Ne MIXTURES

Mixture	T (K)	ϵ/k (K)	σ (Å)	T^*	$\tilde{\gamma}$ (10 ⁻³² cm ⁶ s ⁻¹)	α_2/a_0^3 (for per- turbator)	Λ^*	J
H ₂ -He	298	19.35	2.757	15.3	4.772	1.4	2.215	15.27
H ₂ -He	273	19.35	2.757	14.0	4.772	1.4	2.215	14.78
H ₂ -He	195	19.35	2.757	10.00	4.772	1.4	2.215	13.48
H ₂ -He	77	19.35	2.757	3.96	4.772	1.4	2.215	11.22
H ₂ -Ne	298	36.15	2.854	8.21	5.293	2.7	1.337	13.15
H ₂ -Ne	273	36.15	2.854	7.52	5.293	2.7	1.337	12.91
H ₂ -Ne	195	36.15	2.854	5.37	5.293	2.7	1.337	12.10
H ₂ -Ne	77	36.15	2.854	2.12	5.293	2.7	1.337	11.50

Q' in Eq. (8) is no longer constant. Its values for different transitions in the fundamental band of hydrogen are given by the approximate relation

$$Q' = \frac{1}{r_e(B/\omega)^{\frac{1}{2}}} \langle 0J | Q | 1J' \rangle. \quad (15)$$

The values of Q' were obtained from the matrix elements $\langle 0J | Q | 1J' \rangle$ listed by Birnbaum and Poll (13) and using $r_e = 1.40108 a_0$, $B = 60.9 \text{ cm}^{-1}$, and $\omega = 4162 \text{ cm}^{-1}$.

Since Q' is different for different transitions of the fundamental band of H₂, the binary absorption coefficients of the individual quadrupolar components were calculated first and the total quadrupolar binary absorption coefficient $\tilde{\alpha}_{1b\text{quad}}$ was then obtained from their sum. The details of the calculations are given later. The molecular parameters used in the calculations are listed in Table III. Values of the depth of the Lennard-Jones potential and those of the Lennard-Jones diameter σ were taken from Hirschfelder, Curtiss, and Bird (29). For the mixtures, the geometric mean of the values of ϵ and the arithmetic mean of the values of σ of the component gases were taken. The de Broglie wavelengths Λ^* were calculated from Eq. (14). The integral **J** at different reduced temperatures $T^*(=kT/\epsilon)$ up to a value of 10 were taken from Van Kranendonk and Kiss (30). For T^* greater than 10, \mathbf{J}_{c1} was evaluated using a computer program on IBM 360. In calculating **J**, the quantum corrections $\mathbf{J}^{(2)}$ and $\mathbf{J}^{(4)}$ mentioned in Eq. (13) were applied to the classical values of \mathbf{J}_{c1} . The polarizabilities, α_2 , of helium and neon were taken from Ref. (29).

The values of the binary absorption coefficients of the individual quadrupolar components of the fundamental band of H₂ were obtained from the expression

$$\tilde{\alpha}_{1b\text{quad}}[B(J)] = \left[\frac{(1/r_e)(B/\omega)^{\frac{1}{2}} \langle 0J | Q | 1J' \rangle}{e\sigma^4} \alpha_2 \right]^2 P(J) L_2(J, J') \mathbf{J} \tilde{\gamma}. \quad (16)$$

Here

$$P(J) = \frac{g_T \exp[-J(J+1)B_0hc/kT]}{\sum_J g_T g_J \exp[-J(J+1)B_0hc/kT]}$$

are the normalized Boltzmann factors, normalized in terms of the Racah coefficients $L_2(J, J')$ such that

$$\sum_J (2J + 1)P(J) = 1,$$

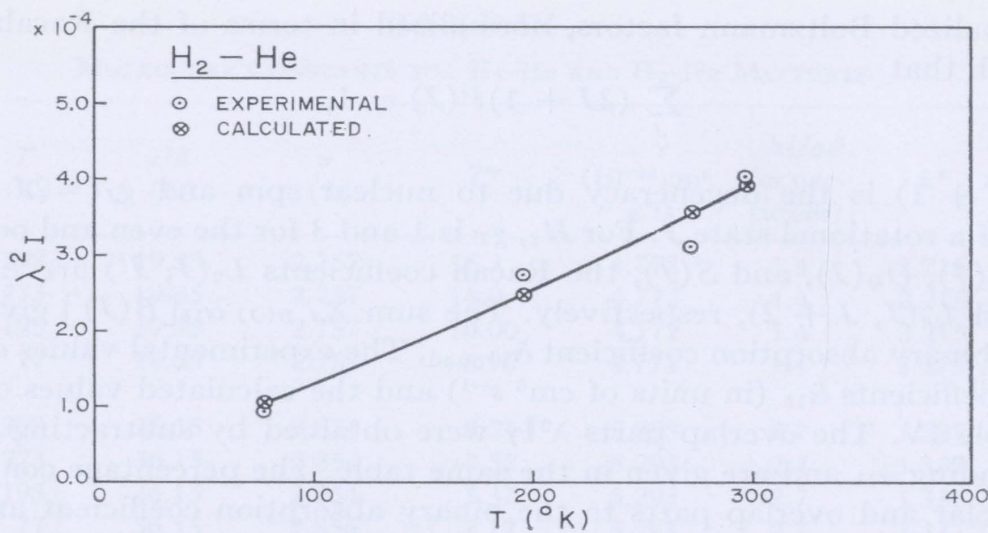
and $g_T (=2T+1)$ is the degeneracy due to nuclear spin and $g_J (=2J+1)$ is the degeneracy of a rotational state J . For H₂, g_T is 1 and 3 for the even and odd rotational states. For $Q(J)$, $Q_Q(J)$, and $S(J)$, the Racah coefficients $L_2(J, J')$ are $L_2(J, J-2)$, $L_2(J, J)$, and $L_2(J, J+2)$, respectively. The sum $\Sigma_{J, B(J)} \tilde{\alpha}_{1b}[B(J)]$ gives the total quadrupolar binary absorption coefficient $\tilde{\alpha}_{1b\text{quad}}$. The experimental values of the binary absorption coefficients $\tilde{\alpha}_{1b}$ (in units of $\text{cm}^6 \text{s}^{-1}$) and the calculated values of $\tilde{\alpha}_{1b\text{quad}}$ are listed in Table IV. The overlap parts $\lambda^2 \mathbf{I} \tilde{\gamma}$ were obtained by subtracting $\tilde{\alpha}_{1b\text{quad}}$ from the corresponding $\tilde{\alpha}_{1b}$ and are given in the same table. The percentage contributions of the quadrupolar and overlap parts to the binary absorption coefficient are also listed in the same table. It is seen that in the temperature range 77–298 K the overlap parts contribute 91 to 97% for H₂–He mixtures and 84–93% for H₂–Ne mixtures.

Determination of the Overlap Parameters for H₂–He and H₂–Ne Pairs

Using the values of $\tilde{\gamma}$ given in Table III the values of $\lambda^2 \mathbf{I}$ for H₂–He and H₂–Ne were obtained from the overlap parts and were then plotted against temperature T in Figs. 5 and 6, respectively. The integral \mathbf{I} given by Eq. (10) depends on the factor σ/ρ , the ratio of the Lennard–Jones diameter of a colliding pair of molecules and the range of the overlap moment. A study of the variation of $\lambda^2 \mathbf{I}$ in H₂–He and H₂–Ne mixtures as a function of temperature enables us to determine the most probable values of σ/ρ for these mixtures. In order to determine the value of ρ/σ for each of the mixtures the following procedure was adopted. The values of \mathbf{I}_{c1} were calculated from Eq. (10) by means of a computer program written for the IBM 360 computer for a series of values of ρ/σ in the range 0.080–0.140 at intervals of 0.002 at reduced temperatures T^* in the range 0.5–20.0 at intervals of 0.5. To obtain appropriate values of \mathbf{I} , quantum correc-

TABLE IV
QUADRUPOLAR AND OVERLAP PARTS OF THE BINARY ABSORPTION COEFFICIENTS

Mixture	Temper- ature (K)	Binary absorption coefficient (10^{-35} cm^6 s^{-1})	Calculated quadrupolar part (10^{-35} cm^6 s^{-1})	Overlap part (10^{-35} cm^6 s^{-1})	Percentage	
					Quad.	Overlap
H ₂ –He	298	1.99	0.06	1.93	3.0	97.0
H ₂ –He	273	1.54	0.06	1.48	3.9	96.1
H ₂ –He	195	1.36	0.05	1.31	3.9	96.1
H ₂ –He	77	0.49	0.04	0.45	9.1	90.9
H ₂ –Ne	298	2.40	0.16	2.24	6.7	93.3
H ₂ –Ne	273	2.07	0.16	1.91	7.7	92.3
H ₂ –Ne	195	1.82	0.15	1.67	8.2	91.8
H ₂ –Ne	77	0.89	0.14	0.75	15.7	84.3

FIG. 5. Variation of $\lambda^2 I$ with temperature for H_2 -He mixtures.

tions $\mathbf{I}^{(2)}$ and $\mathbf{I}^{(4)}$ were applied [Eq. (12)]. These quantum corrections were either directly obtained or extrapolated from the data given by Van Kranendonk and Kiss (8). For one particular value of ρ/σ , λ was calculated from $\lambda^2 \mathbf{I}$ at one of the experimental temperatures using the corresponding value of \mathbf{I} . Assuming λ^2 to be independent of temperature, $\lambda^2 \mathbf{I}$'s were calculated at the other three experimental temperatures. This procedure was repeated until the calculated values of $\lambda^2 \mathbf{I}$ at all the experimental temperatures agreed closely with the observed values. The criterion for the best fit of the curves between $\lambda^2 \mathbf{I}$ and T was that the sum of the squares of the deviations of the calculated values of $\lambda^2 \mathbf{I}$ from the corresponding observed values be a minimum. The temperature dependence of the experimental and calculated values of $\lambda^2 \mathbf{I}$ is shown for H_2 -He and H_2 -Ne in Figs. 5 and 6, respectively. The values of ρ/σ , ρ , λ , and $\mu(\sigma)$ for H_2 -He and H_2 -Ne evaluated in the present work are given in Table V. For the purpose of comparison the values of ρ/σ and ρ for H_2 -He obtained by Sears (30) by an analysis of the collision-induced fundamental band of H_2 in H_2 -He mixtures in terms of force autocorrelation

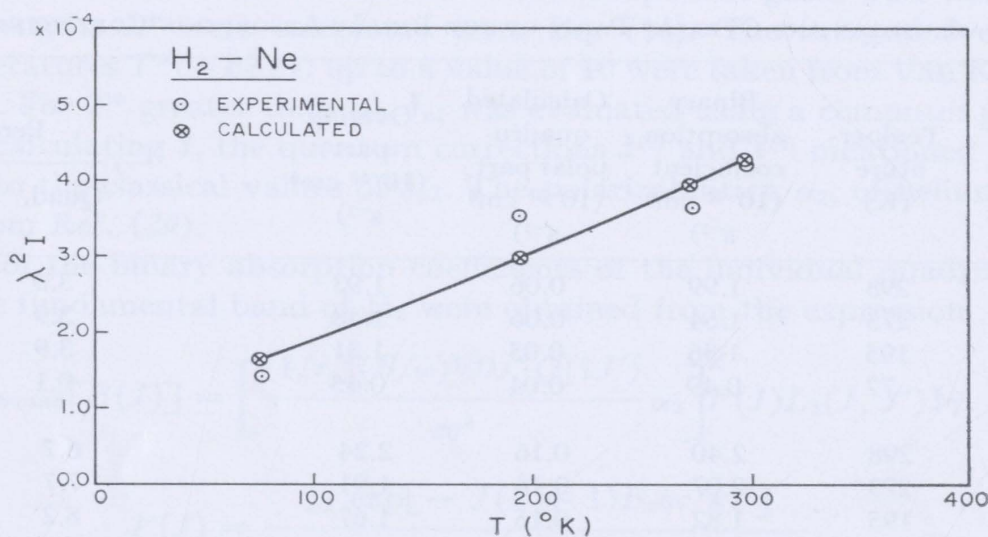
FIG. 6. Variation of $\lambda^2 I$ with temperature for H_2 -Ne mixtures.

TABLE V
OVERLAP PARAMETERS FOR VARIOUS GAS MIXTURES

Mixture	ρ/σ	λ	σ (Å)	ρ (Å)	$\mu(\sigma)$ ($10^{-3} ea_0$)	Reference
H ₂ -He	0.088	5.6×10^{-3}	2.757	0.24	29.2	Present work
H ₂ -Ne	0.100	9.0×10^{-3}	2.854	0.29	48.5	Present work
H ₂ -H ₂	0.126					(8)
H ₂ -He	0.087		2.75	0.24		(30)
He-Ar	0.110		3.0	0.33	4.5	(31)
Ne-Ar	0.092		3.1	0.29	5.9	(31)

function, and for He-Ar and Ne-Ar also obtained by Sears (31) by an analysis of their collision-induced translational absorption are also included in the same table. The value of ρ/σ for H₂-He obtained in the present work is in good agreement with that of Sears (30).

A brief comment must be made on the errors involved in calculating the quadrupolar part of the binary absorption coefficients using the molecular parameters of the colliding pairs of molecules. The major error lies in the uncertainty of the values of σ of the colliding pairs since it occurs in the fifth power in the expression for the binary absorption coefficient. The numerical calculations have shown that the quadrupolar part of the binary absorption coefficients varies from 3% for H₂-He at 298 K to 16% for H₂-Ne at 77 K. For the sake of argument, even if we assume an uncertainty as large as 25% in the calculation of quadrupolar parts, the percentage error in the overlap parts will not be very high; these are less than 1% for H₂-He at 298 K and about 5% for H₂-Ne at 77 K.

Another method of estimating the quadrupolar and overlap parts of the binary absorption coefficient for the given binary mixture is by the method of profile analysis. In this method there is no need to use the molecular parameters of the component gases except the relative strengths of the individual lines of the fundamental band of hydrogen. However, for the H₂-He and H₂-Ne mixtures, particularly at higher temperatures, even the method of profile analysis may not yield more accurate values of the quadrupolar part because the contribution of the overlap parts extends almost to the entire region of the fundamental band.

ACKNOWLEDGMENTS

The authors are thankful to Professor S. W. Breckon for his continued interest in this research.

RECEIVED: August 18, 1972

REFERENCES

1. M. F. CRAWFORD, H. L. WELSH, AND J. L. LOCKE, *Phys. Rev.* **75**, 1607 (1949).
2. H. L. WELSH, M. F. CRAWFORD, AND J. L. LOCKE, *Phys. Rev.* **76**, 580 (1949).
3. G. VARGHESE AND S. P. REDDY, *Canad. J. Phys.* **47**, 2745 (1969).
4. G. VARGHESE, S. N. GHOSH, AND S. P. REDDY, *J. Mol. Spectrosc.* **41**, 291 (1972).
5. J. VAN KRANENDONK, *Physica* **23**, 825 (1957).

6. J. VAN KRANENDONK, *Physica* **24**, 347 (1958).
7. J. L. HUNT, Ph. D. Thesis, University of Toronto, Toronto, Canada, 1959.
8. J. VAN KRANENDONK AND Z. J. KISS, *Canad. J. Phys.* **37**, 1187 (1959).
9. D. A. CHISHOLM AND H. L. WESLH, *Canad. J. Phys.* **32**, 291 (1954).
10. W. F. HARE AND H. L. WELSH, *Canad. J. Phys.* **36**, 88 (1958).
11. S. P. REDDY AND W. F. LEE, *Canad. J. Phys.* **46**, 1373 (1968).
12. G. KARL AND J. D. POLL, *J. Chem. Phys.* **46**, 2944 (1967).
13. A. BIRNBAUM AND J. D. POLL, *J. Atmospheric Sci.* **26**, 943 (1969).
14. C. J. HUMPHREYS, *J. Opt. Soc. Amer.* **43**, 1027 (1953).
15. International Union of Pure and Applied Chemistry: "Tables of Wave Numbers for the Calibration of Infrared Spectrometers." Butterworth's, London, 1961.
16. E. K. PLYLER, L. R. BLAINE, AND E. D. TIDWELL, *J. Res. Nat. Bur. Standards B* **55**, 279 (1955).
17. W. S. BENEDICT AND E. K. PLYLER, *J. Res. Nat. Bur. Standards B* **46**, 246 (1951).
18. E. K. PLYLER, L. R. BLAINE, AND M. J. NOWAK, *J. Res. Nat. Bur. Standards B* **58**, 195 (1957).
19. A. MICHELS, W. DE GRAAFF, T. WASSENAAR, J. M. H. LEVELT, AND P. LOUWERSE, *Physica* **25**, 25 (1959).
20. J. W. DEAN, "National Bureau of Standards Technical Note 120." U. S. Department of Commerce, Washington, D. C., 1961.
21. A. MICHELS AND W. WOUTERS, *Physica* **8**, 923 (1941).
22. D. B. MANN, "National Bureau of Standards Technical Note 154." U. S. Department of Commerce, Washington, D. C., 1962.
23. "American Institute of Physics Handbook," Section 4i, McGraw-Hill, New York, 1963.
24. A. MICHELS, T. WASSENAAR, AND P. LOUWERSE, *Physica* **26**, 539 (1960).
25. K. D. TIMMERHAUS, "Advances in Cryogenic Engineering," Vol. 8, p. 135. Plenum Press, New York, 1963.
26. S. P. REDDY AND C. W. CHO, *Canad. J. Phys.* **43**, 2331 (1965).
27. B. P. STOICHEFF, *Canad. J. Phys.* **35**, 730 (1957).
28. J. VAN KRANENDONK, *Canad. J. Phys.* **46**, 1173 (1968).
29. J. O. HIRSCHFELDER, C. F. CURTISS, AND R. B. BIRD, "Molecular Theory of Gases and Liquids," 2nd ed. Wiley, New York, 1967.
30. V. F. SEARS, *Canad. J. Phys.* **46**, 2315 (1968).
31. V. F. SEARS, *Canad. J. Phys.* **46**, 1163 (1968).

New Rotational Transition in the Hydrogen Molecule*

P. W. Gibbs, C. G. Gray, and J. L. Hunt

Department of Physics, University of Guelph, Guelph, Ontario, Canada

and

S. Paddi Reddy, R. H. Tipping, and K. S. Chang

Department of Physics, Memorial University of Newfoundland, St. John's, Newfoundland, Canada

(Received 22 April 1974)

Pressure-induced rotational-vibrational U transitions ($\Delta J = 4$) of hydrogen gas have been observed for the first time at 195 K for densities in the range 180–300 amagat. The spectrum is interpreted in terms of a hexadecapolar induction mechanism, and from the experimental integrated absorption coefficient of the $U(1)$ line, rough values are obtained for the hydrogen-molecule hexadecapolar moment and its derivative.

We report here the first spectroscopic observations of molecular $U(J)$ rotational transitions in H_2 corresponding to the selection rule $\Delta J = 4$. The $U(1)$ line ($J = 1 - 5$) has been observed in the fundamental rotational-vibrational (near-infrared) band and the integrated absorption coefficient has been obtained. An analysis is given below in terms of hexadecapolar induction.

In Fig. 1 is shown the near-infrared spectrum in the region 5550–5900 cm^{-1} taken at a temperature of 195 K and a density of 300 amagat, together with the computed S -branch ($\Delta J = 2$) and Q -branch ($\Delta J = 0$) contributions following MacTaggart and Welsh.¹ The peak of the observed feature is shifted by about 50 cm^{-1} towards higher frequencies from the calculated position of the

$U(1)$ line for the free molecule. From spectra such as that of Fig. 1 recorded over the density range 180–300 amagat, we have obtained the integrated absorption coefficient $\tilde{\alpha} = \int \tilde{A}(\nu) d\nu$ (as defined by Van Kranendonk²) as a function of the density ρ . In Fig. 2 where we have plotted the experimental $\tilde{\alpha}/\rho$ against ρ , it is apparent that a good fit is obtained for a straight line passing through the origin confirming that the line arises from a binary-collision mechanism.

The theory of the integrated absorption coefficient $\tilde{\alpha}$ has been developed in general by Van Kranendonk² and in detail for higher-multipolar induction by Gray.³ For the hexadecapolar-induced $U(J)$ lines we find that the binary absorption coefficient $\tilde{\alpha}_1$, defined by the density expan-

sion $\tilde{\alpha} = \tilde{\alpha}_1 \rho^2 + \tilde{\alpha}_2 \rho^3 + \dots$, is given by

$$\tilde{\alpha}_1(U(J)) = 10\kappa\sigma^{-9} I_{12}(T) \rho_J(T) C(J \ 4 \ J+4; 0 \ 0 \ 0)^2 [(\Phi' l \alpha)^2 + (\Phi l \alpha')^2], \quad (1)$$

where $\kappa = (4\pi^3/3h)$, $l = \langle 1|R - R_e|0\rangle = (h/8\pi^2 m \nu_0)^{1/2}$ is the $v=0 \rightarrow 1$ vibrational matrix element with ν_0 the vibrational frequency, $C(J \ 4 \ J+4; 0 \ 0 \ 0)$ a Clebsch-Gordan coefficient, σ the Lennard-Jones diameter, α the mean molecular polarizability, and α' its derivative with respect to internuclear separation R . The quantity

$$\rho_J(T) = Z^{-1} g_J(2J+1) \exp(-\epsilon_J/kT) \quad (2)$$

is the normalized Boltzmann factor for the level J , and Φ' is the derivative of the molecular hexadecapole moment Φ , defined by

$$\Phi = \int \rho(\vec{r}) r^4 P_4(\cos \theta) d^3r, \quad (3)$$

where $\rho(\vec{r})$ is the total charge density of the molecule. The quantity $I_{12}(T)$ is a dimensionless inte-

gral⁴

$$I_{12}(T) = 4\pi \int g_0(x) x^{-12} x^2 dx, \quad (4)$$

where $x = R/\sigma$, and $g_0(x)$ is the low-density limit of the pair correlation function. The term involving $(\Phi' l \alpha)$ in (1) corresponds to single transitions in which one molecule of the colliding pair makes both the vibrational and rotational jump, while the term involving $(\Phi l \alpha')$ corresponds to double transitions in which one molecule makes a vibrational and the other a rotational jump. The triangles in Fig. 1 indicate the expected positions of these transitions.

From Fig. 2 we obtain the experimental value $\tilde{\alpha}_1(U(1)) = (0.78 \times 10^{-10} \pm 20\%) \text{ cm}^{-1} \text{ amagat}^{-2}$. Since Eq. (1) depends on both Φ and Φ' , one of these must be known before the other can be obtained from the single experiment.

Previously, Gush and Van Kranendonk⁵ invoked the intermolecular quadrupole-hexadecapolar interaction in solid hydrogen with a value $\Phi = 1.2ea_0^4$, to explain the observed fine structure of the $S_1(0)$ line. A rough theoretical estimate, based on a point-charge model constructed to give the known quadrupole moment $Q = 0.46ea_0^2$, leads to $\Phi = 0.34ea_0^4$. A recent theoretical calculation⁶ using the Heitler-London-Wang wave function to obtain $\rho(\vec{r})$ in (3), gives $\Phi = 0.1ea_0^4$ and $\Phi' = 0.2ea_0^3$. Assuming the hexadecapolar-induction mechanism dominates and using Eq. (1), we obtain from the experimental spectrum upper limits for Φ and Φ' of $|\Phi| = 0.59ea_0^4$ and $|\Phi'| = 0.47ea_0^3$. From the

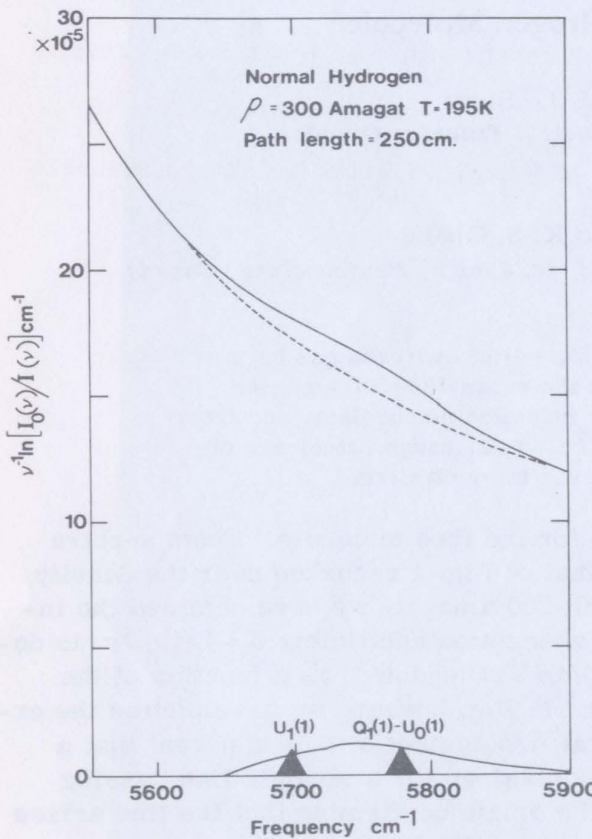


FIG. 1. High-frequency wing of the spectrum of pure normal hydrogen. The dashed curve shows the sum of all $\Delta J = 0, 1$ transitions. The difference of the two curves is shown at the bottom. The triangles indicate the frequencies of the $U_1(1)$ and $Q_1(1) - U_0(1)$ transitions calculated from the molecular constants of the free molecule.

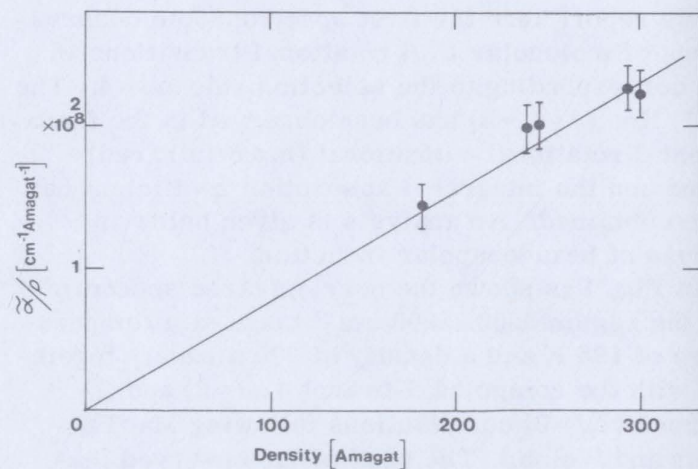


FIG. 2. Variation of transitions probability per unit density with density for pure normal hydrogen at 195 K.

fact that the peak of the experimental spectrum (Fig. 1) falls midway between the single- and double-transition frequencies, and from previous results on the quadrupole-induced lines,⁷ we expect the single and double transitions to contribute roughly equal amounts to the spectrum of Fig.

1. Assuming exactly equal contributions would give $|\Phi| = 0.42ea_0^4$ and $|\Phi'| = 0.33ea_0^3$.

Finally, we mention other possible induction mechanisms, in addition to the hexadecapolar mechanism. The quadrupole-induced double transitions $S_0(1)+S_1(3)$, $S_1(1)+S_0(3)$, and $S_0(2)+S_1(2)$, which fall within the linewidth of Fig. 1, can be ruled out. To do this the group of double-S transitions near 5300 cm^{-1} (outside Fig. 1) were observed⁸ and their intensity compared with the expected intensity of the double-S transitions in question; the latter is expected to be about 5% of the intensity of the lines near 5300 cm^{-1} . Since the observed peak of Fig. 1 is about 50% of the intensity of the 5300 cm^{-1} lines, we see that the double-S transition mechanism fails, by an order of magnitude, to explain the observed peak. Rough estimates of the dispersion and overlap mechanisms indicate that they too are small. The "level-mixing" mechanism of Herman⁹ is estimated to be of importance here only if Φ is of order $0.1ea_0^4$ or less.

Work is now in progress to obtain accurate absorption coefficient for the pure rotational lines of H_2 , and the lines of H_2 -rare-gas mixtures. An analysis of all these experiments together should yield more accurate values for both $|\Phi|$ and $|\Phi'|$.

The authors are grateful to Professor G. Karl, Professor E. Obryk, Professor J. Poll, and professor R. Herman for discussions.

*Work supported by the National Research Council of Canada.

¹J. W. MacTaggart and H. L. Welsh, Can. J. Phys. 51, 158 (1973).

²J. Van Kranendonk, Physica (Utrecht) 23, 825 (1957).

³C. G. Gray, J. Phys. B: Proc. Phys. Soc., London 4, 1661 (1971).

⁴A. D. Buckingham and J. A. Pople, Trans. Faraday Soc. 51, 1173 (1955).

⁵H. P. Gush and J. Van Kranendonk, Can. J. Phys. 40, 1461 (1962).

⁶G. Karl, E. Obryk, and J. D. Poll, Can. J. Phys. 51, 2216 (1974).

⁷A. Watanabe and H. L. Welsh, Can. J. Phys. 45, 2859 (1967).

⁸P. W. Gibbs, M. Sc. thesis, University of Guelph, 1973 (unpublished).

⁹R. M. Herman, J. Chem. Phys. 52, 2040 (1970).

